University of Nevada, Reno

Forest cover controls variability of net shortwave radiation and snow albedo in a mountain watershed

A thesis submitted in partial fulfillment

of the requirements for the degree of

Master of Science in Geography

By

Alexander I. Greenwald

Dr. Anne Nolin

Thesis Advisor

August 2020

THE GRADUATE SCHOOL

We recommend that the dissertation
prepared under our supervision by

Alexander I. Greenwald

entitled

Forest cover controls variability of net shortwave radiation and snow albedo in a mountain watershed

be accepted in partial fulfillment of the
requirements for the degree of

MASTER OF SCIENCE

Anne W. Nolin, Ph.D
Advisor

Stephen A. Drake, Ph.D
Committee Member

Keith S. Jennings
Committee Member

Kenneth E. Nussear, Ph.D
Committee Member

Monica M. Arienzo, Ph.D
Graduate School Representative

David W. Zeh, Ph.D., Dean
Graduate School

August, 2020

Abstract

Snow albedo regulates the surface energy budget of snow-covered regions which governs snowmelt processes, this makes snow albedo a critical parameter for climate models. Spaceborne and airborne remote sensing measurements provide high spatial and temporal resolution snow albedo data but have limited accuracy in forested regions due to the canopy shading effect. Vegetation induces spatial and temporal variability in snow albedo by depositing forest litter on the snow surface, reducing albedo in affected areas. Thus, accurate measurements of snow albedo and forest litter are needed to determine snow albedo characteristics and variability. Here, I present a unique set of field-based results detailing snow albedo and the snowpack energy budget in a temperate and coniferous forest. Data were collected during the 2019 snow season at the Sagehen Creek Field Station in the California Sierra Nevada. Three meteorological stations continuously measured the snowpack energy budget and snow depth across a forest density gradient. A forest density gradient spanned the forest, forest edges, and open meadow at the study site. Using a Spectral Evolution RS-3500 Portable Spectroradiometer, I measured snow spectral albedo during the accumulation and ablation periods. Spectral data and snow samples were collected over the period 14 February – 12 May 2019 and the net radiometer data were collected over the period 22 March – 15 May 2019. These measurements were used to characterize spectral and broadband snow albedo during the ablation season across the forest density gradient. Surface and subsurface snow samples were collected at each site and filtered to determine the mass fraction of forest litter and quantify black carbon content.

Results highlight the spatial and temporal differences of net shortwave radiation and snow albedo across a forest density gradient in the California Sierra Nevada. Differences in spectrally integrated and broadband snow albedo are driven by forest litter concentration, which is variable due to forest density. Forest litter concentration is a function of forest density and increases at the snowpack surface through the accumulation to the end of the ablation period. Snow albedo is 22% less in forest than in open sites because of greater forest litter concentrations. Strong and significant relationships exist between both

percent canopy cover and distance to forest tree stand evaluated with spectral snow albedo measurements. In the forest, net shortwave radiation is determined by canopy shading and snow albedo. In open areas of forest net shortwave radiation is completely dependent on snow albedo because canopy shading is not present. Net shortwave radiation is the largest term in the snowpack energy budget across the forest density gradient. In the forest, net shortwave radiation is a reduced component of the total snow energy budget when compared to open forest. As forest density decreases, albedo and net shortwave radiation are more important for the snowpack energy budget. This implies that, for estimating energy budget in snowy forests, sub-canopy snow albedo does not need to be known as accurately as snow albedo in open areas.

Acknowledgements

This work would not have been possible without the help and support of many individuals. Most notably, I would like to thank my advisor, Dr. Anne Nolin. I am truly honored to have worked with Anne, she is a role model for all and one of the most dedicated scientists in her field. The future of snow-based scientific research continues to grow in many diverse directions thanks to Anne. Second, I would like to thank all my committee members individually. Dr. Keith Jennings pushed me out of my comfort zone and helped me learn RStudio. I owe Keith many thanks for being a mentor and his dedication to my field work, data set analysis, and as an overall friend. To Dr. Steve Drake who shared many days of his time working in the field with me and providing guidance through my project. Steve dedicated a tremendous amount of his time by establishing and maintaining the Sagehen Field Site and sharing his data. Dr. Monica Arienzo and her supporting team at the Desert Research Institute, I offer many thanks for their roles in processing my samples, creating my data set, and providing insight for my project. To Dr. Kenneth Nussear, I appreciate your time and efforts supporting my project. To the University of Nevada, Reno Geography Department for funding me for two years and all the professors and surrounding cohort involved. I would like to give a huge thanks to the entire Computational Mountain Studies Lab group. First, soon to be (Dr.) Mikey Johnson, one of my first friends at UNR. Mikey always supported me both in and out of school and taught me a wealth of RStudio knowledge, I have never met a student who works as hard as Mikey. Second, (Dr. in a few years) Jack Tarricone, your friendship and support both in and out of the academic setting I can't thank you enough for. To Dr. Carl Schmitt, a lifetime of thanks for being my mentor during my entire academic career, inviting me to do research in Peru for two different expeditions, and being a lifetime friend. The McNair Scholars ladies, Susan and Liz, who supported our scholar group at UW, and got me set on a path of academic research and into graduate school. To all my friends through this and many other journeys, especially my two housemates that kept us all working through covid-19. Thank you to both of my sisters, Nicole and Noelle, for constantly supporting me through my whole life. Lastly

and most of all, to my mom Judy, who raised three kids completely alone and has always been the strongest person I know.

Table of Contents

1 Introduction 1
1.1 Significance and Motivation 1
1.2 Research Objectives 2
1.3 Previous Work 3
1.3.1 Snow Albedo 3
1.3.2 Snow and Forest Interactions 6
1.3.3 Snowpack Energy Budget 7
1.3.4 Forests and Radiation 8
1.3.5 Forests and Turbulent Fluxes 10
1.3.6 Other Energy Budget Components 10
2 Forest gradient transition of snow albedo in a temperate forest in the California Sierra Nevada: Spatiotemporal analysis of snow albedo 11
2.1 Introduction 11
2.2 Methods 12
2.2.1 Description of Study Area 12
2.2.2 Forest Density Gradient Description 14
2.2.3 Forest Density Gradient Vegetation and Site Characteristics 15
2.2.4 Spectral Snow Albedo Measurement Sites 16
2.2.5 CNR4 Net Radiometer Snow Albedo Measurements 17
2.2.6 Hyperspectral Snow Albedo Measurements 17
2.2.7 Snow Field Sampling 19
2.2.8 Lidar Data 20
2.2.9 Snow Sample Laboratory Processing 23
2.2.10 Laboratory Analyses of Black Carbon 23
2.2.11 Spectral Reflectance Factor Measurements of Forest Litter 24
2.2.12 Estimated Snow Grain Size from Spectral Data 25
2.2.13 SNICAR Model 25
2.2.14 Statistical Testing Approach 26
2.2.15 Snow Surveys 27
2.3 Results 27
2.3.1 Statistical Analysis of Data Sets 28
2.3.2 Spectral Snow Albedo 30
2.3.3 Accumulation Period Spectral Snow Albedo 31

2.3.4 Ablation Period Spectral Snow Albedo 33
2.3.5 Spatial Variability Snow Albedo Summary 34
2.3.6 Net Radiometer Broadband Snow Albedo Temporal and Spatial Variability 36
2.3.7 Snow Albedo and Distance from Forest Stand Relationship 38
2.3.8 Snow Albedo and Percent Canopy Cover Relationship 39
2.3.9 Estimated Effective Snow Grain Radius 41
2.3.10 Forest Litter 42
2.3.11 Laboratory Determinations of Black Carbon Concentrations 44
2.3.12 Spectral Albedo Measurements and Snow Impurities 45
2.3.13 Spectral Reflectance of Forest Litter 47
2.3.14 SNICAR Model Versus Spectral Albedo Measurements 48
2.4 Error assessment 49
2.4.1 CNR4 Albedo 49
2.4.2 Spectrometer 50
2.4.3 Snow Sample Collection 50
2.4.4 Snow Sample Analysis 50
2.5 Discussion 51
2.5.1 Snow Albedo and Forest Litter 51
2.5.2 Black Carbon 53
2.5.3 Conclusion 53
3 Snow Albedo and its Role in the Energy Budget of a Forest Snowpack 54
3.1 Introduction 54
3.2 Methods 54
3.2.1 Description of Forest Characteristics at the Meteorological Stations 55
3.2.2 Meteorological Station Instrumentation 57
3.2.3 Snow Skin Temperature 59
3.2.4 Energy Balance Calculations 59
3.3 Results 63
3.3.1 Snow Depth and SWE 64
3.3.2 Shortwave radiation 65
3.3.3 Longwave radiation 67
3.3.4 Sensible Heat Fluxes 70
3.3.5 Latent Heat Fluxes 71
3.3.6 Turbulent Fluxes Combined 72
3.3.7 Ground Heat Fluxes 74

3.3.8 Total Energy Budget 75
3.3.9 Net Shortwave Radiation and the Relation to Broadband Snow Albedo 77
3.4 Error Assessment 79
3.4.1 CNR4 net radiometers 79
3.4.2 Energy Budget Calculation 80
3.5 Discussion 80
3.5.1 Snowpack Energy Budget Component Variability 80
3.5.2 Shortwave Radiation 81
3.5.3 Longwave Radiation 81
3.5.4 Turbulent Fluxes 82
3.5.5 Snowmelt 82
3.5.6 Conclusion 83
4 Synthesis of the Research 83
4.1 Key findings 83
4.2 Effects of Forest Litter and Light Absorbing Particles 84
4.3 Effects of Forest on Net Solar Radiation 84
4.4 Bigger Picture 85
4.5 Recommendations for future research 86
5 References 88
6 Appendices 95

List of Tables

Table 2. 1: Forest structure statistics of measurement sites from LiDAR data, (*) indicate snow sample sites, all other sites represent spectrometer measurement sites. 21

Table 2. 2: Kruskal-Wallis rank sum test results for grain radius, spectrally integrated albedo, and broadband albedo data sets during the accumulation and ablation periods 28

Table 2. 3: Pairwise comparisons using Dunn's test for grain radius, spectrally integrated albedo, and broadband albedo data sets during the accumulation and ablation periods**.** 29

Table 2. 4: Summary of mean spectral integrated albedo (350-1850 nm) and visible albedo (400-700 nm) during the entire observed accumulation period (March 2019). Standard deviations are in parentheses. .. 33

Table 2. 5: Summary of mean spectral integrated albedo (350-1850 nm) and visible albedo (400-700 nm) during the observed ablation period (April 2019). Standard deviations are in parentheses. 34

Table 2. 6: Summary of mean spectrally integrated snow albedo values during the observed Accumulation period (15 March, 29 March, 30 March, WY 2019) and observed Ablation period (12 April, 26 April, WY 2019). 35

Table 2. 7: Statistics generated from spectrally integrated albedo versus distance to tree stand linear model. 39

Table 2. 8: Statistics generated from spectrally integrated albedo versus percent canopy cover linear model. 40

Table 3. 1: Summary of forest stand type, ground cover vegetation type, and LiDAR derived canopy cover and tree stand height metrics at each station. 56

Table 3. 2: Summary of Met station instrumentation and nominal accuracy. 58

Table 3. 3: Snow water equivalent and snow disappearance date from local SNOTEL sites (*) and Sagehen Field Site 64

Table 3. 4: Reported statistical values of broadband snow albedo and net shortwave radiation. 78

Table 3. 5: Accumulation (acc.) and ablation (abl.) period daily average broadband albedo and incoming shortwave radiation with LiDAR forest metrics at each station. Standard deviations are reported in parentheses. 79

List of Figures

Figure 2. 1: a) Sagehen Watershed (black polygon) and Study Area (red lines), and b) locator map of Sagehen location in California. 14

Figure 2. 2: Sagehen Field Site spectral albedo measurement sites (green circles), snow sample sites (green crosses), transect line (blue). Stations are represented by white text. 16

Figure 2. 3: Use of RS-3500 field spectrometer at Sagehen Field Site. 19

Figure 2. 4: Dates of spectral albedo measurements, snow impurities, SWE and snow depth transects. 19

Figure 2. 5: LiDAR metrics of percent canopy cover (%) and tree height (m) across the Sagehen Field site. 21

Figure 2. 6: Experimental setup for spectral reflectance factor measurements. 25

Figure 2. 7: Average spectral snow albedo (solid lines) measured at the Open, Forest Edge, and Forest sites spanning the forest density gradient. Dashed lines represent spectrally integrated albedo (350-1850 nm). All measurements were taken on or near solar noon under diffuse (clear) sky conditions. 31

Figure 2. 8: Mean spectrally integrated broadband albedo (350-1850 nm) during the accumulation and ablation period. 35

Figure 2. 9: Temporal changes to broadband snow albedo at Forest (S1), Forest Edge (S4), Open (S3). Dashed vertical lines indicate snow disappearance date and missing data was due to a 27 March snow event that obstructed the measurements 37

Figure 2. 10: Differences in broadband albedo for each of the stations during the accumulation and ablation periods. 38

Figure 2. 11: Relationship between distance from nearest tree stand and spectrally integrated snow albedo. 39

Figure 2. 12: Relationship between percent canopy cover and spectrally integrated snow albedo. 40

Figure 2. 13: Estimated snow grain radius (μm) during the accumulation and ablation periods showing distribution and density. 42

Figure 2. 14: Mean forest litter concentrations from surface and shallow sub-surface snow samples during the accumulation and ablation periods. 43

Figure 2. 15: Forest litter samples from the forest density gradient with associated dates of collect. A clean-blank white filter illustrates clean versus dirty filters. These samples are from surface collected snow. 44

Figure 2. 16: Mean black carbon concentration from surface and shallow sub-surface snow samples during the accumulation and ablation period. 45

Figure 2. 17: Relationship between in-situ measured spectrally integrated snow albedo and forest litter concentrations. 46

Figure 2. 18: Relationship between in-situ measured spectrally integrated snow albedo and black carbon concentrations. 46

Figure 2. 19: Mean spectral reflectance factors during the period of observation. 48

Figure 2. 20: In-situ measured snow albedo versus SNICAR calculated snow results, in-situ measurements were made with a field spectrometer and snow samples were taken immediately after for further processing of black carbon content. Dashed red line indicate 1:1 line and black line indicate linear regression line. 49

Figure 3. 1: Map of Sagehen Field Site meteorological stations. 55

Figure 3. 2: Photographs of S3 (Open), S4 (Forest Edge), and S1 (Forest). 56

Figure 3. 3: Daily mean net shortwave radiation, vertical dashed lines indicate snow disappearance date. 66

Figure 3. 4: Daily mean incoming incident radiation, vertical dashed lines indicate snow disappearance date. 66

Figure 3. 5: Daily mean snow albedo, vertical dashed vertical lines indicate snow disappearance date per station. 67

Figure 3. 6: Daily mean longwave radiation, vertical dashed lines indicate snow disappearance date. 68

Figure 3. 7: Daily mean incoming longwave radiation, vertical dashed lines indicate snow disappearance date. 69

Figure 3. 8: Daily mean outgoing longwave radiation, vertical dashed lines indicate snow disappearance date. 69

Figure 3. 9: Daily sensible heat flux, vertical dashed lines indicate snow disappearance date. 71

Figure 3. 10: Mean daily latent heat fluxes, vertical dashed lines indicate snow disappearance date. 72

Figure 3. 11: Mean daily net turbulent fluxes, vertical dashed lines indicate snow disappearance date. ... 73

Figure 3. 12: Daily wind speed, solid blue line is daily mean value and light blue line is daily range of values. 74

Figure 3. 13: Daily mean ground heat flux. Dates are removed past 3 May 2019 due to snow disappearance at the stations beginning. 75

igure 3. 14: S1 (Forest) daily mean energy budget components (bars)..... 76

Figure 3. 15: S3 (Open) daily mean energy budget components (bars)..... 76

Figure 3. 16: S4 (Forest Edge) daily mean energy budget components (bars). 77

Figure 3. 17: Daily values of net radiometer measured broadband snow albedo and net shortwave radiation during the end of the accumulation and entire ablation period. 78

List of Equations

Eq. 1. 1 8

Eq 3. 1 59
Eq 3. 2 60
Eq 3. 3 60
Eq 3. 4 61
Eq 3. 5 61
Eq 3. 6 61
Eq 3. 7 62
Eq 3. 8 62
Eq 3. 9 62
Eq 3. 10 63
Eq 3. 11 63

1 Introduction

1.1 Significance and Motivation

Snow has the highest variability across the electromagnetic spectrum of any natural land cover. The presence of snow on Earth is essential to the planetary energy budget because it controls net solar radiation at local to global scales. More than one half of the Northern Hemisphere's land surface is covered by snow during winter (Lemke et al., 2007). The earth's snow-covered surfaces play an important role in the global albedo-temperature feedback. High snow albedo reflects most incoming solar radiation and maintains cool air temperatures. Decreased albedo allows snow to absorb a larger fraction of solar radiation and can amplify the melting of surface snow. Warming air temperature and positive snow-albedo feedbacks have reduced the extent of annual Northern Hemisphere snow cover (Brown & Robinson, 2011). Snow albedo therefore is important in weather and climate models but requires parameterization because of the canopy shading effect on sub-canopy snow (Betts & Ball, 1997). Use of satellite and airborne remote sensing has aided global monitoring of snow albedo and is essential for assimilation into weather and climate models.

Snow albedo is a primary control on snowmelt because it governs net solar radiation (Wiscombe & Warren, 1980). More than one-sixth of the Earth's population lives in regions that rely on snowmelt for water resources (Barnett et al., 2005). Snowmelt provides water that is critical for ecosystems, human energy production, agricultural uses, and drinking water. Understanding snow albedo on global and regional scales can allow us to better predict the rate and duration of snowmelt. In particular one challenge is estimating snow albedo in heterogenous forested areas. Roughly one-third of snow-covered regions are forested (Sturm et al., 2017) and snow albedo in these regions remains poorly constrained.

Snow-forest interactions create snow albedo variability due to differences in forest structure (Gleason et al., 2013), forest disturbance state (e.g. wildfire, beetle kill) (Harpold et al., 2014; R. Winkler et al., 2010), and snow climate (e.g. temperate, continental). Forest canopy cover affects the snowpack radiation

budget by reducing solar irradiance via canopy shading and contributing longwave radiation from vegetation (Roth & Nolin, 2017). Forest density affects wind speed and therefore influences sensible and latent heat fluxes (Boon, 2009). Of these energy balance components, it is well known that for open areas net shortwave radiation is the largest contributor to snowmelt (Marks et al., 1992). In such areas small changes in albedo can have a major impact on snowmelt timing and rate. However, the importance of snow albedo in heterogenous forested landscapes is not well understood.

The two components that have the largest effect on snow albedo in forested regions are forest litter and snow grain size. Yet measurements of these components are limited to a few sites in the northeastern US and Canada (Melloh et al., 2001; R. Winkler et al., 2010a). Moreover, none of these studies simultaneously measured spectral snow albedo, grain size, and forest litter concentrations. Recent studies have measured spectral snow albedo, grain size, and burned woody debris, but were focused on understanding the effects of charred woody debris on snowmelt rates and the impacts of forest fires on snow albedo across the western United States (Gleason et al., 2013, 2019a; Gleason & Nolin, 2016).

Satellite remote sensing of snow in forests is challenging because of mixed pixel effects and forest canopy obscuring the snow surface. Models can be employed to account for snow albedo effects in forested areas. However, the models themselves need improved parameterizations of snow albedo to account for spatial and temporal variability. Therefore in-situ measurements are needed to understand snow albedo characteristics across forest density gradients. This study provides the first comprehensive measurements of snow albedo and forest litter concentrations across a forest density gradient. It provides important context for the role of snow albedo in overall snowpack energy budget in forests.

1.2 Research Objectives

This study serves to determine how forest canopy affects snow surface albedo and the snowpack energy budget covering a forest density gradient in a temperate-coniferous forest in the California Sierra Nevada Mountain Range. Previous studies have found forest vegetation canopy modifies the snowpack energy budget by affecting the radiation balance and turbulent fluxes (Boon, 2009; T. E. Link & Marks, 1999; T.

Link & Marks, 1999). I document snow albedo across a forest density gradient to better understand the spatiotemporal variability of snow albedo due to forest cover and density. The meteorological variables and properties of the snowpack were measured and used to calculate the energy budget across the forest density gradient to determine the importance of snow albedo.

This thesis has three following chapters. Chapter 2 documents the field collected snow albedo measurements and shows the spatial and temporal variability of snow albedo during the accumulation and ablation period. Chapter 3 computes the snowpack energy budget at our forest, open and forest edge sites to show where and when snow albedo is a major contributing factor to the overall snowpack energy budget. Chapter 4 in this thesis reviews the key findings of the previous chapters and provides a broader context for these findings.

1.3 Previous Work

1.3.1 Snow Albedo

Albedo is a measure of surface reflectivity and drives the planetary energy budget which is an important part of Earth's climate. Energy is emitted from the Sun in the form of shortwave radiation (typically 300-2500 nm). Shortwave radiation encounters Earth's atmosphere and surfaces where it can be absorbed, reflected, or transmitted, the sum of these three components equals the dimensionless value of albedo (0-1.0). Albedo describes the reflective properties of a surface. Generally, lighter (white) surfaces reflect most of the incoming shortwave radiation encountered, while darker (black) surfaces absorb more. The amount of solar radiation that is absorbed or reflected is an important control on temperature as less absorbed energy means less heating of a surface. Albedo can be represented as the spectrally averaged value of all wavelengths, or as spectral albedo, the measurement of albedo at individual wavelengths.

Snow is one of the most highly reflective surfaces on the Earth in the visible spectrum; therefore it has a high albedo. The snow-albedo feedback is determined by the amount of snow cover and is an important

parameter in climate models because of its strong feedback properties that determine temperature and snowmelt (Henderson-Sellers & Wilson, 1983). Greater snow cover increases albedo and reflects more solar radiation and decreases temperatures, less snow cover decreases albedo and absorbs more solar radiation causing warmer temperatures and decreasing albedo as more snow melts. Under most atmospheric conditions the absorption of shortwave radiation is the largest energy source for snow melt (Male & Granger, 1981).

Net shortwave radiation and shortwave albedo are a primary control on snowmelt (Wiscombe & Warren, 1980). Net shortwave radiation is dependent on both solar irradiance and the surface albedo, both of which can have high spatiotemporal variability (Klok et al., 2004). Solar irradiance and snow albedo can have high spatiotemporal variability due to the position and angle of the sun which seasonally varies and regional differences in factors that determine albedo. Therefore, snowmelt rates are controlled by snow albedo and understanding snow albedo is important for predicting snowmelt and use in land surface modeling.

Warren and Wiscombe (1980) created a model of the albedo of pure snow which explains pure snow has a high albedo of 0.95 in the visible portion of the electromagnetic spectrum (VIS, 400-700 nm) and decreases with wavelength in the near-infrared (NIR, 700-1000 nm) and shortwave near-infrared (SWIR, 1000-2500 nm). In the visible portion snow reflects almost all energy, however in the thermal spectrum snow is almost a perfect black body (Warren, 1982). Due to the high reflectivity of snow in the visible wavelengths, small changes to visible snow albedo can greatly increase net shortwave radiation (Dozier et al., 2009). Snow albedo that is spectrally integrated across the shortwave spectral range (300-2500 nm) of "new snow" is between 0.8-0.9 and is referred to as broadband albedo.

Snow albedo is variable across the entire range of shortwave radiation (350-2500 nm) and is affected by snow grain size, solar zenith angles, visible versus near-infrared radiation, impurities in snow, and snow depth (Warren Wiscombe 1980; Wiscombe & Warren, 1980). Snow albedo is a function of snow grain size in the near-infrared region and light absorbing particle content in the visible region. Snow grain size

and light absorbing particle content generally increase through time. Therefore, snow albedo decreases with time and is refreshed by new snowfall (O'Neill & Gray, 1973). Snow albedo can rapidly decrease over short periods which can increase the absorption of solar radiation and increase melt rate.

Snow albedo can significantly be reduced in the visible spectrum by the addition of light absorbing particles. Common light absorbing particles include black carbon, brown carbon, dust, ash, fire soot, and forest litter. Due to the importance of snow albedo, light absorbing particles and their effect on snow and the climate system have been studied and detailed (Flanner et al., 2007a; Hadley & Kirchstetter, 2012; Skiles et al., 2012).Concentrations of black carbon, ranging from 10-100 (ppb) deposited on snow can decrease snow albedo by 1-5% (Hansen & Nazarenko, 2004; Warren & Wiscombe 1980). Charred woody debris was found to reduce snow albedo in a burned forest by 40% compared to a healthy forest during the ablation period (Gleason et al., 2013). Forest litter is known to effectively reduce snow albedo (Hardy et al., 2000; Melloh et al., 2001). However, forest litter influence on snow albedo has not been fully understood due to its high variability.

The spectral properties of snow make it possible to measure snow albedo using instrumentation and models. Field based measurements of snow albedo are usually collected using pyranometers or field spectrometers. Pyranometers have been used in snow albedo and snowpack energy balance studies and offer high temporal measurements but do not capture spatial variability (Gleason et al., 2013; Hardy et al., 2004). In-situ measurements from spectroradiometers offer high spectral and spatial, but low temporal resolution. Both methods offer the ability to validate remote sensing observations, derive surface snow properties such as snow impurity content, and collect measurements in complex terrain.

Spaceborne sensing platforms can measure snow albedo with greater spatial and temporal coverage (Bair et al., 2019; Dozier, 1984, 1989; Painter et al., 2009). Measurements from these platforms are spatially confined in forest and mountainous regions where these measurements are most important (Betts & Ball, 1997). Satellite measured albedo is dependent on clear skies and can be inaccurate due to complex terrain (Stroeve et al., 1997).

Snow grain radius is an important property of snow and snow albedo because larger grain size increases the chance of a photon of light to be absorbed (Warren, 1982). Due to the scattering properties of snow grains and the sensitivity in the NIR and SWIR regions, techniques have been developed to retrieve snow grain sizes from in-situ and remotely sensed snow reflectance observations (Nolin & Dozier, 1993, 2000; Painter et al., 2003). Nolin (1993, 2000) was able to estimate snow grain size using the ice absorption feature centered at $\lambda = 1.03$ μm.

Models incorporate snow albedo as fixed (new snow versus old snow), variable (aging snow), or physically derived albedo decay parameterizations (Essery, 2013). Physically based representations usually incorporate known albedo values (maximum and minimum) that decay across time, refresh from snowfall events, and decline during dry periods. Parameterizing snow albedo in models becomes complicated in heterogenous regions where snow albedo spatial variability is greater. Snow albedo can vary from open gaps in the forest to the sub-canopy snow surface where different processes govern the primary controls on snow albedo. Melloh et al., (2002) created a model that accounts for snow albedo sub-canopy and in open forest. The model is physically based and includes accounting for solar zenith angles, cloud cover, canopy, snow grain size, litter amounts, snow events, snow depth, and patchy snow cover. Hardy (Hardy et al., 1998, 2000) included forest litter deposition rates and effects on snow albedo in the snowpack energy balance model SNTHERNM (Jordan, 1991). The need to accurately represent snow albedo in these models is essential to model the timing and intensity of snowmelt.

1.3.2 Snow and Forest Interactions

Snow-forest interactions create complexities in understanding patterns of accumulation and melt of snow. The presence of a forest and forest canopy creates multiple factors that affect snow accumulation. Differences in forest structure, elevation, and wind control snow accumulation patterns in forests.

Accumulation of snow under the canopy is known to be less than open forest due to canopy interception (Jost et al. 2007; Winkler et al., 2005). In the open forest or forest edges, more snow can reach the surface and accumulate into a snowpack (Musselman et al., 2008). Snow accumulation is known to decline with

greater canopy density because of canopy snow interception and sublimation (Gelfan et al., 2004; Pomeroy et al. 1998; Varhola et al. 2010). For example in coniferous forests up to 40% of annual snowfall intercepted by the canopy can be lost to sublimation (J. W. Pomeroy et al., 1998). Forest canopies can redistribute snow via "canopy sloughing" or "mass unloading" unequally to the forest floor. Snow intercepted by the canopy can sublimate, melt or refreeze. Forests that have undergone changes to the canopy (e.g. fire, beetle kill) can accumulate more snow because of canopy removal (Boon, 2009; Gleason et al., 2013; Harpold et al., 2014). Changes to the forest canopy can increase snow accumulation and snow-water equivalent.

Wind is known in forests to drive snow accumulation patterns based on precipitation, wind patterns, vegetation influences, and topography (Hiemstra et al., 2002, 2006). The influence of wind can strip snow from windward aspects and redistribute to leeward. This wind driven process can create greater depths of snow on forest edges and in open areas of the forest. Wind can effectively strip vegetation (e.g. needles, cones) from the canopy and redistribute it as forest litter to the underlying snowpack.

Understanding these processes is complicated due to regional differences in forest types (e.g. coniferous, deciduous, boreal, clear-cut, burned) and their climates (e.g. cold, warm, continental, maritime). The interactions of radiation, vegetation, and topography are challenging to incorporate into our understanding of snow forest interactions but need considered (Link & Marks, 1999; Rinehart et al., 2008).

1.3.3 Snowpack Energy Budget

The energy budget of a snowpack controls the timing and duration of snowmelt, therefore accurately calculating the energy budget is necessary to determine snowmelt timing and rates. The components of the snowpack energy budget are the sums of net shortwave radiation, net longwave radiation, net sensible heating flux, net latent heating flux, energy inputs from rainfall, and ground heating flux (Eq. 1.1) (Anderson 1968; Marks & Dozier 1992).

$$Q_{Total} = Q_{Net\ SW} + Q_{Net\ LW} + Q_{Net\ Sensible} + Q_{Net\ Latent} + Q_{Rainfall} + Q_{Ground} \qquad \text{Eq. 1. 1}$$

Total net radiation is the sum of the difference in incident and reflected shortwave radiation and incident and emitted longwave radiation. Sensible heat fluxes are dependent on temperature gradients while latent heat fluxes are dependent on vapor pressure gradients, both fluxes are a function of turbulence. Energy inputs from rainfall tend to add positive energy from liquid water into a snowpack. Ground heat flux is the amount of heat the ground contributes to the snowpack. These components mirror a global energy budget with slight differences when applied to a snow surface and snowpack.

Positive and negative snowpack energy fluxes both can physically alter the snowpack. Positive energy inputs into the snowpack lead to warming and snow melt once internal storage of cold content is overcome, while negative energy fluxes from the snowpack leads to cooling and preservation of the snowpack (Marks et al., 1992). A snowpack cannot efficiently begin to melt until it reaches an internal temperature of 0˚C or is “isothermal”.

Snowpack energy budgets in forests depend on different factors (e.g. forest type, elevation, topography, vegetation, regional climate) that can alter energy transfer. The forest canopy is important because it affects snow surface energy budget processes which influence snow accumulation and ablation (Link & Marks, 1999; Roth & Nolin, 2017). Forest composition is heterogenous and snowpack energy budget components are not uniform across forests creating differences in snow melt across fine spatial scales (Winkler et al., 2005). Elevation, topography, and forest cover are important considerations when studying snowmelt in forests (Jost et al., 2007). The following section addresses the importance of understanding the forest in the snowpack energy budget.

1.3.4 Forests and Radiation

Detailed measurements of the snowpack energy budgets components in different forest types have shown that net radiation is the dominant energy components for snowmelt followed by turbulent fluxes (Boon,

2009; Link & Marks, 1999; Roth & Nolin, 2017). The forest canopy structure (e.g. forest composition and gaps) influences the amount of solar radiation that can reach a sub-canopy snow surface. The amount of shortwave radiation that can reach the snow surface is key to snowmelt. In forests that have had reduced or removed forest canopy, total snow water equivalent (SWE) may increase, but snowmelt can shift earlier due to increased net shortwave radiation on the snow surface (Gleason et al., 2013; Harpold et al., 2014). As the canopy can reduce snow accumulation it can effectively reduce snow ablation by reducing solar insolation below the canopy.

Energy budget studies have found that forest type is important to snowmelt. Boon (2009) found that dead forest stands have greater net shortwave radiation, reduced net longwave radiation, and minor increases in sensible heat flux. Gleason (2013) found that burned forests allow more incoming shortwave radiation to reach the snow surface and contribute organic burned material that further reduce snow albedo and increase snowmelt compared to a healthy forest stand in the Oregon Cascades. Roth and Nolin (2017) found that in maritime forests shortwave and longwave radiation are important factors for snowmelt depending on if the snowpack is in the open or under the canopy. Hardy et al., (2004) found that sub-canopy net solar radiation is spatially and temporally variable in a coniferous forest. Incoming shortwave radiation reaching the sub-canopy snow surface can vary with tree species, canopy gaps, and solar incidence angles. Detailed shortwave radiation measurements using sub-canopy pyranometers or canopy radiation models are needed to accurately understand the sub-canopy energy budget (Hardy et al., 2004).

On the contrary, longwave radiation is limited in the open due to lack of sources (e.g. vegetation, exposed surfaces, tree stands) and snows emissivity, however in the forest it is a primary component. Forest canopies is a contributor of net longwave radiation to the snowpack by absorbing incoming shortwave radiation and re-emitting it as longwave radiation to the sub-canopy surface (Essery et al., 2008). Energy exchange processes above the forest canopy can warm the canopy (radiation and sensible heating) and can increase longwave radiation emitted back to the snowpack (Boon, 2009). Tree stands are known

sources of longwave radiation, thus the melting of snow around tree-wells. Net longwave radiation is known to be greater in alive forest stands than dead stands (Boon, 2009)

Snowmelt contributions in forests from longwave radiation is determined by characteristics of the forest (e.g. elevation, warm versus cold forest, aspect). Roth and Nolin (2017) found in a warm forest in Oregon snowmelt was driven under the canopy by long-wave radiation at certain elevations. These results suggest that in other warm forested environments like the Sierra's the importance of longwave radiation to snowmelt. Longwave radiation during rain on snow events in forests can be a strong energy budget component and create snowmelt (Mazurkiewicz et al., 2008).

1.3.5 Forests and Turbulent Fluxes

Sensible and latent heating fluxes are affected by the forest canopy both above and below the canopy. Wind speed is reduced by the forest canopy and tree stands which reduces turbulent transfer of energy (Boon, 2009). Studies have found sensible heating fluxes tend to be towards (positive) and latent heating flux away (negative) from the snowpack (Marks et al., 1992). It is important to consider how these fluxes can affect snowmelt when the snow cover is no longer uniform and becomes patchy. As snow becomes patchy and bare ground exposed sensible heat fluxes from bare ground to surrounding snow can contribute more to snowmelt (Marsh & Pomeroy, 1996). In Marks & Dozier's study they found that the turbulent fluxes tend to cancel each other in the winter. Roth & Nolin (2017) found that turbulent fluxes in low-mid-high forest were minimal, and only at open mid-high exposed sites that encountered wind did they contribute to the energy budget. Boon (2009) found that turbulent fluxes are minimal in a dead and alive forest plot but have an impact in clear cut forest due to differences in wind speeds.

1.3.6 Other Energy Budget Components

Advective energy can be sensible heat additions from "warm rain", latent heat releases from rainfall freezing on snowpack, or condensation on snowpack due to high humidity (DeWalle & Rango, 2008). Rainfall energy is more important to understand in warmer regions that experience rain during winter like the Pacific Northwest or the Sierra Nevada. In several studies (Boon, 2009; Marks et al., 1992; Roth &

Nolin, 2017) rainfall energy was not included in their energy budget calculations. However, studies have shown that in warm regions that experience large rain-on-snow events heat advection from precipitation could be important for snowpack energy budget and snowmelt (Jennings & Jones, 2015) Ground heat conduction is the heat transferred from the ground to the snowpack and has been found minimal with contributions averaging 1-3 Wm^{-2} (Cline, 1997; Marks et al., 1992).

2 Forest gradient transition of snow albedo in a temperate forest in the California Sierra Nevada: Spatiotemporal analysis of snow albedo

2.1 Introduction

Snow albedo controls the amount of net shortwave radiation received by a snow surface and determines the timing and rate of snowmelt. Measuring snow albedo in forests is difficult due to the heterogenous composition of a forest that create spatial and temporal variability. The subject of snow albedo in forests has been limited in study, mainly by evaluating the role of charred woody debris in the Pacific Northwest ,beetle kill deposited forest litter in the Canadian Boreal forest, or forest litter deposited in a mixed-hardwood forest in Vermont (Gleason et al., 2013; Melloh et al., 2001; R. Winkler et al., 2010b). However, a study has not measured snow albedo and forest litter across a forest density gradient in the California Sierra Nevada.

While the importance of snow albedo is well understood, it is not understood in forests the characteristics of snow albedo spatially and temporally. Furthermore, it is not understood what creates differences in snow albedo values across a forest in the California Sierra Nevada. The objective of this research is to understand forest effects on snow albedo. Specifically, the following set of questions is asked: What are the effects of differential forest density on snow albedo across a forest gradient? What are the differences both spatially and temporally of snow albedo values across a forest density gradient? What is the effect of forest litter and other light absorbing particles on snow albedo across a forest density gradient?

2.2 Methods

A field study site was designed prior to the 2019 snow season. Data sets were created using a combination of field measurements and observations paired with laboratory analyses. I collected hyperspectral snow albedo measurements spanning a forest density gradient to measure snow albedo at fine spatiotemporal scales. Snow samples were collected with the in-situ snow albedo surveys to examine the snow for light-absorbing impurities such as forest litter, black carbon, and dust. I analyzed the snow samples out of the field for concentrations of impurities in an ice core laboratory. Instrumentation was dispersed across the forest density gradient to measure temporal snow albedo and snowpack properties. I created forest canopy metrics from a LiDAR data set to describe the forest density gradients relationship to the snow albedo and snow impurity measurements. Standard snow community measurement techniques were used to measure snow depth, snow-water equivalent, and analyze snow pits. I used empirical methods to evaluate the observational data that was collected during the 2019 field season. The specific methods are described below.

2.2.1 Description of Study Area

The Sagehen Experimental Forest is located about 13 kilometers north of Truckee, CA within the Tahoe National Forest, and is a part of the northern Sierra Nevada Mountain Range. Sagehen Experimental Forest is operated by the USDA Forest Service, with an included field station operated by the University of California Berkeley for research purposes. Sagehen Creek is the main drainage feature of this basin. The Sagehen watershed drains an area of 27 km^2 that is the primary tributary flowing east into Stampede Reservoir, which is a part of the Truckee River Watershed (Mast & Clow, 2000).

The California Sierra Nevada receives 67% of annual precipitation as snowfall and snowmelt provides the majority of surface water that is under high demand and sensitive to climatic variability (Serreze et al., 1999). The Sagehen Watershed receives an average of 85-94 centimeters of precipitation annually, of which 80% is snowfall (Kirchner, 2005). Sagehen Creek is snowmelt fed, with peak flows during spring, tapering off into summer. The climate is temperate; there is a wet winter and spring season, followed by a

dry summer leading into fall. The watershed is composed of mixed conifer, pine, fir, brush, ferns, and mountain meadows. Topography is steep in the upper reaches of the watershed and the elevation gradient decreases to the east; elevations range from about 2600 m to 1900 m.

The study site for this project is located to the south (200 m) of the research field station and Sagehen Creek (Figure 2.1). Dr. Anne Nolin (Director of the Graduate Program of Hydrologic Sciences, Department of Geography) in coordination with Dr. Stephen Drake (Department of Physics), both at the University of Nevada Reno, established the field site for forest-snow interactions and snow sublimation experiments in the fall of 2018. The field site was operational for the winter and spring of water year 2019. Five meteorological towers (Met stations) were installed in the fall and early winter of 2018-2019 to house instrumentation for several field projects. The stations run east to west and cover 5 different forest zones; upwind forest (S1), upwind forest edge (S2), open meadow (S3), downwind forest edge (S4), and downwind forest (S5) (Figure 2.2). The five stations share a mean elevation of 1941 m, and a relatively uniform slope (0-4˚) and aspect (0-5˚). The established study site provides an idealized heterogenous representation of a temperate-coniferous forest in the Sierra Nevada Mountain Range to serve our forest-snow interactions study.

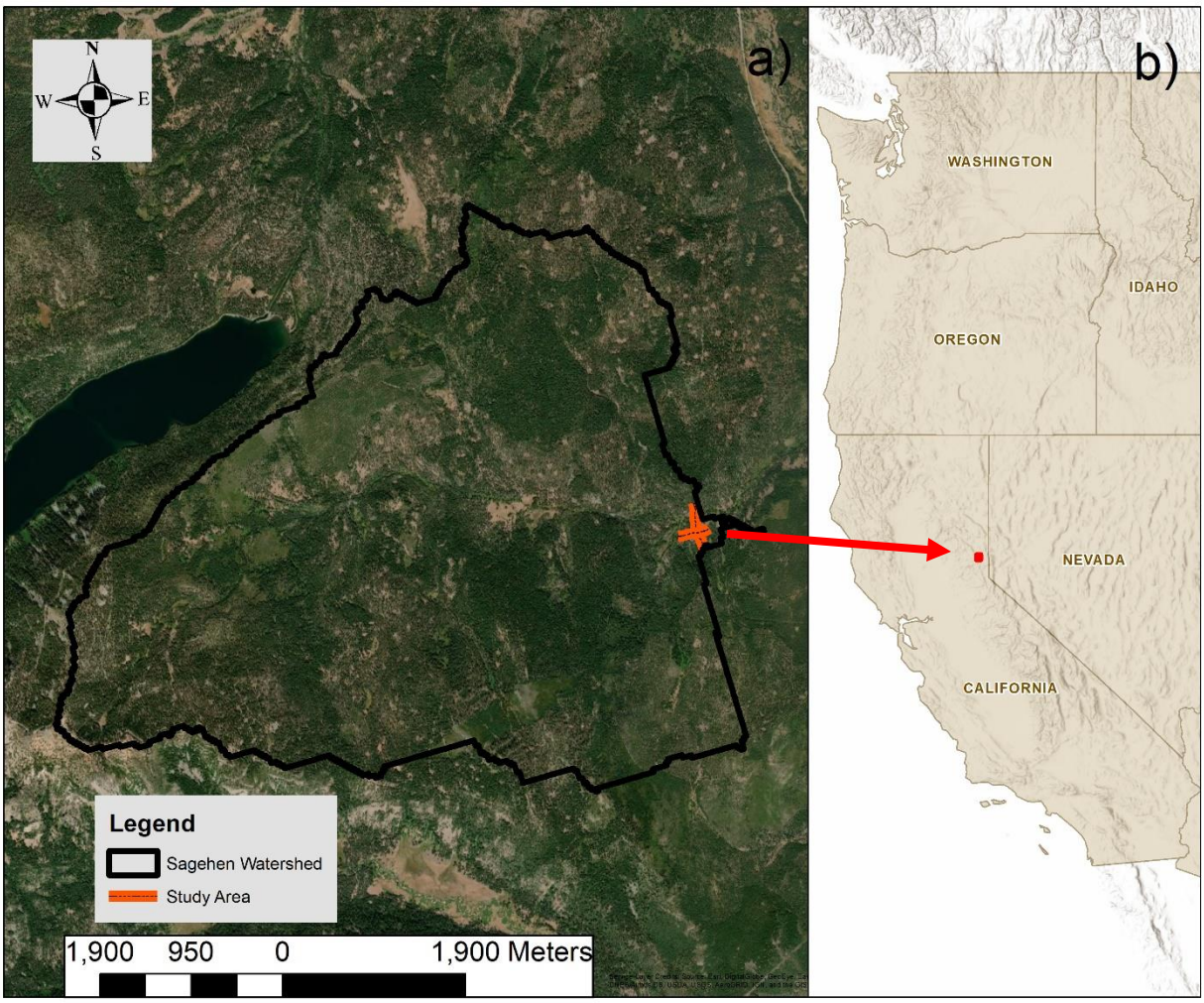

Figure 2. 1: a) Sagehen Watershed (black polygon) and Study Area (red lines), and b) locator map of Sagehen location in California.

2.2.2 Forest Density Gradient Description

The forest density gradient was established prior to the field season and is composed of a transect spanning the field site and was supported by five meteorological stations (Figure 2.2). The meteorological stations measured meteorological variables, snow depth, and broadband snow albedo. The forest density gradient was categorized in three types of forest structure: Open, Forest Edge, and Forest to capture the differences from forest effects on snow albedo. The forest density gradient categories were developed using a combination of location characteristics (e.g. vegetation, elevation,) and a LiDAR data set that

describes forest structure. Two transects spanned the forest density gradient (Figure 2.2). The west-to-east transect captured the dominant westerly wind patterns and included all five meteorological stations. The north-to-south transect captured the southern edge of the forest, open meadow, and south-facing forest.

2.2.3 Forest Density Gradient Vegetation and Site Characteristics

Across the sampling transects forest structure and vegetation characteristics were documented. The Open sites included S3 and surrounding locations in the open meadow (Figure 2.2). There are several individualized trees stand composed of lodgepole pine (*Pinus contorta* subspecies *Murrayana*), both mature and young near the open sites but canopy shading did not disturb the sites. The dominant ground cover at the Open sites is primarily sedge (*Cyperaceae exerta),* with clusters of greenleaf manzanita *(Arctostaphylos patula),* jeffrey shooting-star *(Dodecatheon jeffreyi),* and bolanders clover *(Trifolium bolanderi)*. During the ablation period the open meadow becomes a seasonal marsh and snowmelt flows north to Sagehen Creek

The Forest Edge sites included two stations (S2 and S4) and additional sites at the north and south perimeter of the open meadow. The Forest Edge sites are composed of mature and young lodgepole pine (*p. contorta* subsp. *Murrayana*), and sparse white fir (*Abies concolor)* and red fir (*Abies magnifica)*. Ground cover at the Forest edge sites are dominated by sedge (*C. exerta)* The Forest Edge sites include vegetation composed of mixed greenleaf manzanita *(A. patula),* jeffrey shooting-star *(D. jeffreyi),* and bolanders clover *(T. bolanderi)*. A tree well next to S2 was included as a Forest Edge site due to it's location and forest structure characteristics.

The Forest included two stations (S1 and S5) and additional sites in the south-facing forest at the northern end of the transect. The Forest sites are composed of primarily lodgepole pine (*p. contorta* subsp. *Murrayana*), sparse white fir (*A. concolor)* and red fir (*A. magnifica)*. Ground cover at the Forest sites is composed of sedge (*C. exerta),* with clusters of greenleaf manzanita *(A. patula),* and Currant species (*Ribes*). The south facing forest sites are composed of mature jeffery pine (*P. jeffreyi),* mature ponderosa

pine (*P. ponderosa*), with limited ground cover represented by clusters of greenleaf manzanita *(A. patula)*, and Currant species (*Ribes*). All of the Forest sites were developed underneath the canopy in the forest.

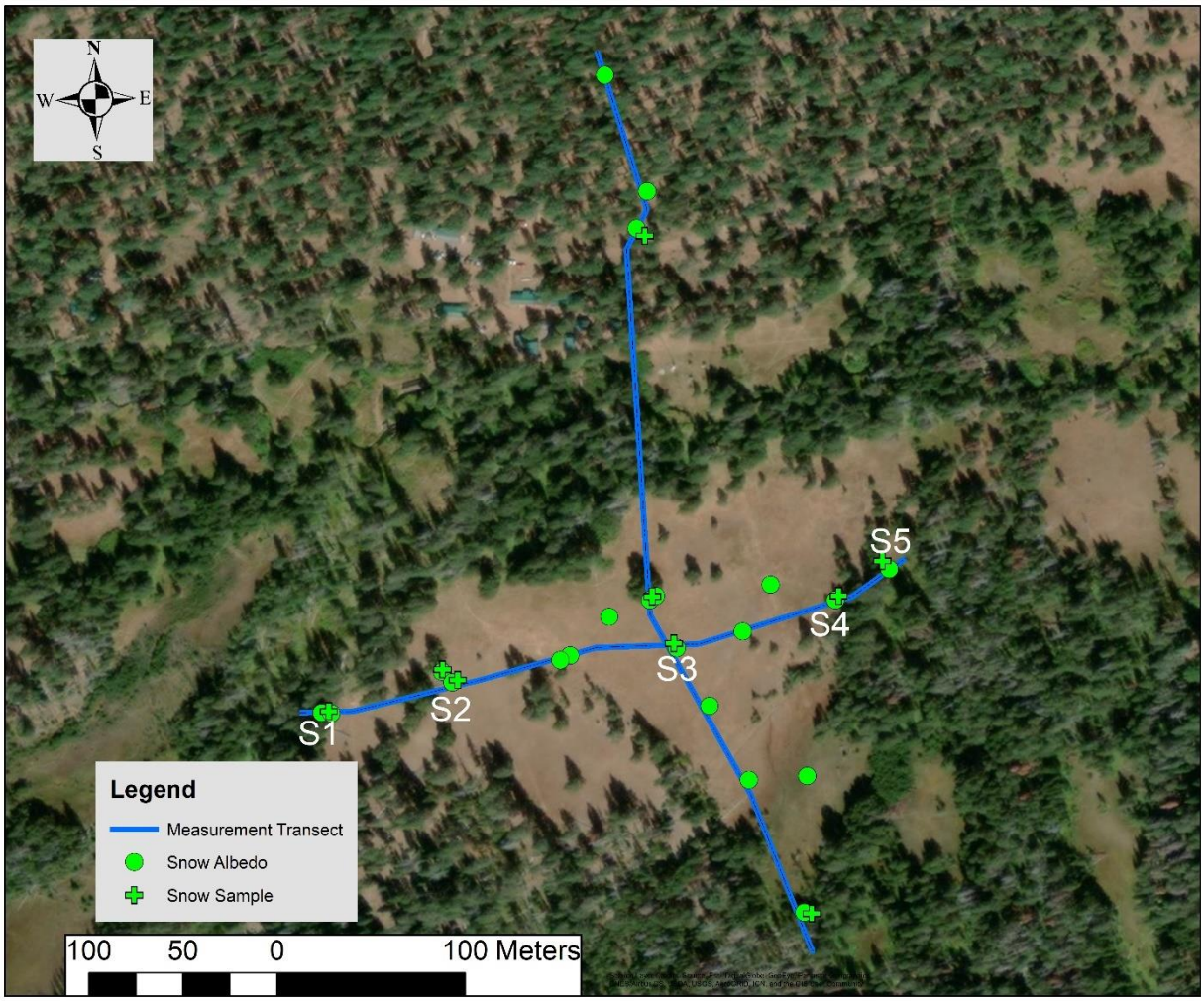

Figure 2. 2: Sagehen Field Site spectral albedo measurement sites (green circles), snow sample sites (green crosses), transect line (blue). Stations are represented by white text.

2.2.4 Spectral Snow Albedo Measurement Sites

Figure 2.2 provides context to the sampling and measurement sites, field site transects, and meteorological stations at Sagehen Field Site. Repeat measurements of spectral snow albedo were made at 20 sites. The same sites were revisited using markers and GPS coordinates to ensure the same location. selected for repeat measurements of spectral snow albedo (350-2500 nm) using a field spectroradiometer.

Table 2.1 provides forest structure metrics derived from LiDAR data for all the measurement sites. These sites were selected to represent the characteristics of the forest within the entire study site. Field measurements of snow albedo captured the snow accumulation (March 2019) and ablation period (April – May 2019). Several field data collection days targeted snowfall events and dry periods that captured snow albedo change.

2.2.5 CNR4 Net Radiometer Snow Albedo Measurements

Figure 2.2 shows the three stations (S1, S3, S4) which were equipped with Kipp & Zonen™ CNR4 Net Radiometers. The CNR4 net radiometers measured broadband snow albedo (305-2800 nm), and incoming and outgoing shortwave radiation at one-minute averaged time steps to provide temporal coverage of snow albedo from 22 March to the date of snow disappearance. These stations represented the three categories of the forest density gradient; S1 (Forest), S3 (Open), and S4 (Forest Edge). The CNR4 net radiometers were mounted approximately three meters above the ground surface on the meteorological stations. The CNR4 net radiometer is composed of upward and downward facing pyranometer and pyrgeometer. The pyranometer measures shortwave radiation (305-2800 nm) and pyrgeometer measures longwave radiation (4500-42000 nm). The field of view for the upward facing sensor is 180˚ and the downward sensors are 170˚ (shortwave), 150˚ (longwave). The CNR4s were calibrated before field deployment. Following most snowfall events, snow was manually removed from the upward facing pyranometer and pyrgeometer sensors.

2.2.6 Hyperspectral Snow Albedo Measurements

Snow albedo was measured with a field spectroradiometer to measure the spatial variability of snow albedo along the transects at the Sagehen Field Site. A Spectral Evolution RS-3500 Portable Spectroradiometer™ (RS-3500) equipped with a 180˚ field of view (FOV) diffuser measured snow albedo (Figure 2.3). The RS-3500 has three detectors (visible-short wave near infrared range) that cover a spectral resolution of 1 nm over the spectral range of 350-2500 nm (Spectral Evolution, 2014). The

diffuser was mounted to an extendable pole with a bubble level attached so the operator could level the sensor.

Snow albedo varies depending on solar zenith angle and atmospheric conditions and to control for these variations, measurements were taken at or near solar noon on clear sky days following the methods described in Gleason et., al. (2013). Measurements that may have been affected by clouds, vegetation, and sun-speckling due to canopy shading were discarded from the dataset. The measurement periods began in March 2019 and ended in May 2019. Each measurement was taken approximately 60 cm from the snow surface. Additional field observations were noted with all measurements (e.g. time of day, slope, aspect, recent snow, height of snow).

As measurement sites melted to the surface or the snowpack became optically thin (height of snow <20 cm) the measurements were discarded from the data set. The hyperspectral measurements were used to create datasets of spectral snow albedo, spectrally integrated snow albedo (350-1850 nm), solar irradiance, and outgoing shortwave radiation. The spectral albedo data required post-processing in order to remove sensor noise effects in the SWIR region at wavelengths longer than 1850 nm. The spectral albedo comparisons and integrated broadband albedo values span the range of 350-1850 nm. These measurements are referred to in the results as spectrally integrated snow albedo. Snow albedo data sets were further processed to correct measurements based on field observations of slope, aspect, and time of day to account for solar geometry.

Figure 2. 3: Use of RS-3500 field spectrometer at Sagehen Field Site.

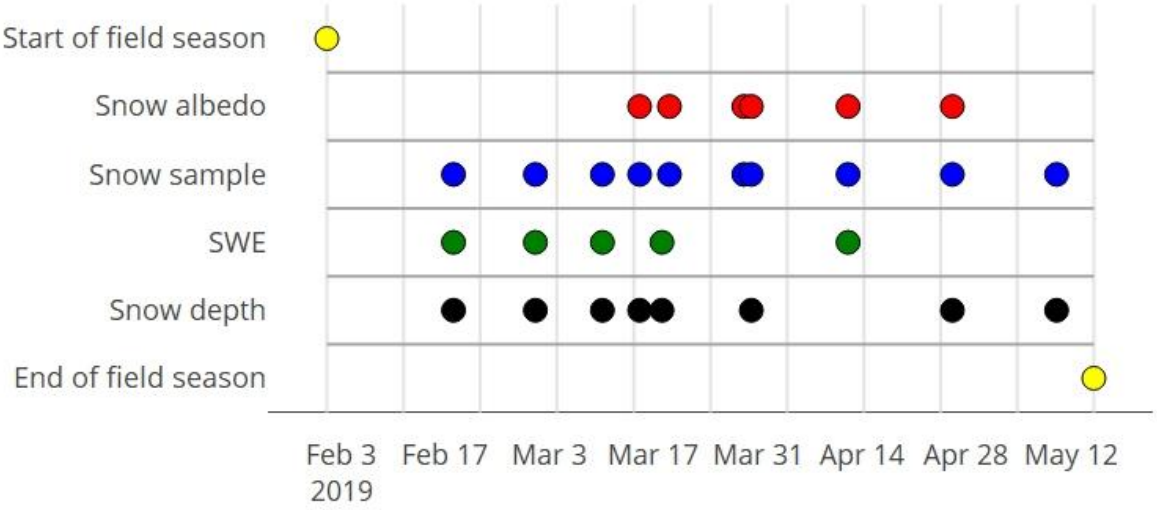

Figure 2. 4: Dates of spectral albedo measurements, snow impurities, SWE and snow depth transects.

2.2.7 Snow Field Sampling

Snow samples were collected to measure and characterize impurities in the snowpack that may be affecting snow albedo. The snow sampling technique closely followed the methods described in Gleason

et al., (2013; 2019). Snow was sampled at all five stations (S1-S5), two tree-well sites (S2, north of S3), the south meadow edge, and at the south-facing old growth forest site (Figure 2.2). Surface and sub-surface samples were collected at locations that were adjacent to or representative of snow albedo measurements made with the RS-3500 spectroradiometer. Surface samples were taken from measurement plots (1 m^2 x 0.5 m^2 area by 3 cm depth) with sterile gloves, acid-washed plastic scoops cleaned with "proximal snow" and were stored in 1-2 L whirl-pack bags. Shallow snow pits were dug (30 cm depth), and shallow pit snow samples were collected (30 cm x 3 cm) and stored in whirl-pack bags. In total, 8-days of snow samples were collected that totaled 61 samples. Snow samples were kept frozen and stored in a cooler during field workdays and immediately transported to the Desert Research Institute's (DRI) ice core freezer for storage prior to further processing.

2.2.8 Lidar Data

LiDAR data was used to characterize the forest structure at each site along the measurement transects and across the forest density gradient. The data was a 1 m processed bare ground digital elevation model (DEM) raster from a 2014 U.S. Forestry Service LiDAR flight. The raster product provided canopy height (average height in meters) and canopy density (percent of cover) metrics. The LiDAR data was incorporated into ESRI's Arc products and used with georeferenced point data for the stations, snow albedo measurement sites, and snow sampling sites. The LiDAR data were (planar) buffered at an area of 1.5 m to account for the forest metrics around each site. Forest structure metrics were extracted from the dataset to show the statistics of canopy density and tree height at each site (Figure 2.5). The LiDAR dataset was spatially joined with the snow albedo and snow impurity data sets.

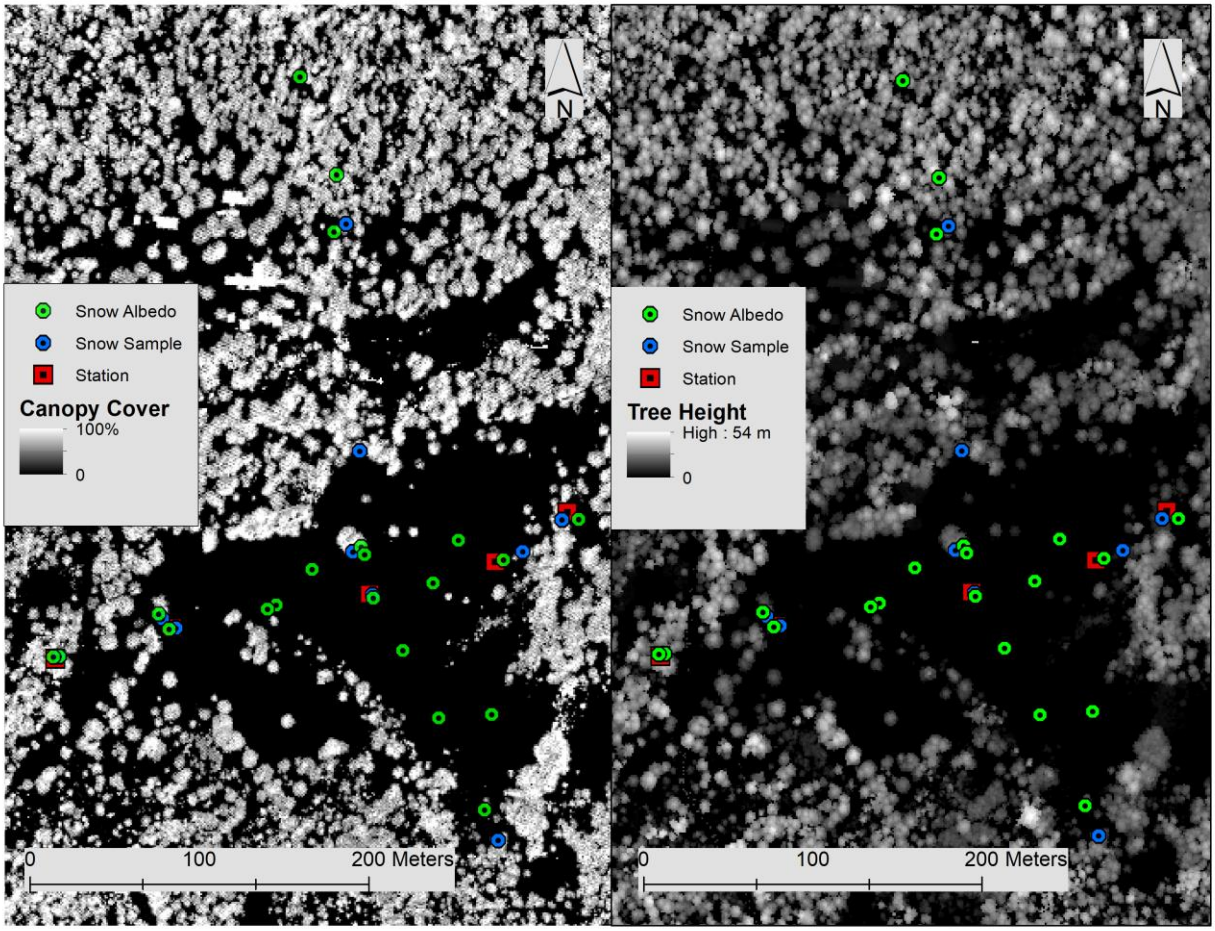

Figure 2. 5: LiDAR metrics of percent canopy cover (%) and tree height (m) across the Sagehen Field site.

Table 2. 1: Forest structure statistics of measurement sites from LiDAR data, (*) indicate snow sample sites, all other sites represent spectrometer measurement sites.

Site ID	Latitude	Longitude	Percent Canopy Cover				Tree Height (m)			
			Mean	Min.	Max.	Std. Dev.	Mean	Min.	Max.	Std. Dev.
South Face: Site 1*	39.4321	-120.24	35	0	69	25	7	0	11	5

South Face: Site 2	39.4324	-120.23997	78	57	100	16	24	21	26	2
South Face: Site 3	39.43292	-120.2402	74	55	92	11	18	10	22	4
Station 1: Forest, Sun*	39.4301	-120.24207	39	0	70	29	9	0	16	5
Station 1: Forest, Shade*	39.42991	-120.242	84	56	100	15	18	15	21	2
Station 2: Forest Edge*	39.43004	-120.2412	None				None			
Station 3: Open *	39.43017	-120.23981	None				None			
Station 4: Forest Edge*	39.43035	-120.23892	5	0	40	13	1	0	4	1
Station 4: Forest Edge Site 2	39.4304	-120.2389	6	0	38	14	1	0	3	1
Station 5: Forest*	39.43055	-120.2384	66	29	100	28	7	3	9	2
Open Sites: n=7	39.4	-120	None				None			
South Meadow: Forest Edge	39.42904	-120.2391	42	18	70	19	9	8	10	1
Tree Well 1: Open*	39.4304	-120.23988	51	0	100	33	6	0	10	3

Tree Well 2: Forest Edge*	39.43012	-120.24127	65	40	83	16	8	4	10	2

2.2.9 Snow Sample Laboratory Processing

Snow samples were processed at the Desert Research Institute (DRI) Ice Core Laboratory. The Ice Core laboratory has instrumentation and processing lines to analyze snow and ice samples for concentrations and properties of black carbon, dust, and forest litter. Snow samples were rapidly melted from their frozen states using low temperature heating lamps. The samples were sonicated with an ultrasonic bath to suspend the particles within the liquid samples in a homogenous mixture. Each melted and sonicated sample had 50 ml of liquid removed and placed in a plastic vial which was pre-rinsed with ultra pure deionized water where it would be used for further analysis.

The remaining volume of liquid from the snow samples was measured for total mass and prepped for vacuum filtration. A vacuum filtration line was used to separate the forest litter from the liquid sample using Whatman™ Glass Microfiber Filters, 47 mm diameter, 1.6 µm pore size. These filters are composed of quartz fibers with no binding agents and are designed for filtration of impurities from liquids. The filters were pre-weighed before vacuum filtration. Post filtration, the filters were baked in a furnace oven at 30 ˚C for 24 hours to remove any remaining liquid. The filters were post-weighed and mass fractions of forest litter were quantified from each sample based on the mass of water (snow) to the mass of forest litter present.

2.2.10 Laboratory Analyses of Black Carbon

In order to measure black carbon concentrations from field collected snow samples the separated 50 ml liquid samples were processed with a Droplet Measurement Technologies Single Particle Soot Photometer™ (SP2). The SP2 uses laser-induced particle incandescent (LII) to measure individual aerosol particles for mass and was designed specifically for refractory black carbon (soot) (Stephens et al., 2003). By combining the theories of light scattering, absorption and emission; the diameter, mass, and

incandescence temperature of individual aerosol particles in the diameter range of 0.15-1 μm can be measured (Baumgardner et al., 2004) (Stephens et al., 2003). The technique used by the SP2 can be found in detail via [Stephens et al., 2003] and it's use with black carbon on snow or ice has been detailed in [Sampson et al., 2007]. The SP2 instrument is calibrated before use with controls of carbon particles with a known density and specific sizes. Liquid samples are loaded on an autosampler and a line is inserted per sample which pumps the liquid through a 20 μm stainless steel filter that removes oversized particles. Next the sample liquids are split for black carbon measurements in the size range of 0.09-0.6 μm and insoluble particles between 0.8-10 μm are ran through an Abakus® laserbased particle counter. The Abakus® measures dust particle concentration based on particle sizes (Gleason et al., 2019a).

Several samples were unable to be processed for black carbon content as they exceeded the laboratory instruments capabilities due to high forest litter concentration. However, these samples were processed for forest litter mass fraction and spectral reflectance.

2.2.11 Spectral Reflectance Factor Measurements of Forest Litter

The spectral reflectance factors of the filtered forest litter samples were measured using the RS-3500 spectroradiometer. These measurements are the spectral reflectance factor of the filter with the added effect of filtered forest litter. The measurements were made between 12:00 and 13:00 at solar noon on a clear sky day in the spring of 2020 to remove atmospheric effects. The RS-3500 was equipped with a calibrated 8˚ fore-optic and was mounted on a tripod pointed perpendicular to the filters, which were mounted on another tripod (Figure 2.6). The use of tripods was employed to remove shadows caused by the operators and other effects of natural features from the underlying surface. A polytetrafluoroethlyene spectralon target and clean calibration filters were used as a reference standard. The reflectance measurements covered a spectral range of 350-2500 nm and were processed to remove noise at the longer wavelengths. The final reflectance measurements covered a spectral range of 350-1350nm. Slight noise was noted around 980 nm when the spectrometer switch sensors, however the noise did not significantly alter the measurements.

Figure 2. 6: Experimental setup for spectral reflectance factor measurements.

2.2.12 Estimated Snow Grain Size from Spectral Data

Snow grain radius was estimated following the Nolin & Dozier (2000) grain size retrieval technique. Spectral albedo measurements from the RS-3500 spectrometer were taken and filtered to retrieve the endpoints at $\lambda = 0.95$ μm and $\lambda = 1.08$ μm to calculate the continuum slope. The known albedo across $\lambda =$ 0.95–1.08 μm was next computed on the known continuum slope and used to compute the scaled band area for each observation. These estimations of snow grain radius are representative for the top 0.5-3 cm of the snowpack and do not necessarily reflect grain size distribution of the entire snowpack.

2.2.13 SNICAR Model

The Snow, Ice, and Aerosol Radiative model (SNICAR) simulates radiative transfer in the snowpack by incorporating Wiscombe and Warren (1980) snow albedo theory with the two-stream, multilayer radiative approximation of Toon et al. (1989) (Flanner et al., 2007). The SNICAR model simulates the radiative forcing of black carbon and dust concentrations on snow. Laboratory analyses of black carbon concentration are the primary input for SNICAR. Snow albedo is sensitive to impurities in the visible spectrum and grain size in the near-infrared region, therefore the SNICAR model has several other key adjustable parameters. Field observations of snowpack density, snow depth, snow grain radius, measured black carbon content (ng/g) and dust (ppm, 4 bins based on size and concentration) were used. Solar zenith angle of 61˚, mid-latitude clear sky, and direct incident radiation on the surface were all assumed.

SNICAR results were compared to in-situ spectral albedo measurements taken from the same location snow samples were collected for black carbon analyses.

2.2.14 Statistical Testing Approach

Kruskal-Wallis rank sum test was conducted in RStudio to determine if the samples for each dataset represent different populations. The Kruskal-Wallis rank sum test is a non-parametric method for testing if sampling populations originate from the same distribution (Daniel, 1990). The Kruskal-Wallis does not assume the data are normally distributed and can be used when evaluating the differences of three or more independent (unmatched) groups. The spectrally integrated snow albedo values, broadband snow albedo values, and estimated grain radius data are the dependent variables and were categorized into forest density gradient categories (Forest, Forest Edge, and Open) or three independent variables (categorical). The datasets were separated into two periods (accumulation, ablation) and the Kruskal-Wallis test was performed for each period.

Significant Kruskal-Wallis test results can indicate that at least one samples population originates from a different distribution but does not indicate which sample population. Therefore, Dunn's test of multiple comparisons using rank sums is necessary to evaluate the results of the Kruskal-Wallis test to indicate the specific sample pairs. The Dunn's test generates adjusted and unadjusted p-values for each pairwise comparison among the groups, a Z test statistic for each comparison is also created. I used RStudio to perform the Dunn's test using the Bonferroni correction method.

Linear models were created in RStudio to determine relationships between spectrally integrated snow albedo values and forest metrics that were derived from the LiDAR data set. Percent canopy cover and distance from nearest tree stand were the forest metrics evaluated. I used ESRI Arc GIS products to classify the nearest tree stands based on the assumption of tree height ≥3 m using the LiDAR data set. From the linear models p-values and values of R^2 were generated and included in our analysis to determine relationship strength and significance.

2.2.15 Snow Surveys

During the 2019 snow season, snow-water equivalent (SWE), snow pits, and snow depth surveys were manually conducted across the established forest density gradient. The SWE surveys covered the east-west station transect across all stations (S1- S5). SWE was measured with a Federal Snow Sampler at each station and between each station. The SWE measurements were collected to monitor the transition of the snowpack from the accumulation to ablation period across the forest density gradient. These data were compared with local SNOTEL site data at Independence Camp (2127 m), and Independence Creek (1962 m). Snow pits were excavated to measure density, stratigraphy, and monitor the snowpack. Snow depth transects followed the east-west SWE transect but had higher spatial resolution (8 m) and included a south-north transect to measure snow depth through the open meadow. Snow depth measurements were acquired with a 240 cm snow avalanche probe.

During the ablation period snow depth was measured with all spectral snow albedo measurements. The purpose of these measurements was to track when the snowpack became optically thin for snow albedo measurements. Each station (S1-S5) was equipped with a Campbell Scientific® SR-50A-L snow depth sensor that monitored snow depth through the entire field season at each station at a 1-minute temporal resolution.

2.3 Results

The results presented in the following section are based on the field measurements that highlight the spatiotemporal variability of snow albedo across a forest density gradient during the accumulation and ablation periods of the 2019 snow season. To better characterize snow albedo across the forest density gradient, measurements are grouped into the following categories: Open (7 sites), Forest Edge (6 sites), and Forest (5 sites). Spatial and temporal variability of snow albedo values are determined from standard deviations. In total 303 spectral albedo and spectrally integrated observations and 47 broadband albedo observations were used in the analysis of the results. The results characterize snow albedo across the

forest density gradient and illustrate the effect that forest litter and light absorbing particles have on snow albedo.

2.3.1 Statistical Analysis of Data Sets

Kruskal-Wallis rank sum test applied to all data sets show statistically significant difference when evaluating p-values and chi-squared distributions during both the accumulation and ablation periods Table 2.2 reports the results of the test and shows that during the accumulation and ablation period p-values and chi-squared values all indicate the sampling populations are from different distributions.

Pairwise comparisons using Dunn's test can be seen in Table 2.3. Results show that all the data sets were significantly different during the accumulation period except the broadband albedo data sets between S3-S4 data sets. During the ablation period grain radius data sets between Forest-Forest Edge and Forest Edge-Open are not significantly different. Spectrally integrated albedo between Forest Edge-Open are not significantly different. Broadband albedo between S3-S4 are not significantly different.

Table 2. 2: Kruskal-Wallis rank sum test results for grain radius, spectrally integrated albedo, and broadband albedo data sets during the accumulation and ablation periods

Accumulation Period		
Data set	**P-value**	**Chi-squared**
Grain radius	2.2e-16	98.22
Spectrally integrated albedo	2.2e-16	117.57
Broadband albedo	4.13e-05	20.19
Ablation Period		
Grain radius	1.92e-06	26.33
Spectrally integrated albedo	6.62e-12	51.48
Broadband albedo	1.29e-13	59.36

Table 2. 3: Pairwise comparisons using Dunn's test for grain radius, spectrally integrated albedo, and broadband albedo data sets during the accumulation and ablation periods**.**

Accumulation Period				
Data Set	**Comparison**	**Z-score**	**Adjusted p-value**	**Significance**
Grain radius	Forest - Forest Edge	2.89	1.15e-02	Yes
Grain Radius	Forest - Open	9.65	1.54e-21	Yes
Grain Radius	Forest Edge - Open	5.92	9.38e-09	Yes
Spectrally integrated albedo	Forest – Forest Edge	-5.48	1.25e-07	Yes
Spectrally integrated albedo	Forest - Open	-10.84	6.48e-27	Yes
Spectrally integrated albedo	Forest Edge - Open	-4.29	5.39e-05	Yes
Broadband albedo	S1 – S3	-4.27	5.94e-05	Yes
Broadband albedo	S1 – S4	-3.35	2.39e-03	Yes
Broadband albedo	S3 – S4	0.91	1.0	No
Ablation Period				
Data Set	**Comparison**	**Z-score**	**Adjusted p-value**	**Significance**
Grain radius	Forest – Forest Edge	-2.09	1.09e-01	No
Grain Radius	Forest - Open	-5.13	8.75e-07	Yes
Grain Radius	Forest Edge - Open	-1.89	1.78e-01	No
Spectrally integrated albedo	Forest – Forest Edge	-4.29	5.39e-05	Yes
Spectrally integrated albedo	Forest - Open	-6.96	1.05e-11	Yes
Spectrally integrated albedo	Forest Edge - Open	-1.12	7.92e-01	No
Broadband albedo	S1 – S3	-6.74	4.91e-11	Yes
Broadband albedo	S1 – S4	-6.61	1.18e-10	Yes
Broadband albedo	S3 – S4	0.13	1.0	No

2.3.2 Spectral Snow Albedo

Figure 2.7 shows the measured spectral snow albedo for the three categories of forest density on five dates. Snow albedo decreased through period of observation. At the Open and Forest Edge sites spectral snow albedo decreased through the accumulation and ablation season. However, at the Forest sites spectral snow albedo was more variable, lower, and decreased more rapidly. Snow albedo values at the Open sites were always higher than the Forest sites and Forest Edge sites throughout the period of observation. Forest Edge albedo values were consistently lower than those in the Open sites. The higher observed snow albedo values at the Open sites compared to the Forest site in Figure 2.7 demonstrate that forest litter effectively reduces snow albedo. During all the measurement dates in Figure 2.7, forest litter was observed on the surface snow at all the Forest sites.

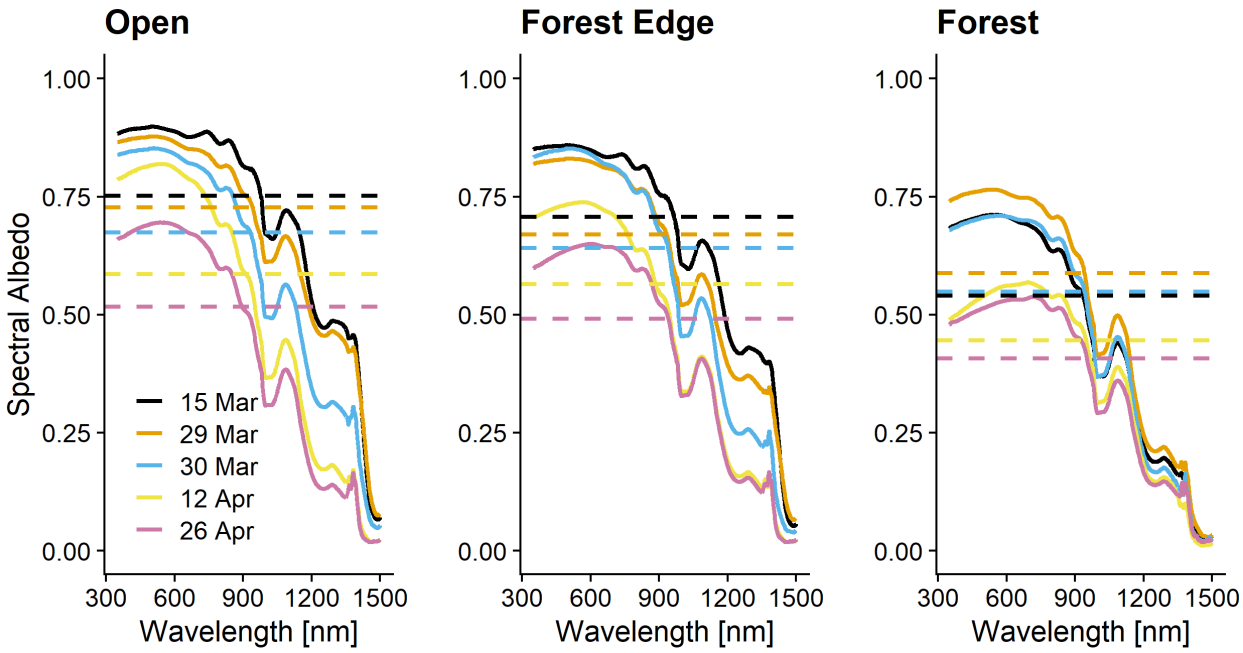

Figure 2. 7: Average spectral snow albedo (solid lines) measured at the Open, Forest Edge, and Forest sites spanning the forest density gradient. Dashed lines represent spectrally integrated albedo (350-1850 nm). All measurements were taken on or near solar noon under diffuse (clear) sky conditions.

2.3.3 Accumulation Period Spectral Snow Albedo

Snow albedo was measured following two snowfall events during the period of observation. On 12 March 2019, snow depth sensors recorded 9 cm of new snow and on 27 March 2019, snow depths sensors recorded 8 cm of new snow. As seen in Figure 2.7, each of these snowfall events refreshed the albedo, though the Forest sites albedo was still lower than in the Open and Forest Edge sites.

Spectral snow albedo was measured on the 15 March 2019 three days after a snowfall event. Measurements from the 15 March 2019 showed high spatial variability across the forest density gradient in both spectrally integrated broadband and visible (VIS) snow albedo. There was a 34% difference in spectral snow albedo between the Open and Forest sites (Open higher). There was a 7% difference between the Open and Forest Edge sites (Open higher). The Open sites had the highest snow albedo values and least spatial variability: 0.76 ± 0.02, VIS 0.89 ± 0.03. The Forest Edge sites had lower snow

albedo values than the Open sites and higher spatial variability: 0.71 ± 0.08, VIS 0.85 ± 0.09. The Forest sites had the lowest observed albedo and the highest spatial variability: 0.54 ± 0.08, VIS 0.70 ± 0.11.

Spectral snow albedo was measured on the 29 March 2019 two days after a snowfall event. Spectral snow albedo values were aligned with the previously discussed snowfall event, this event again showed the spatial differences of snow albedo across the forest density gradient. There was a 21% difference in spectral snow albedo between the Open and Forest sites (Open higher) and a 9% difference between the Open and Forest Edge sites (Open higher). The Open sites had the highest albedo snow values and low spatial variability: 0.73 ± 0.02, VIS 0.87 ± 0.02. The Forest Edge sites had lower snow albedo values and low spatial variability: 0.67 ± 0.02, VIS 0.82 ± 0.02. The Forest sites had the lowest observed snow albedo values and highest spatial variability: 0.59 ± 0.06, VIS 0.76 ± 0.07.

These measurements were made after the final measurable snowfall event of the 2019 field season. During this period the snowpack was near isothermal and ablation was beginning based on field observations. The relatively high snow albedo values in the VIS region for the Open and Forest Edge sites suggest relatively little effect on albedo reduction from impurities at the time. The low spectrally integrated albedo and VIS albedo values at the Forest sites suggest that forest litter and other light absorbing particles were present in the surface snow immediately after snowfall events.

Table 2.4 provides a summary of mean broadband and VIS albedo values collected during the entire accumulation period of observation. Snow albedo was highest at the Open sites and lowest at the Forest sites. There was a 25% difference in spectral snow albedo (Open higher) indicating that snow albedo in the Forest was being affected by a factor not present in the Open. The Forest Edge sites snow albedo was in between the other two sites. These results imply that open areas of forest have higher snow albedo values, lower spatial variability, and decrease closer to or in the forest (Figure 2.8). The lowest snow albedo values are in the forest. Results of just the VIS albedo values show high spatial variability at Forest sites, and effects of impurities reducing the VIS albedo. There were no measurable snowfall events after March 27 until date of snow disappearance.

Table 2. 4: Summary of mean spectral integrated albedo (350-1850 nm) and visible albedo (400-700 nm) during the entire observed accumulation period (March 2019). Standard deviations are in parentheses.

Location	Albedo (broadband)	VIS albedo
Forest	0.56 (± 0.07)	0.72 (± 0.09)
Forest Edge	0.66 (± 0.05)	0.83 (± 0.05)
Open	0.72 (± 0.05)	0.87 (± 0.04)

2.3.4 Ablation Period Spectral Snow Albedo

Here I present results for spectral albedo measurements collected during month of April. There were no measurable snowfall events during this time, therefore this is referred to as the ablation period. Following this time our sampling sites were no longer valid due to patchy snow cover and excessive forest litter at some sites, obscuring the snow surface.

On 12 April 2019, following 16 days of no snowfall, the snow albedo had decreased at all three sites (Figure 2.7). Figure 2.8 shows differences in spectrally integrated albedo for the three categories and the spatial variability within each category. Open sites had low spatial variability: 0.60 ± 0.02, VIS 0.81 ± 0.03. The Forest Edge sites had greater spatial variability: 0.55 ± 0.04, VIS 0.73 ± 0.05. The Forest sites had the highest spatial variability and the lowest snow albedo values: 0.43 ± .05, VIS 0.54 ± 0.06. There was a 34% difference in snow albedo values when comparing the Open and Forest sites.

On 26 April 2019, following 30 days of no snowfall snow albedo had further decreased at the Open and Forest Edge sites, but remained similar at the Forest site through the ablation period. The Open sites had low spatial variability: 0.52 ± 0.02, VIS 0.68 ± 0.03. The Forest Edge sites had similar albedo to the Open: 0.50 ± 0.02, VIS 0.64 ± 0.04. The Forest sites albedo resembled measurements from 12 April: 0.42 ± .04, VIS 0.52 ± 0.06. Following 26 days of ablation, the Open and Forest Edge sites snow albedo decreased but the Forest sites snow albedo remained relatively constant.

Table 2.5 provides a summary of changes of spectrally integrated broadband and VIS snow albedo values for each of the three categories through the ablation period. During the ablation period broadband and VIS snow albedo decreased differently at all sites. Spatial variability was consistent between all sites. There was little change from both measurement periods in snow albedo values at the Forest sites indicating a minimum snow albedo threshold being reached through the ablation period until snow disappearance date. The Open and Forest Edge sites snow albedo continued to decline from 12-26 April. Changes in the VIS albedo at both the Open and Forest Edge sites indicate as the snow melted impurities and grain size throughout the snowpack began to increase and further reduce albedo. The large snow albedo changes throughout the ablation period at the Open and Forest Edge sites, and lack of changes at the Forest sites indicate differences in temporal snow albedo change across the forest density gradient.

Table 2. 5: Summary of mean spectral integrated albedo (350-1850 nm) and visible albedo (400-700 nm) during the observed ablation period (April 2019). Standard deviations are in parentheses.

Location	Albedo (broadband)	VIS albedo
Forest	0.43 (± 0.05)	0.53 (± 0.07)
Forest Edge	0.52 (± 0.04)	0.67 (± 0.06)
Open	0.54 (± 0.04)	0.71 (± 0.06)

2.3.5 Spatial Variability Snow Albedo Summary

During the snow accumulation period observed spatial differences in snow albedo were lower for the Open and Forest Edge categories, but there was a greater spatial variability in the Forest category (Figure 2.8). The Forest category displayed much lower albedo through both accumulation (0.56 ± 0.07) and ablation periods of observation (0.43 ± 0.05). The Forest category had albedo values during the accumulation period that represented the Open and Forest Edge category during their ablation period. Table 2.6 shows albedo values decreased at relatively similar rates at all the sites from the observed

accumulation through the observed ablation periods; snow albedo value decreases (25% at the Open, 21% Forest Edge, and 25% Forest).

Table 2. 6: Summary of mean spectrally integrated snow albedo values during the observed Accumulation period (15 March, 29 March, 30 March, WY 2019) and observed Ablation period (12 April, 26 April, WY 2019).

Site	Accumulation				Ablation			
	Mean	Min.	Max.	Std. Dev.	Mean	Min.	Max.	Std Dev.
Forest	0.56	0.40	0.65	0.07	0.42	0.53	0.35	0.05
Forest Edge	0.66	0.57	0.78	0.05	0.52	0.47	0.61	0.04
Open	0.72	0.62	0.78	0.05	0.54	0.49	0.64	0.04

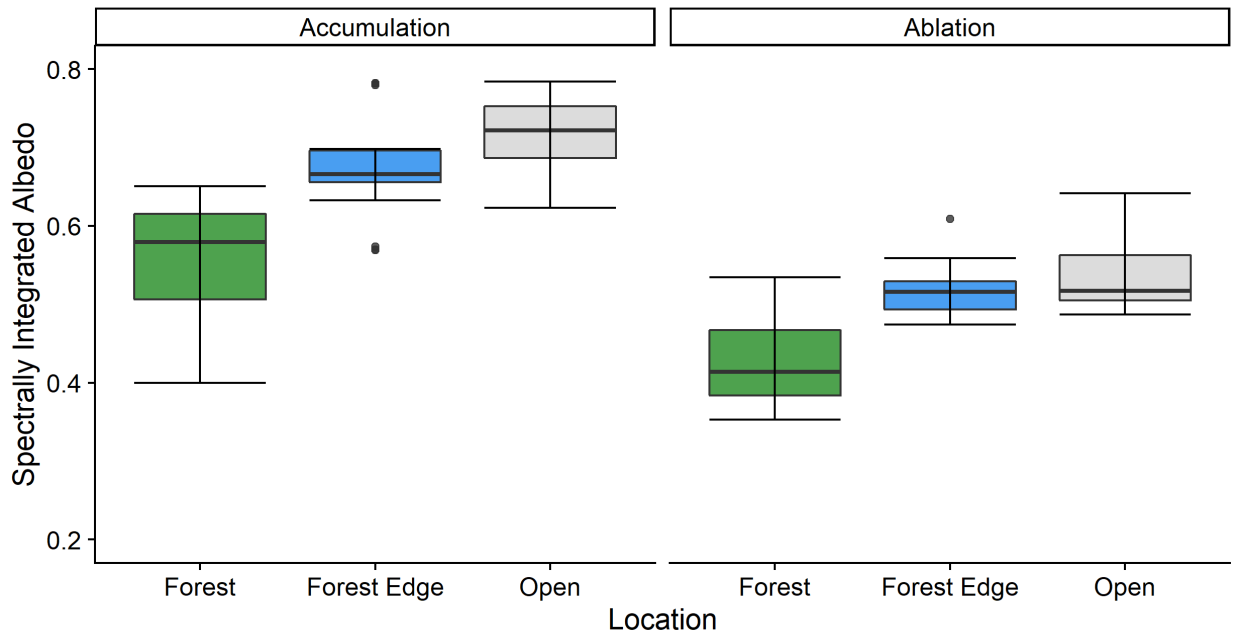

Figure 2. 8: Mean spectrally integrated broadband albedo (350-1850 nm) during the accumulation and ablation period.

2.3.6 Net Radiometer Broadband Snow Albedo Temporal and Spatial Variability

Results of broadband snow albedo temporal variability and incoming shortwave radiation from three CNR4 pyranometers located at S1, S3, and S4 (Figure 2.2) are presented from 22 March 2019 until snow disappearance date at each station. Figure 2.9 shows temporal decreases in broadband albedo through the period of observation for the CNR4 instruments. S3 (Open) and S4 (Forest Edge) stations show nearly identical broadband albedo values and they were consistently higher than those in the Forest.

Over the snow accumulation period of observation, mean broadband albedo values at S3 (0.71 ± 0.04) are nearly identical to the spectrally integrated values from the Open sites (0.72 ± 0.05). At S4 (Forest Edge), mean broadband albedo values (0.71 ± 0.07) are consistent to the spectrally integrated values from the Forest Edge sites (0.66 ± 0.07). At S1 (Forest), mean broadband albedo values (0.45 ± 0.06) are lower than the spectrally integrated values from the Forest sites (0.56 ± 0.07). These CNR4 measurements at S1 (Forest) might be affected by the dense forest surrounding the station and within the FOV thereby leading to lower albedo.

Over the snow ablation period of observation, mean broadband albedo values at S3 (Open) (0.62 ± 0.05) are higher than the spectrally integrated values from the Open sites (0.54 ± 0.04). At S4 (Forest Edge), mean broadband albedo values are similar to S3 (Open) (0.61 ± 0.05) and are higher than the spectrally integrated values from the Forest Edge sites (0.52 ± 0.04). At S1 (Forest), mean broadband albedo values (0.37 ± 0.03) are the lowest and are lower than the spectrally integrated values from the Forest sites (0.43 ± 0.05).

Our results show that during the ablation period of observation the CNR4 broadband albedo values do not agree well with spectrally integrated albedo values that cover a larger spatial extent. This result implies an issue of spatial representation. The stations (S3, S4) are measuring more reflective snow and missing the forest litter effect on snow albedo that S1 (Forest) station picks up. During the ablation period of observation broadband snow albedo at all three sites declined over time. Mean albedo values from accumulation to ablation changed relatively uniform at all three sites consistent with the observed changes

found from the spectral measurements. Broadband snow albedo values changed by 18% at S1 (Forest), 13% at S3 (Open), and 14% at S4 (Forest Edge).

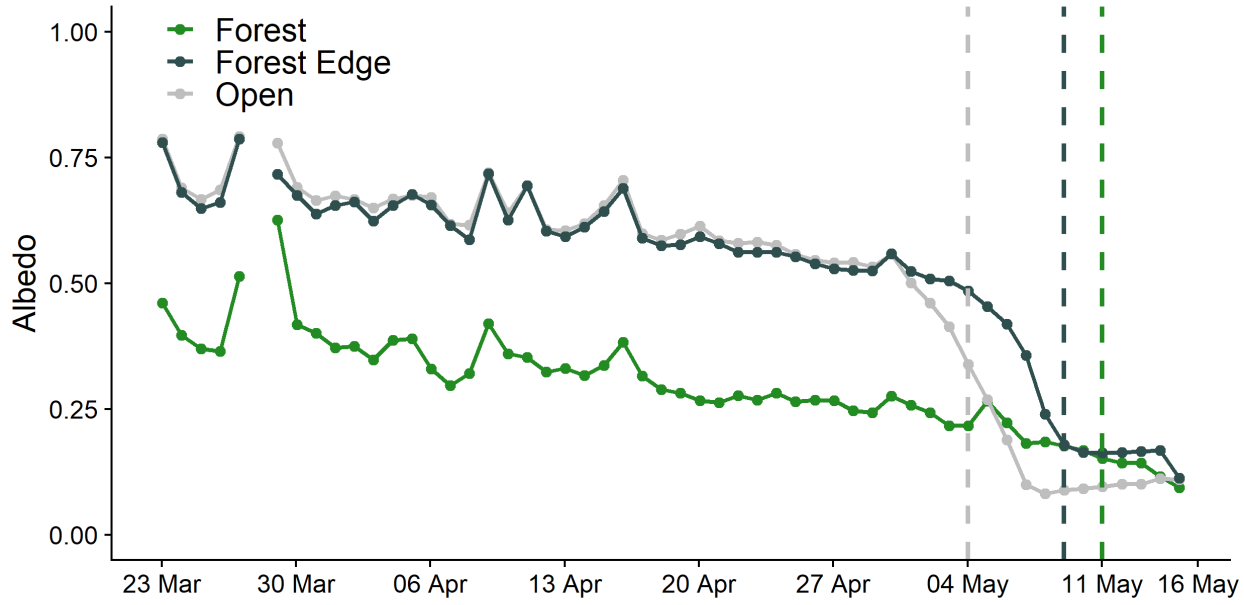

Figure 2. 9: Temporal changes to broadband snow albedo at Forest (S1), Forest Edge (S4), Open (S3). Dashed vertical lines indicate snow disappearance date and missing data was due to a 27 March snow event that obstructed the measurements.

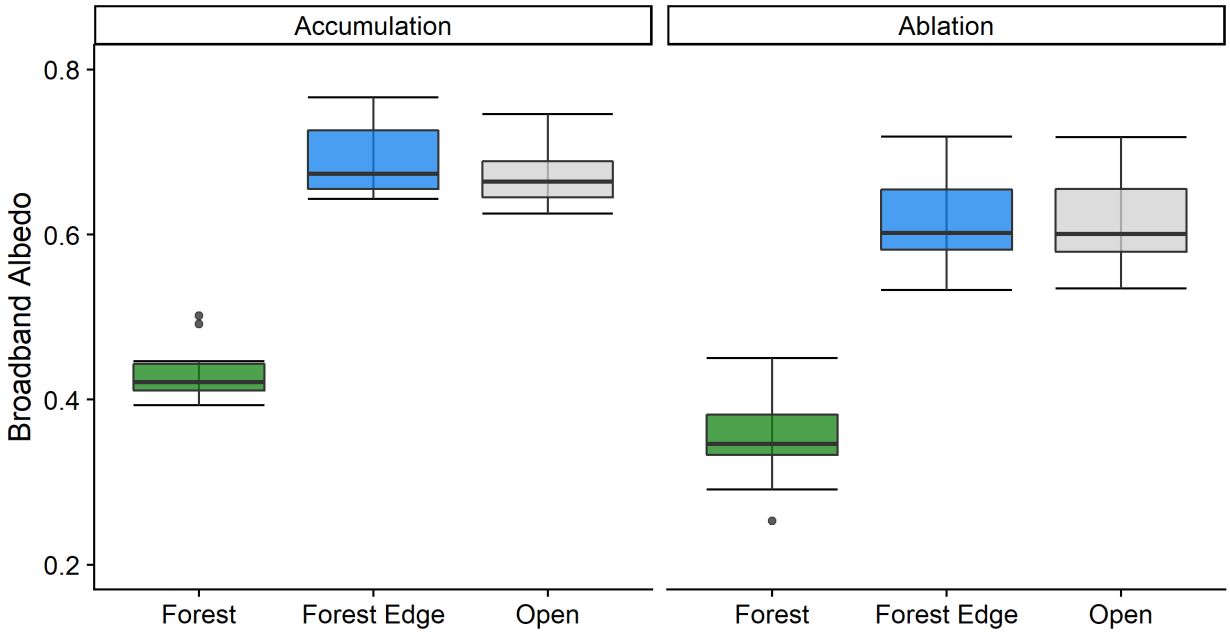

Figure 2. 10: Differences in broadband albedo for each of the stations during the accumulation and ablation periods.

2.3.7 Snow Albedo and Distance from Forest Stand Relationship

A linear model was created to evaluate the relationship between the spectrally integrated snow albedo measurements (n=303) and distance from nearest tree stand. Spectrally integrated snow albedo was the dependent variable and distance from nearest tree stand was the independent variable. Results were split into the accumulation and ablation periods and tree stands were classified as >= 3 m in height. Figure 2.11 shows the relationship that spectrally integrated snow albedo increases, as distance from nearest tree stand increases. Statistics generated from the linear models in Table 2.7 show that during both accumulation and ablation periods a statistically significant relationship exists between both variables. The relationship implies that higher snow albedo values are found further from the forest. These findings support our results from the averaged snow albedo values from the three different forest density gradient categories.

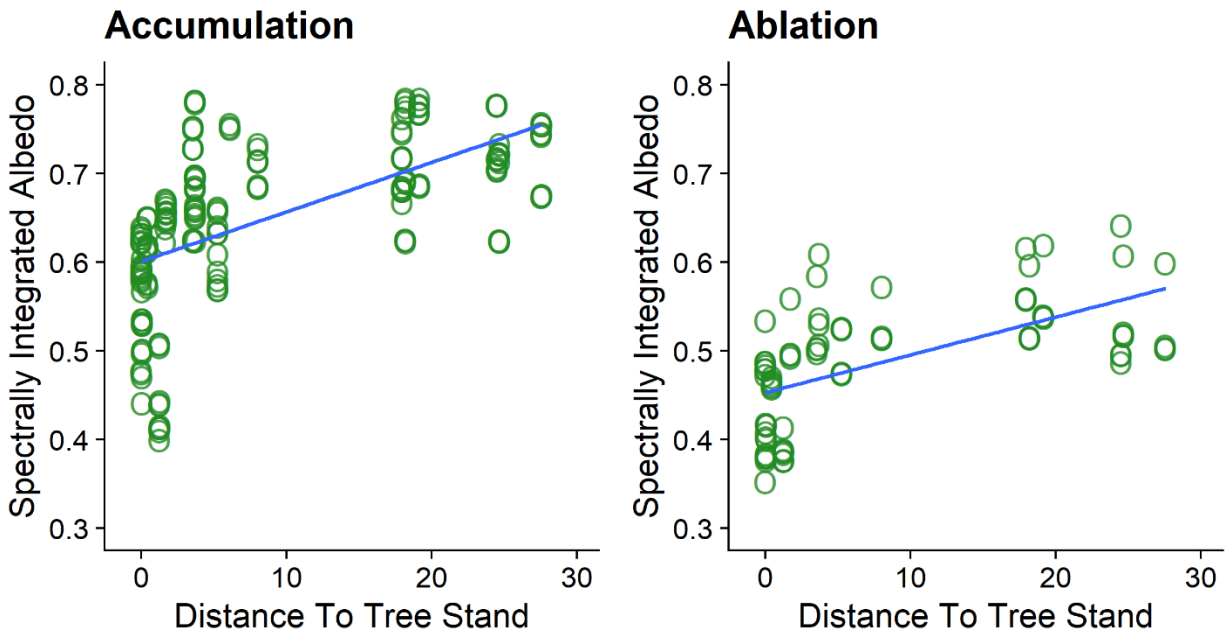

Figure 2. 11: Relationship between distance from nearest tree stand and spectrally integrated snow albedo.

Table 2. 7: Statistics generated from spectrally integrated albedo versus distance to tree stand linear model.

Period	**R^2**	**P-value**
Accumulation	0.34	P < 0.00001
Ablation	0.35	P < 0.00001

2.3.8 Snow Albedo and Percent Canopy Cover Relationship

A linear model was created to evaluate the relationship between spectrally integrated snow albedo measurements (n=303) and percent canopy cover derived from the LiDAR data during both the accumulation and ablation periods. Figure 2.12 shows the relationship that spectrally integrated snow albedo increases with decreasing canopy cover. A strong and statistically significant relationship can be seen in Table 2.8. Statistical results were created from the linear model and are separated for both the accumulation and ablation periods. These results support the point-based broadband albedo values and

averaged spectrally integrated snow albedo values from the three different forest density gradient categories. The Forest station and Forest sites that have the greatest canopy cover, have the lowest snow albedo values.

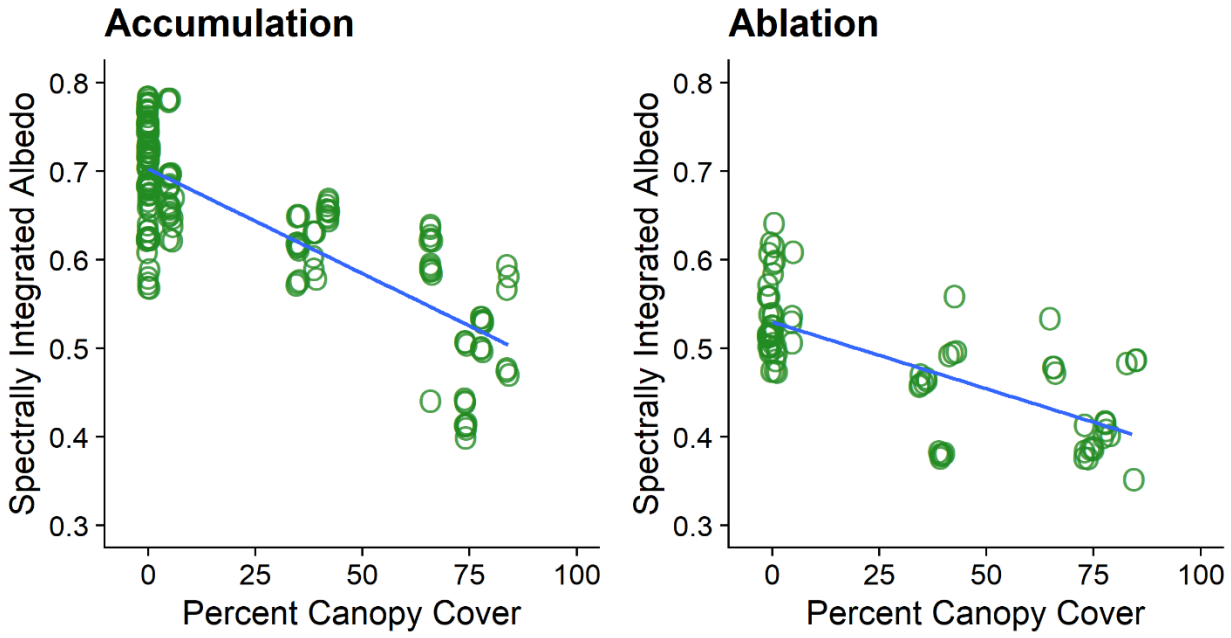

Figure 2. 12: Relationship between percent canopy cover and spectrally integrated snow albedo.

Table 2. 8: Statistics generated from spectrally integrated albedo versus percent canopy cover linear model.

Period	**R^2**	**P-value**
Accumulation	0.62	P < 0.00001
Ablation	0.49	P < 0.00001

2.3.9 Estimated Effective Snow Grain Radius

Effective grain radius values were estimated from spectral albedo measurements and showed responses to snow events, dry periods, and the ablation season. Following two snow accumulation events mean grain radius at the Open sites (297 ± 43), Forest Edge sites (469 ± 178), and Forest sites (1271 ± 273). The Forest Edge and Forest sites had high spatial variability based on standard deviations compared to the Open sites. Fresh snow has a grain radius between 100-500 μm and rapidly ages upon deposition (>500 μm) due to metamorphism. These measurements were made several days following new snowfall events, so metamorphism had begun. Estimated snow grain radius at the Forest sites following two accumulation events indicated a difference in estimated size of snow grains than the observations from both the Open and Forest Edge sites where snow grains were much smaller and resembled fresh snow following the observed events.

Figure 2.13 shows during ablation period of observation effective snow grain radius was relatively similar at all sites. Estimated mean grain radius at the Open sites displayed the highest spatial variability based on standard deviation (1820 ± 292). The Forest Edge sites grain radius increased over the ablation period in size and variability (1637 ± 200). The Forest sites decreased in spatial variability and did not change significantly from the accumulation to ablation period (1445 ± 190). Estimated snow grain radius increased at the sites through the period of observation.

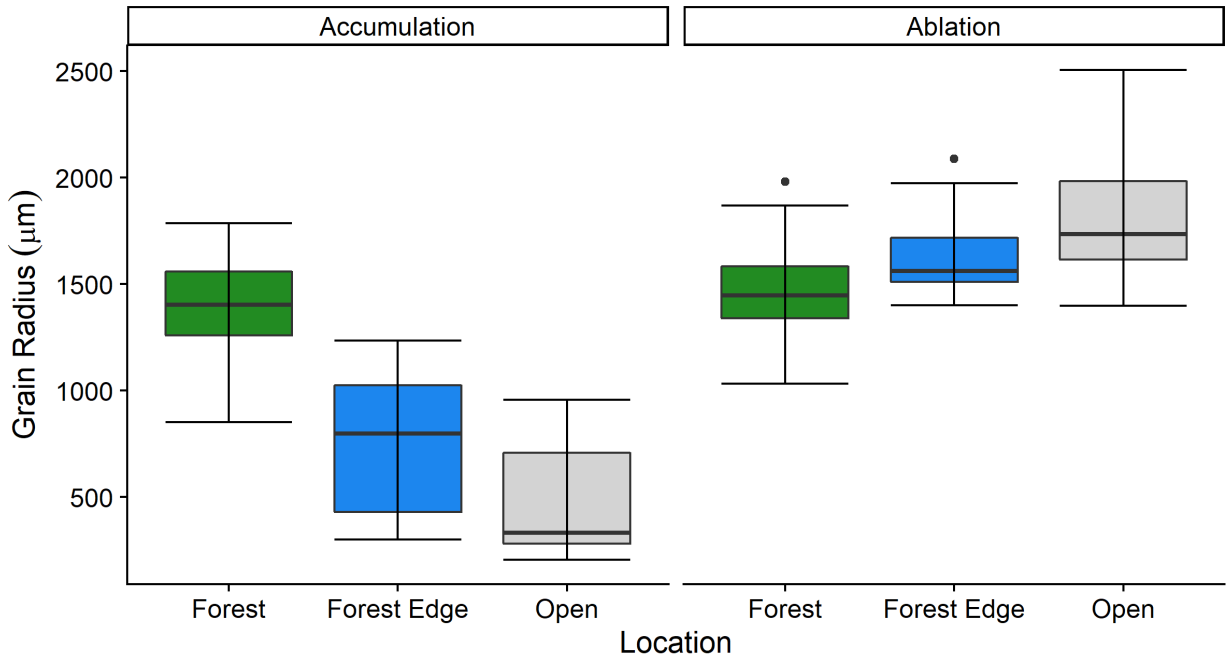

Figure 2. 13: Estimated snow grain radius (µm) during the accumulation and ablation periods showing distribution and density.

2.3.10 Forest Litter

The results from the field collected snow samples illustrate the spatial and temporal differences of forest litter across the forest density gradient. Mass fractions of forest litter across the forest density gradient show large differences when comparing Open sites to Forest sites (Figure 2.14). Forest litter was present in the snowpack at the Forest and Forest Edge sites throughout the accumulation and increased during the ablation period. Our results show that forest litter is most present in the forest and decreases towards the open forest areas. These results are based on the range of measurements from surface and shallow sub-surface pit samples.

Forest litter was most concentrated below the canopy in parts of the forest, at the edges of the forest, with little concentration at the Open sites. I observed in the field and in the lab analysis of snow samples that there is a large difference in the composition and size of forest litter and light absorbing particles that depends on the sampling location. Larger debris composed of needles, bark, small branches, wax and sap

are present at the Forest sites, while the open sites composition resembles dust and fine particles. Figure 2.15 shows the forest litter and light absorbing particles that were collected on several filters.

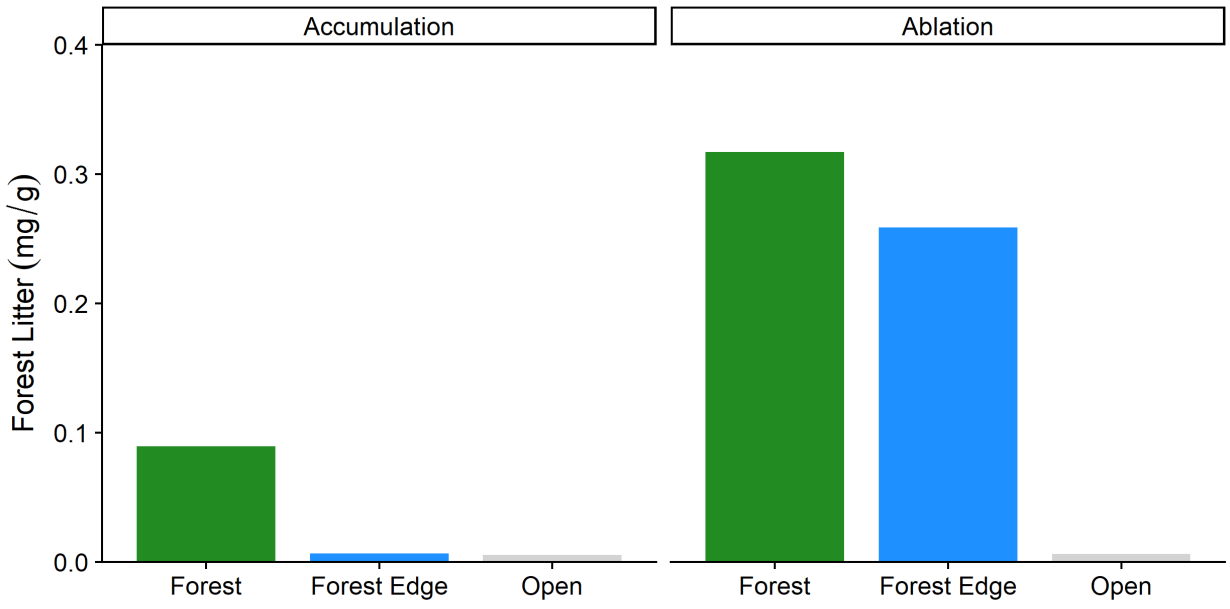

Figure 2. 14: Mean forest litter concentrations from surface and shallow sub-surface snow samples during the accumulation and ablation periods.

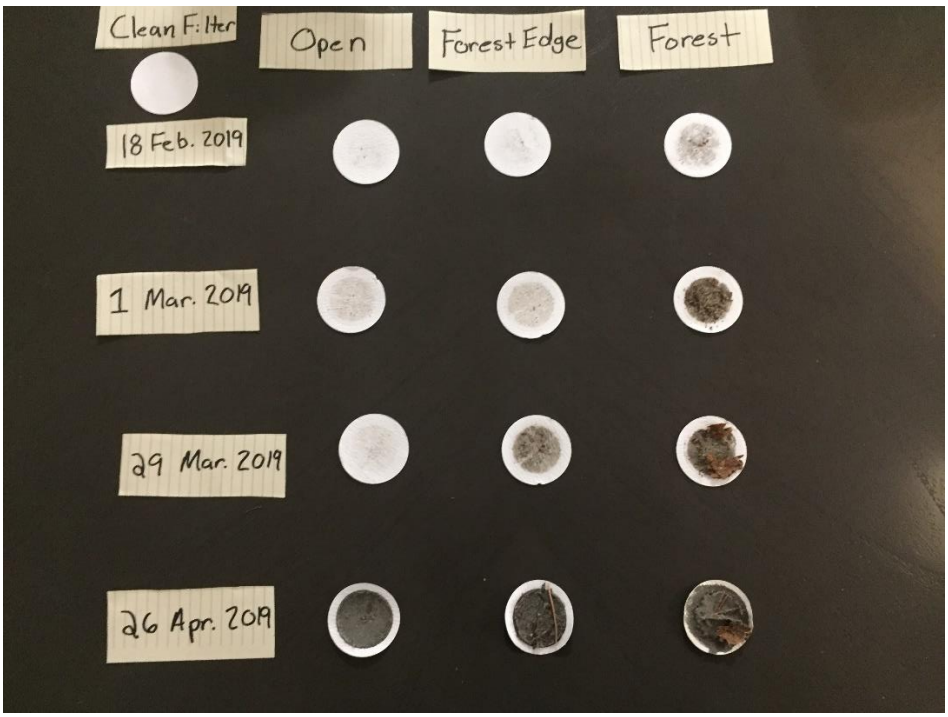

Figure 2. 15: Forest litter samples from the forest density gradient with associated dates of collect. A clean-blank white filter illustrates clean versus dirty filters. These samples are from surface collected snow.

2.3.11 Laboratory Determinations of Black Carbon Concentrations

Our laboratory analysis of snow samples indicate that black carbon was present in all samples and that the concentrations show spatial and temporal differences across the forest density gradient. Figure 2.16 shows the concentrations of black carbon per site during accumulation and ablation periods. During the accumulation period, mean black carbon concentrations very similar between all sites and approximately 5-10 ng/g. However, as the snowpack began melting, black carbon effectively increased in concentration across all sampling sites. At the Forest and Forest Edge sites mean black carbon concentration increased from 5 ng/g to over 30 ng/g from the accumulation to the ablation period, respectively. Black carbon concentrations doubled at the Open sites from the accumulation period through the ablation period but was consistently lower than at the Forest and Forest Edge sites. These results are based on the range of measurements from surface and shallow sub surface pit samples.

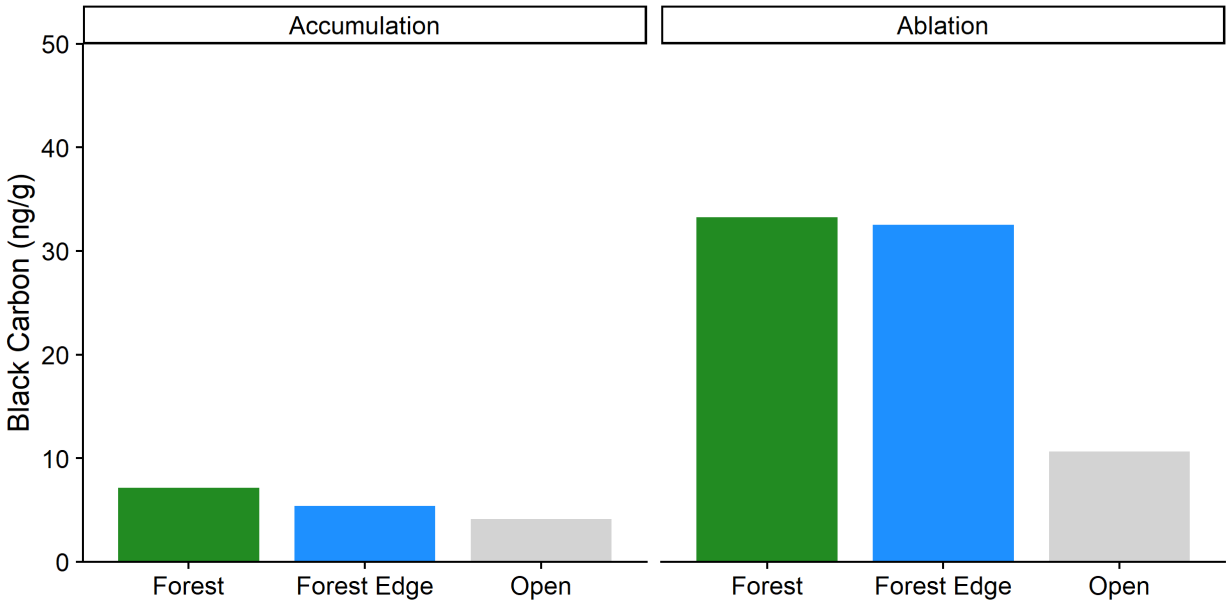

Figure 2. 16: Mean black carbon concentration from surface and shallow sub-surface snow samples during the accumulation and ablation period.

2.3.12 Spectral Albedo Measurements and Snow Impurities

Results from the analysis of snow samples were compared with in-situ spectral albedo measurements to evaluate the effects of forest litter and light absorbing particles on snow albedo. Figure 2.17 shows the inverse linear trend between spectrally integrated snow albedo and forest litter concentrations (n=25). As forest litter increases in concentration in the snow, snow albedo declines. Figure 2.18 shows a weak correlation and inverse relationship between spectrally integrated snow albedo and black carbon concentrations (n=22).

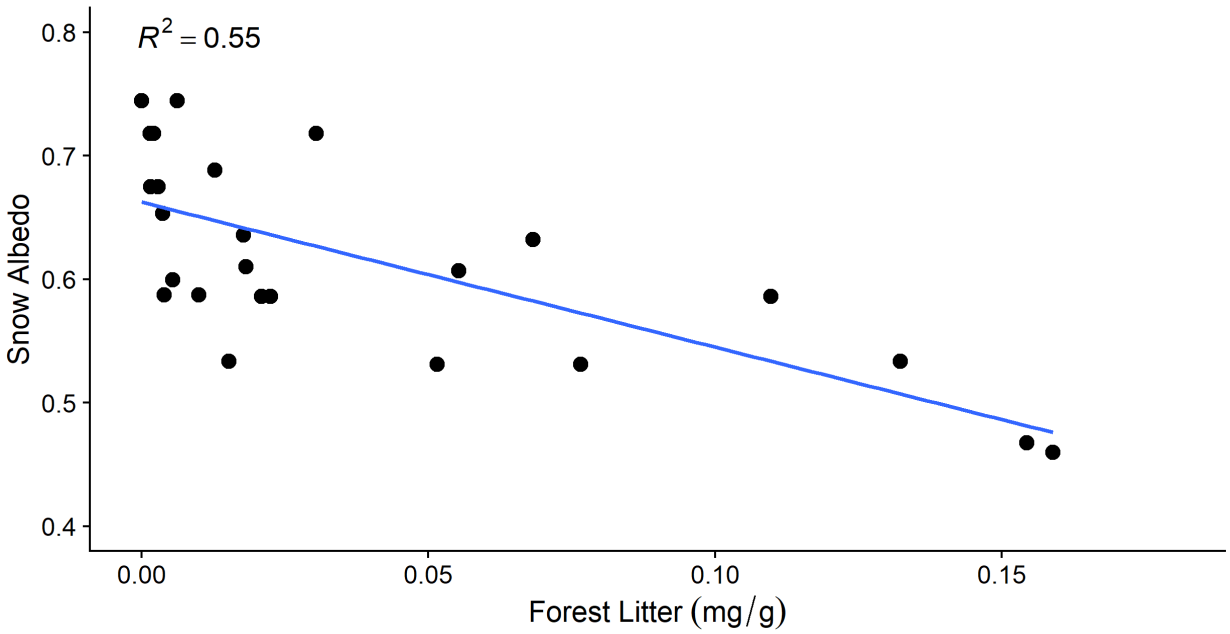

Figure 2. 17: Relationship between in-situ measured spectrally integrated snow albedo and forest litter concentrations.

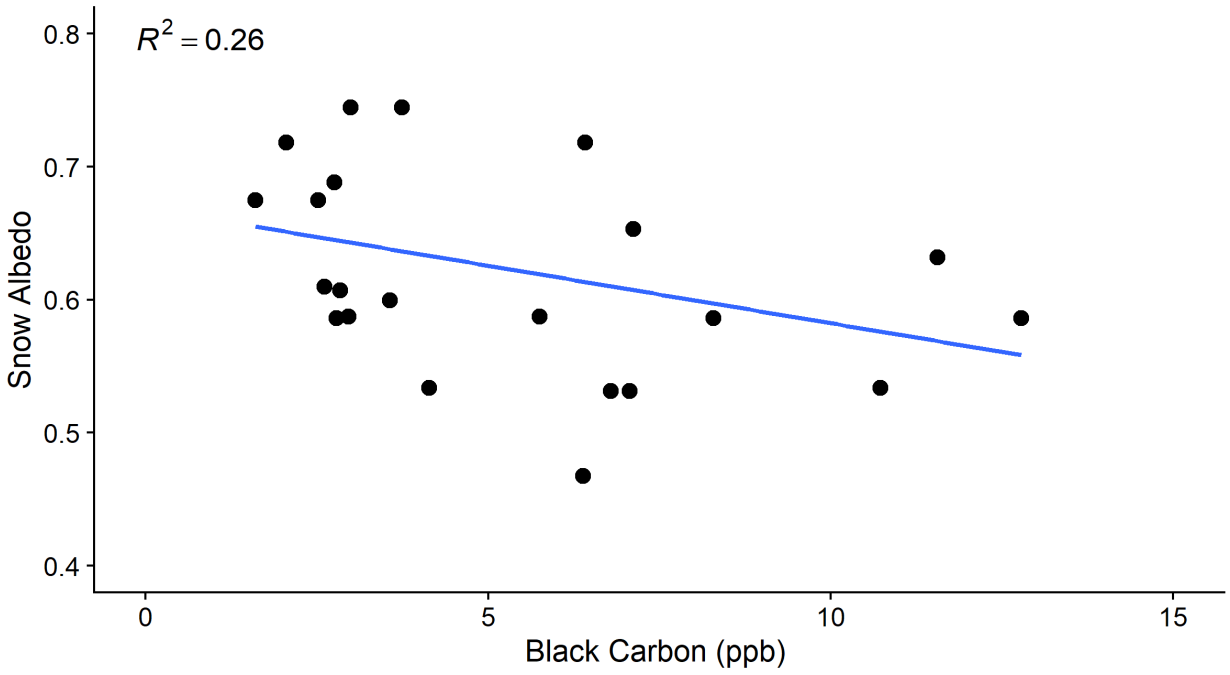

Figure 2. 18: Relationship between in-situ measured spectrally integrated snow albedo and black carbon concentrations.

2.3.13 Spectral Reflectance of Forest Litter

Results presented here are reflectance factor measurements of the forest litter material plus any exposed portion of the white filter. Reflectance factor measurements of a clean, white filter was approximately 0.96 (not shown). Reflectance factor measurements of forest litter + white filter from the Open and Forest Edge sites had high values (>0.8) and at the Forest sites were lower (<0.58) during the accumulation period. Results from Open sites show consistently higher reflectance factor values, mainly due to exposed white filter background. Measured reflectance factors for cleaner snow show a correspondence with concentrations of forest litter in the snow samples.

Snow is more contaminated closer to the Forest during the accumulation and ablation period and reflectance of forest litter decreases through the period of observation at the Forest and Forest Edge sites (Figure 2.19). During the ablation period spectral reflectance values of forest litter + white filter at the Open site decreased while. at the Forest and Forest Edge sites values decreased to a similar value (<0.35). The filters from the Forest and Forest Edge sites during the later ablation period were completely covered by forest litter and there was less of a discernible effect of the white filter on the measured spectral reflectance factor. Thus, it is assumed that these measurements represent the spectral reflectance of forest litter.

Visual inspection of the filtered materials showed a range of concentrations of forest litter and fine particulates (Figure 2.15). In the Open sites, the filters were contaminated with fine particulates. In the Forest and Forest Edge sites the filters were contaminated with bark, needles, cones, and other unidentified fine particulates. Sizes of the forest litter materials on the filters ranged from millimeters to several centimeters. During field sampling, it was noted even larger pieces of debris such as tree branches and large cones, which were not collected.

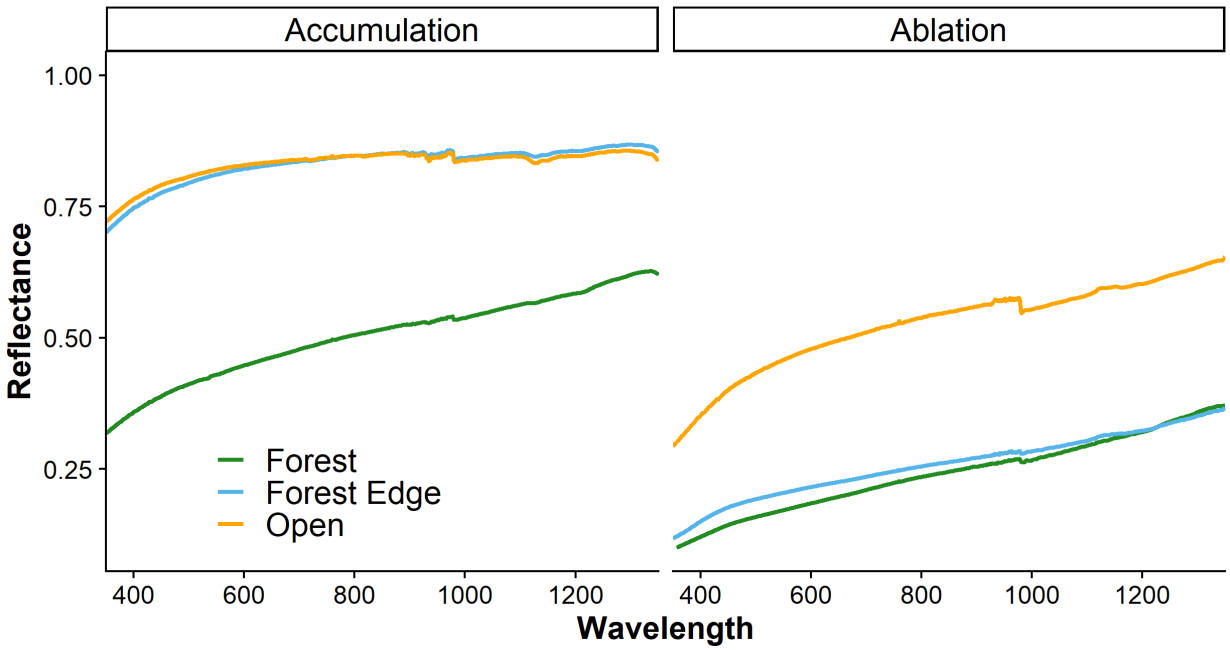

Figure 2. 19: Mean spectral reflectance factors during the period of observation.

2.3.14 SNICAR Model Versus Spectral Albedo Measurements

Snow albedo was modeled using the Snow, Ice, and Aerosol Radiation Model (SNICAR). Black carbon concentrations from the snow samples collected during the accumulation and ablation periods and field collected data were used as input parameters, no assumptions were made. The results of SNICAR (n=16) corresponded with in-situ spectral snow albedo measurements that were collected at the exact site snow was sampled for black carbon concentration. The results (Figure 2.20) show that at all sites the modeled observations do not agree well with the field measurements. P-value for the linear model was < 0.005 and R^2 was reported at 0.79. As the in-situ measured albedo values decrease, the SNICAR model overestimates snow albedo, which is expected because SNICAR cannot account for the effects of forest litter on snow albedo.

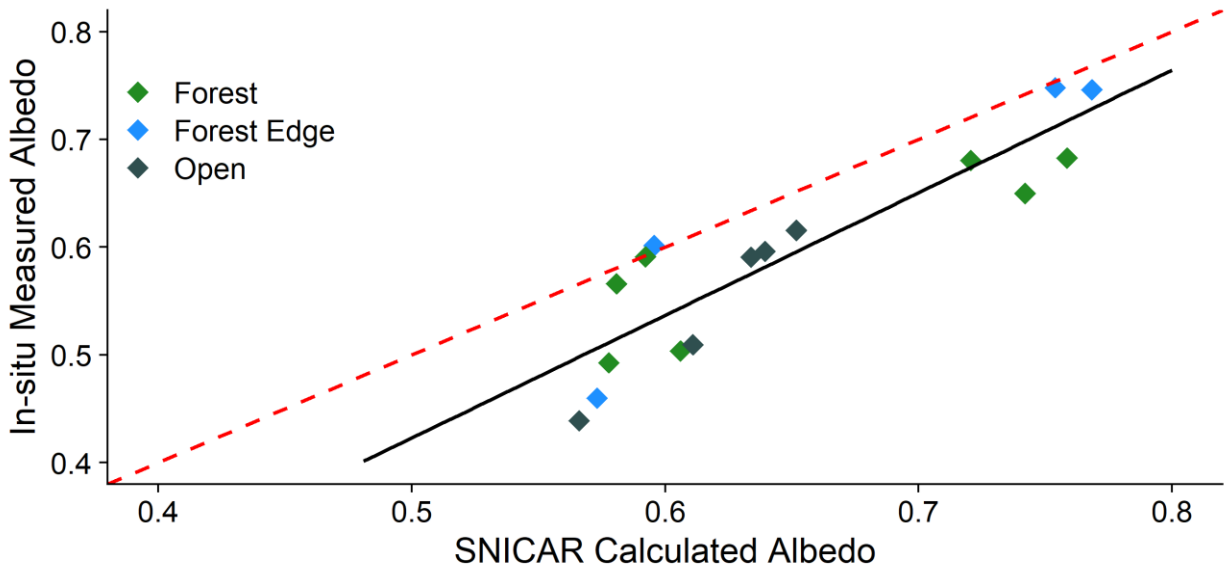

Figure 2. 20: In-situ measured snow albedo versus SNICAR calculated snow results, in-situ measurements were made with a field spectrometer and snow samples were taken immediately after for further processing of black carbon content. Dashed red line indicate 1:1 line and black line indicate linear regression line.

2.4 Error assessment

2.4.1 CNR4 Albedo

The Kipp and Zonen CNR4 net radiometers have a pair of pyranometers (upward and downward) that have an expected daily accuracy of ± 10% the daily reported values and < 5% uncertainty in daily totals. The pyranometer has an upward facing detector field of view (FOV) measures 180˚, the lower facing detector FOV measures 150˚ to prevent illumination at low zenith angles.

Previous studies (e.g. Gleason et al., 2013) have shown sub-canopy use of pyranometers can introduce bias to pyranometer measurements. Shading and sun-speckle can influence incoming solar radiation. Reflections from vegetation can also affect measured radiation at the A significant source of error in the net radiation measurements is due to precipitation. During and after snowfall events, the upward pointing

instruments were blocked by snow. Precipitation events were monitored in order to clear off the upward-pointing pyranometers. I noted these events and omitted data that may have been affected.

2.4.2 Spectrometer

The Spectral Evolution RS-3500 Spectroradiometer measured snow albedo with a 180-degree FOV diffuser. Use of the diffuser in forest areas may have error introduced to the measurement due to vegetation interference in the FOV during a measurement. Human operator interference and error in the measurements can exist in several ways. Operator interference in the FOV can occur, an extension pole was used to mitigate this issue. A non-level measurement could be taken if the operator does not correctly use the bubble level. Atmospheric conditions can rapidly change especially if clouds are present in the sky and moving, even if they are not blocking the sun.

2.4.3 Snow Sample Collection

Snow samples were subject to minor error introductions via sampling technique which greatly depended on snow conditions. Ideally, within the sampling area about 2-3 cm of snow would be removed from the surface plot of 1m x 0.5m x 3 cm. Due to snow metamorphism, differences in snow density, sampling conditions based on the day (frozen/melting snow surfaces); error in sample collection could be introduced. Large concentrations of forest litter could introduce error in the amount of snow sampled, especially in the ablation season when litter was highly concentrated at the forest sites. During sampling at the forest during the ablation period very large pieces of debris (e.g. tree branches, bark, cones) were not collected because filter analysis could not separate them.

2.4.4 Snow Sample Analysis

Analysis of snow samples at the DRI ice core laboratory were carried out over consecutive days. Processing of snow samples involves melting the snow to liquid water and sonicating the entire sample to evenly mix the sample. Once sonicated a smaller liquid sample is removed for black carbon and dust analysis, this sample may not fully represent the impurity load present. Impurities in the sample can stick

to the sampling bags, thus introducing an under-biased representation of the actual impurity load. Black carbon measurements processed via the SP2 method have a 5% measurement error (Gleason et al., 2019).

2.5 Discussion

2.5.1 Snow Albedo and Forest Litter

Our measurements and snow sample analyses show that snow albedo decreases with increasing forest density, that this decrease is a function of forest litter concentration, that Forest snow albedo was consistently lower than elsewhere during both accumulation and ablation periods. These results are consistent with Winkler et al., (2010). They measured large concentrations of forest litter below a coniferous forest stand, while in an adjacent clear-cut forest, no forest litter concentrations were found. There results also found the lowest measured snow albedo values corresponded with the greatest concentrations of forest litter.

Our measurements of spectral snow albedo during the accumulation period and following snowfall events were similar to Gleason et al., (2013, 2016) for the Open and Forest Edge sites compared to their unburned forest sites, however our spectral albedo values at the denser Forest sites were much lower through the study suggesting the impact of forest litter on snow albedo being greater. These results suggest that forest structure and composition in different regions can create snow albedo variability.

Visible snow albedo of new snow is well above 0.80 and between 0.5-0.6 for older and dirty snow (Lek & Ramaswamy, 1983). During the accumulation period the Open and Forest Edge sites visible snow albedo values resembled clean and fresh snow, but the Forest sites visible albedo values indicated impurities reducing visible albedo. Visible albedo reductions of soot (black carbon) contaminated snow have been well documented (Warren & Wiscombe, 1980), however studies have quantified visible snow albedo effected by forest litter. Our results suggest that forest litter effectively reduces visible snow albedo, but future work needs to extract the full effect.

Estimated snow grain radius at the Open and Forest Edge sites following snowfall events are consistent with the literature of fresh snow and small grain radius (Wiscombe & Warren, 1982). However, at the Forest sites following snowfall events estimated snow grain radius resembled old dirty snow. It is unclear what caused large grain sizes at the Forest sites during the accumulation period. The variability discovered in snow grain radius estimates during the accumulation period shows the importance of collecting spectral snow albedo and estimated snow grain size measurements. These measurements allow snow albedo to be broken down into separate regions (e.g. visible, near-infrared). The effects of visible snow albedo reductions caused from impurities or near-infrared albedo reductions caused from snow grain radius can be determined.

Through the ablation period forest litter concentrated at the surface of the snowpack to a maximum until the snow melted completely at the Forest and Forest Edge sites. Forest litter is too large to scavenge via snowmelt processes unlike black carbon which Delaney et al., (2015) hypothesize large snowmelt events can remove small particles (black carbon and dust). During the ablation period forest litter increases as snowpack layers consolidate and snow grain radius grows from aging snow, these combined effects greatly reduce snow albedo during peak snow melt timing and intensity. Which suggests measuring snow albedo and forest litter during the ablation period is most important.

Spectral reflectance factor measurements of filters and forest litter show that greater concentrations of forest litter mean increased absorption of shortwave radiation, thus reduced snow albedo. Gleason et al., (2013) measured spectral reflectance factors of charred woody debris and forest litter from ablation period snow samples and suggest that greater concentrations of darker debris have greater radiative impact on snowmelt. This study was unable separate the full effect of forest litter on snow albedo, however I suspect that forest litter effects on snow vary in other forest regions because of differences in forest litter distribution and composition.

2.5.2 Black Carbon

Laboratory analysis of black carbon always showed higher concentrations at the Forest Edge and Forest sites, that increased in concentration during the ablation period. The greater concentrations of black carbon in and near the forest may point to black carbon being collected and redistributed by the forest. Black carbon may collect in tree branches from wind events and dry deposition and sloughed off the canopy to the snow surface from precipitation. Black carbon concentrations increased at all sites during the ablation period from surface and sub-surface samples which indicates that concentrations increase as snow melts and sublimates from beneath the surface. Sterle et al., (2013) noted that surface black carbon concentration was retained through the ablation period at a higher elevation site in the Central California Sierra Nevada until a snowmelt flush event decreased concentrations later in the ablation period.

The SNICAR model does not incorporate the effect of forest litter on snow albedo, therefore our model results overpredicted snow albedo where forest litter was greater. This finding is similar to Gleason et al. (2019), who notes SNICAR includes fine-grained (black carbon and dust) impurities but misses larger debris (e.g. charred wood, charcoal) that reduce snow albedo. Based on these findings future work requires a greater sampling size of snow contaminated with forest litter and in-situ spectral albedo measurements. Development of a model that incorporates forest litter effects on snow albedo is needed to fully understand the albedo reduction effect from forest litter.

2.5.3 Conclusion

These results focus on snow albedo variability in a mixed temperate-coniferous forest in the California Sierra Nevada and may be used to better characterize snow albedo in land surface models in this region. In different forest regions and snow climates snow albedo may be affected by other factors that need better understood. Our in-situ measurements of snow albedo across a forest density transect show that spatiotemporal variability exists across small spatial scales. Results indicate denser areas of forest have reduced snow albedo and open areas of forest have higher snow albedo. Snow albedo reductions across the forest density gradient are driven by forest litter concentration. Distance from a forest tree stand and

percent canopy cover have a clear relationship on snow albedo values. Future work incorporating forest structure metrics and snow albedo measurements can provide forest empirical relationships between forest density and snow albedo. Forest litter and snow albedo are most important to measure during the snowmelt period when both effects are greatest. Further research is needed to separate the full effect of forest litter on snow albedo. Although this study was unable to create snow albedo decay rates future work with a larger data set will generate albedo decay functions dependent on forest density.

3 Snow Albedo and its Role in the Energy Budget of a Forest Snowpack

3.1 Introduction

The snowpack energy budget determines the timing and rate of snowmelt and is important to account for when modeling snowmelt across large spatial scales. Net radiation, the sum of net shortwave and net longwave radiation, is the dominant component of the snowpack energy budget and is important to accurately quantify when calculating the energy budget components. Snow albedo varies across a forest density gradient but the relative importance of albedo to net shortwave radiation is unclear. While its know that forest litter decreases snow albedo, it is not known the extent to which this influences net shortwave radiation and total energy budget of a forest snowpack. The objective of this component of the research is to quantify and understand the role of forest snow albedo in the total snowpack energy balance. Specifically, I ask the following set of questions: What are the effects of forest cover on the snowpack energy budget components across a forest density gradient? What is the role of snow albedo on the energy budget of a forest? Across a forest density gradient, where is snow albedo most important for the energy budget?

3.2 Methods

Snow albedo data from the previous chapter was used as a starting point for the research in this chapter. Meteorological data from selected stations: S1 (Forest), S3 (Open) and S4 (Forest Edge) to compute the snowpack energy budget. Data from only these three stations was used because these sites had net

radiometer measurements. Snowpack properties were measured to track changes through accumulation and ablation periods. LiDAR data were used to describe the forest structure at each of the three sites.

3.2.1 Description of Forest Characteristics at the Meteorological Stations

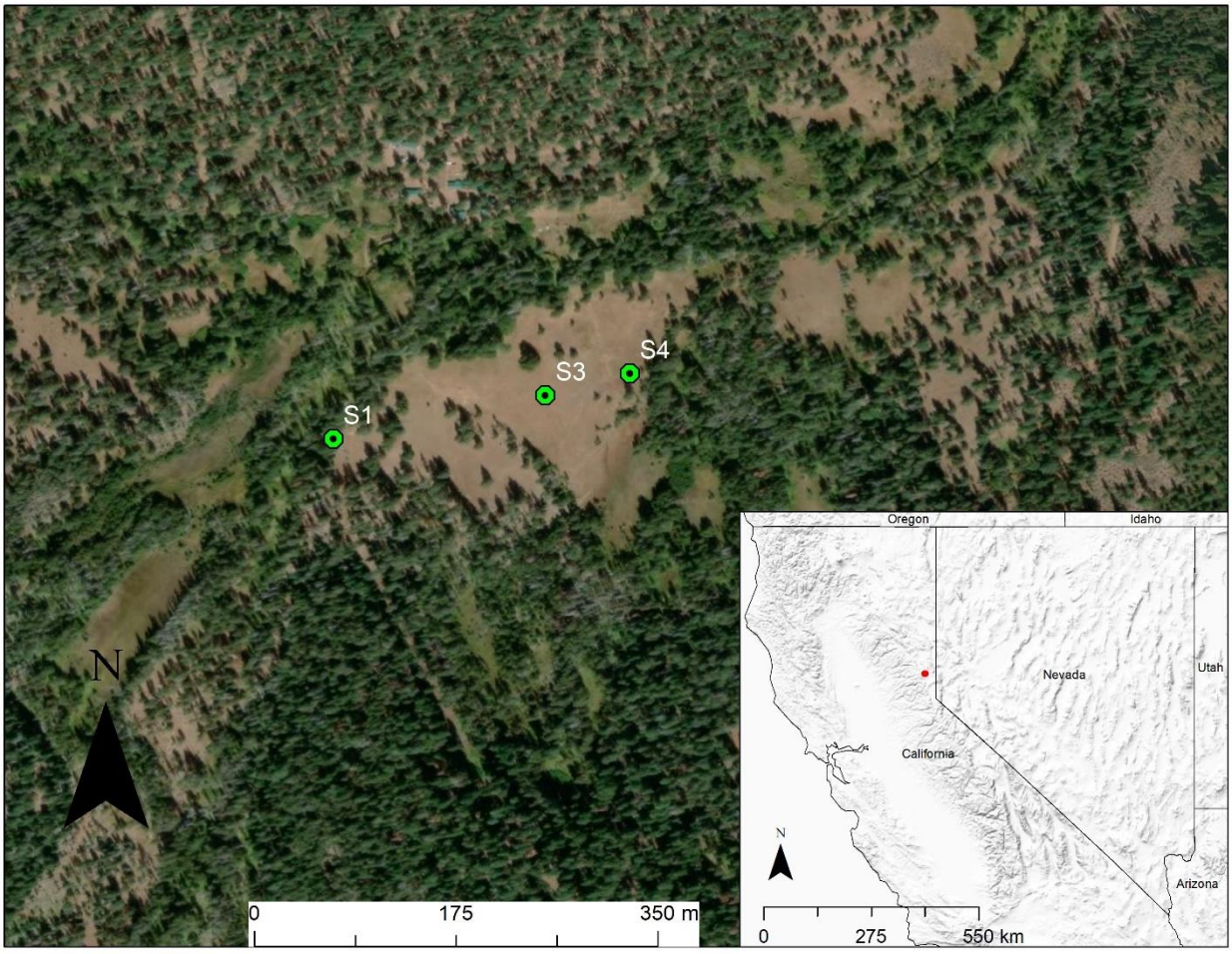

Figure 3. 1: Map of Sagehen Field Site meteorological stations.

Figure 3. 2: Photographs of S3 (Open), S4 (Forest Edge), and S1 (Forest).

Forest and vegetation characteristics at the meteorological stations were documented. S1 is dominated by both mature and young lodgepole pine (*p. contorta* subsp. *Murrayana*), with sparse White fir (*A. concolor)* and Red fir (*A. magnifica)*. The ground cover is composed of Currant (*Ribes*) and assorted Sedge species (*C. exerta)*. S3 has no tree stands and is centered in a large open meadow, dominant ground cpver vegetation is Sedge (*C. exerta*), Jeffrey shooting-star *(D. jeffreyi), and* Bolanders clover *(T. bolanderi)*. There are no canopy influences at S3, and it is exposed to the dominant westerly wind pattern. S4 is surrounded by both mature and young lodgepole pine (*p. contorta* subsp. *Murrayana*), with Sedge (*C. exerta),* Greenleaf manzanita *(A. patula),* Jeffrey shooting-star *(D. jeffreyi),* Bolanders clover *(T. bolanderi)* as the dominant ground cover that is shared with S3 and S4.

Table 3. 1: Summary of forest stand type, ground cover vegetation type, and LiDAR derived canopy cover and tree stand height metrics at each station.

Station	Forest Stand Type	Ground cover Vegetation Type	Canopy cover (%)				Stand height (m)			
			Mean	Min.	Max.	Std. Dev.	Mean	Min.	Max.	Std. Dev.

S1 (Forest)	Lodgepole pine -*P. contorta* subsp. *Murrayana*	Currant – (*Ribes)*	84	56	100	15	18	15	21	2
S3 (Open)	None	Nebraska sedge – (*C. nebraskensis)*	None				None			
S4 (Forest Edge)	Lodgepole pine – *(P. contorta* subsp. *Murrayana)*	Nebraska sedge – (*C. nebraskensis)*	5	0	40	13	1	0	4	1

3.2.2 Meteorological Station Instrumentation

The stations were all equipped with IRGASons, thermohygrometers, Apogee IR radiometers, SR-50 snow depth sensors, upward facing Li-Cor pyranometers, soil moisture/ temperature sensors, temperature probes, and data loggers. Three of the stations: S1, S3, and S4, were equipped in mid-March 2019 with CNR-4 net radiometers (Figure 3.1, Figure 3.2). The stations recorded data at one-minute intervals of meteorological conditions and snow depth. See Table 2 for full documentation of the instrumentation on each station.

Table 3. 2: Summary of Met station instrumentation and nominal accuracy.

Instrument	Measurement	Variable measured	Accuracy
Campbell Scientific® IRGASon Infrared Gas Analyzer + Sonic Anemometer	CO_2, H_2O, Wind vectors	Wind speed (u, m s^{-1}) Wind direction (0-360˚)	2% Std. Dev Calibration Res.
Campbell Scientific® CSAT3 Sonic Anemometer + EC150	CO_2, H_2O, Wind vectors	Wind speed (u, m s^{-1}) Wind direction (0-360˚)	±0.7˚ at 1 m s^{-1} (horizontal wind) 2% Std. Dev Calibration Res.
Vaisala HMP 155	Air temperature	($T_{air,}$ ˚C)	± 0.12˚C
Thermohygrometers	Relative humidity	(RH, %)	±1% RH
Apogee SI-111 Infrared Radiometer	Snow skin temperature	($T_{s,}$ ˚C)	± 0.2˚C
Kipp & Zonen CNR-4 net radiometer	Pyranometer	($K_{in,}$ W m^{-2}), (K_{out} , W m^{-2})	< 5% uncertainty
	Pyrgeometer	($L_{in,}$ W m^{-2}), ($L_{out,}$ W m^{-2})	< 10% uncertainty
Campbell Scientific® SR-50	Snow depth	(Hs, cm)	± 1cm
LI-COR Par LI-200R Pyranometer	Incoming direct and diffuse shortwave radiation	($K_{in,}$ W m^{-2})	± 3%

Decagon 5TM	Soil moisture/temperature	($T_{ss,}$ ˚C)	± 1˚C
Campbell Scientific® 107 Temperature Probe	Temperature at the snow-ground interface	(T_{sb}, ˚C)	± 0.2 ˚C

3.2.3 Snow Skin Temperature

Snow surface temperature ("skin" temperature) is a critical measurement in calculating the energy budget of a snowpack. In this study two Apogee SI-111 infrared radiometers were pointed at the surface of the snowpack at S3 and S4, only in water year 2019. In water year 2020 the Apogee SI-111's were deployed at three sites (S1, S2, S3). I used the Apogee SI-111 data from water year 2020 to estimate the skin temperature for S1 for WY 2019. Using a simple linear regression model, I computed values for S1 based on data from water year 2002 using both S1 and S3 (Equation 3. 1). The model had an R^2 of 0.73. I used the slope and intercept of the model results to estimate values for S1 in water year 2019 using S3 values.

$$y = 0.47103x - 0.07568 \quad \text{Eq 3. 1}$$

3.2.4 Energy Balance Calculations

In the following section I define the terms of the energy balance equation and show the measured and calculated parameters. In each section there is an explanation of the measurements, calculations, uncertainties, and key assumptions.

A simple 1-D energy balance equation was used to calculate the point-based energy budget for each station as described in DeWalle & Rango (2008) with slight adjustments:

$$Q_m = R_{net} + H + L_vE + A + G \quad \text{Eq 3. 2}$$

Total energy is represented by Q_m (W m^{-2}), R_{net} is net radiation (W m^{-2}), H is sensible heat flux (W m^{-2}), L_vE is latent heat flux (W m^{-2}), A is the energy from advected mass (e.g. rainfall) (W m^{-2}), and G is ground heat flux (W m^{-2}). Internal snowpack processes were not calculated due to lack of snowpack temperature profile measurements. Net shortwave and longwave radiation were calculated as:

$$R_{net} = (SW_{in} - SW_{out}) + (LW_{in} - LW_{out}) \quad \text{Eq 3. 3}$$

where SW_{in} is incoming shortwave radiation, SW_{out} is outgoing shortwave radiation, L_{in} is incoming longwave and L_{out} is outgoing longwave. The net radiometers recorded minutely averages of incoming and outgoing shortwave and longwave radiation used in the calculation. They had a spectral range of 305-2800 nm (shortwave) and 4500-42000 nm (longwave). To calculate the turbulent fluxes the use of the bulk aerodynamic method corrected for stability was applied with minor assumptions within acceptable error limits (Anderson, 1976; Brutsaert, 1982; Kustas et al., 1994; Marks et al., 1992). Based on bulk aerodynamic theory the sensible heat flux can be calculated from the temperature gradient as Kustas et al., (1994):

$$H = \rho_a \, c_p \, C_h \, u_a \, (T_a - T_s) \qquad \text{Eq 3. 4}$$

the density of air is represented by ρ_a (kg m^{-3}), c_p is the specific heat of air (J kg^{-1} K^{-1}), C_h is the dimensionless bulk transfer coefficient for sensible heat, u_a is wind speed at height z_a (m s^{-1}), T_a is air temperature at height z_a (K), and T_s is air temperature at the snowpack surface (K).

The latent heat flux is driven by vapor pressure gradient above the snow surface and is calculated as the latent heat flux from the bulk aerodynamic equation that follows Kustas et al., (1994):

$$L_v E = (\rho_a \, 0.622 \, L / P_a) \, C_e \, u_a \, (e_a - e_0) \qquad \text{Eq 3. 5}$$

the density of air is represented as ρ_a (kg m^{-3}), L is latent heat of vaporization or sublimation (J kg^{-1}), P_a is total atmospheric pressure (Pa), C_e is bulk transfer coefficient for vapor exchange, u_a is wind speed at height z_a (m s^{-1}), e_a is atmospheric vapor pressure at height z (Pa), and e_0 is vapor pressure at the snowpack surface (Pa). This method requires a correction for atmospheric stability based on the bulk transfer coefficient C_{en} and C_{hn} to correct C_e and C_h, this assumes these variables to be equal. To account for atmospheric stability conditions interacting with the snow surface I used the bulk Richardson number to index through stability conditions:

$$Ri_B = \frac{g \, Z \, (T_{air} - T_{snow})}{0.5 \, (T_{air} + T_{snow}) \, U \, (z)^2} \qquad \text{Eq 3. 6}$$

where g is the acceleration due to gravity, 9.8 m s^{-2}, Z is the height of the measurement above the snow surface (m) (reflects changes in snowpack height through the season) and $U(z)^2$ is wind speed in in m s^{-1} at height z. Positive values of Ri_B indicate stable conditions, negative Ri_B indicate instability:

$$Unstable: \frac{C_e}{C_{en}} = (1 - 16Ri_B)^{0.75}; \quad \text{Eq 3. 8}$$

$$Stable: \frac{C_e}{C_{en}} = (1 - 5Ri_B)^2. \quad \text{Eq 3. 9}$$

Under neutral stability C_{en} and C_{hn} are calculated as:

$$C_{en/hn} = \left[ln\left(\frac{Z}{Z_0}\right)\right]^{-2} \quad \text{Eq 3. 10}$$

where k is von Karman's constant 0.4, Z has been defined, and Z_0 is the surface roughness length, a median value of 0.003 m that spans the average values for a seasonal snowpack was used and has been used in Roth and Nolin (2017). The bulk aerodynamic approach has seen success (Marks et al., 1992), however is difficult to implement at a below-canopy height.

Energy inputs from rainfall are accounted for as

$$R = P_r \rho_w c_w (T_r - T_s) \quad \text{Eq 3. 11}$$

However, during the period of observations no rainfall events occurred. Energy released from the ground into the snowpack is generally assumed at a constant, our stations were equipped with 3 Decagon 5TM soil moisture and temperature sensors at 3 heights. I used the simple equation to calculate ground heat conduction:

$$G = k_g (T_g - T_{sb}) / (z_2 - z_1) \quad \text{Eq 3. 12}$$

which assumes the thermal conductivity of soil k_g (W m $^{-2}$) at a constant based on the soil properties at Sagehen; T_g is soil temperature at depth z_2 (˚C), and T_{sb} is temperature at base of snowpack at depth z_1 (˚C). Based on this simple equation and the sum of the energy budget components I can calculate the total energy of the snowpack.

3.3 Results

The results presented in this section highlight the spatial and temporal differences in the snowpack energy budget along the forest density gradient during the accumulation and ablation periods of the 2019 snow season. In the next subsections I describe the data collected at Open, Forest Edge, and Forest stations and the results from our energy budget calculations. Data collection at our sites started in the last week of January 2019 so there is data during most of the accumulation period. However, the net radiometers were not installed until mid-March, so our full energy budget calculations extend during the end of the accumulation period through the end of the ablation period. Our results show the differences in energy budget components across three sites: Forest, Open, and Forest Edge.

3.3.1 Snow Depth and SWE

The 2019 snow season had above average snow accumulation during the months of January and February and a deep snowpack developed across the study site. April 1st snow-water equivalent at nearby SNOTEL sites were 53 cm Independence Creek (1962 m) and 105 cm at Independence Camp (2127 m). Our study site is situated in the same watershed as both these SNOTEL sites with a mean elevation of 1941 m. There was a measured maximum SWE of 76 cm at the Forest Edge station, 75 cm for the Open station, and at the Forest station 47 cm all on 18 March 2019.

The month of March had minor snow accumulation, warm-sunny weather. Snowmelt began in late March and snow at the tree stations lasted through early May. Snow disappearance date (SDD) varied across the study site (Table 3.3). However, the meadow surrounding the Open station started to develop surface melt gaps by 25 April and SDD occurred on 4 May. SDD at the Forest Edge station occurred on 9 May and at the Forest station, SDD occurred on 11 May. These differences are also reflected in the energy budgets at each station.

Table 3. 3: Snow water equivalent and snow disappearance date from local SNOTEL sites (*) and Sagehen Field Site.

Site	**Peak SWE (cm)**	**Peak SWE Date**	**(SDD) Snow disappearance date**	**Elevation**
Independence Camp*	105 cm	2019-04-01	2019-05-14	2127 m
Independence Creek*	57 cm	2019-03-20	2019-05-05	1962 m
Forest (S1)	57 cm	2019-03-18	2019-05-11	1941 m
Forest Edge (S4)	76 cm	2019-03-18	2019-05-09	1940 m

Open (S3)	75 cm	2019-03-18	2019-05-04	1940 m

3.3.2 Shortwave radiation

Net shortwave radiation increased at the Open and Forest Edge stations through the end of the accumulation period (end of March 2019) until SDD. Figure 3.3 shows the steady increase in net shortwave radiation at the Open and Forest Edge stations, while daily net shortwave radiation at the Forest station remains relatively constant. From the end of accumulation period to snow disappearance date, net shortwave radiation increased by 128 Wm^{-2} at the Open station and 90 Wm^{-2} Forest Edge station. During the same period net shortwave radiation increased by 19 Wm^{-2} at the Forest station. Net shortwave radiation and incident radiation did not significantly increase due to canopy shading at the Forest station. At all the stations, net shortwave radiation and incident radiation was variable based on daily conditions for example stormy or cloudy days (Figure 3.3, Figure 3.4). Daily broadband snow albedo values calculated from the net radiometers were similar for the Open and Forest Edge sites and decreased during the ablation period, albedo was already reduced at the Forest site before the ablation period began and continued to decrease (Figure 3.5). The differences between the stations in net shortwave radiation can be explained by the available shortwave radiation and snow albedo.

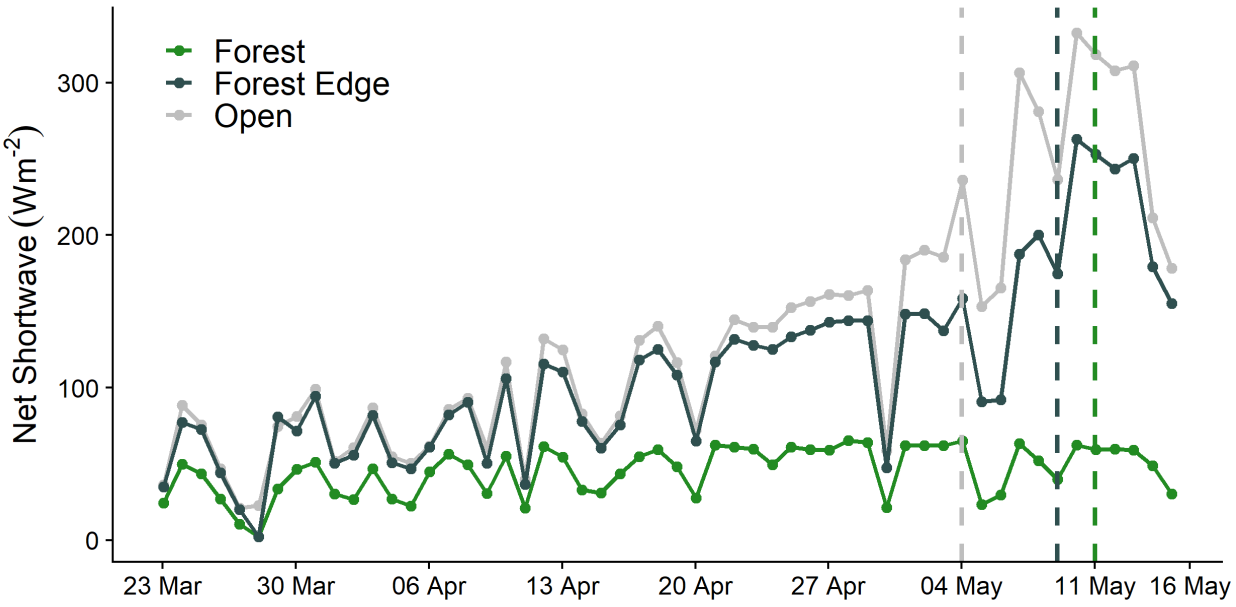

Figure 3. 3: Daily mean net shortwave radiation, vertical dashed lines indicate snow disappearance date.

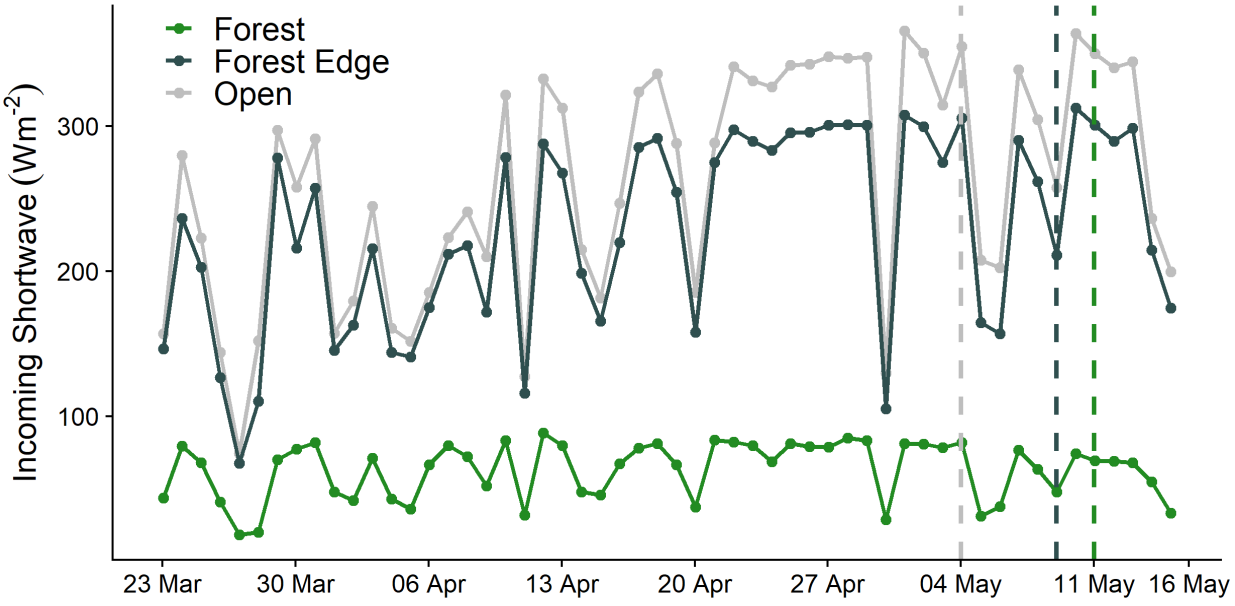

Figure 3. 4: Daily mean incoming incident radiation, vertical dashed lines indicate snow disappearance date.

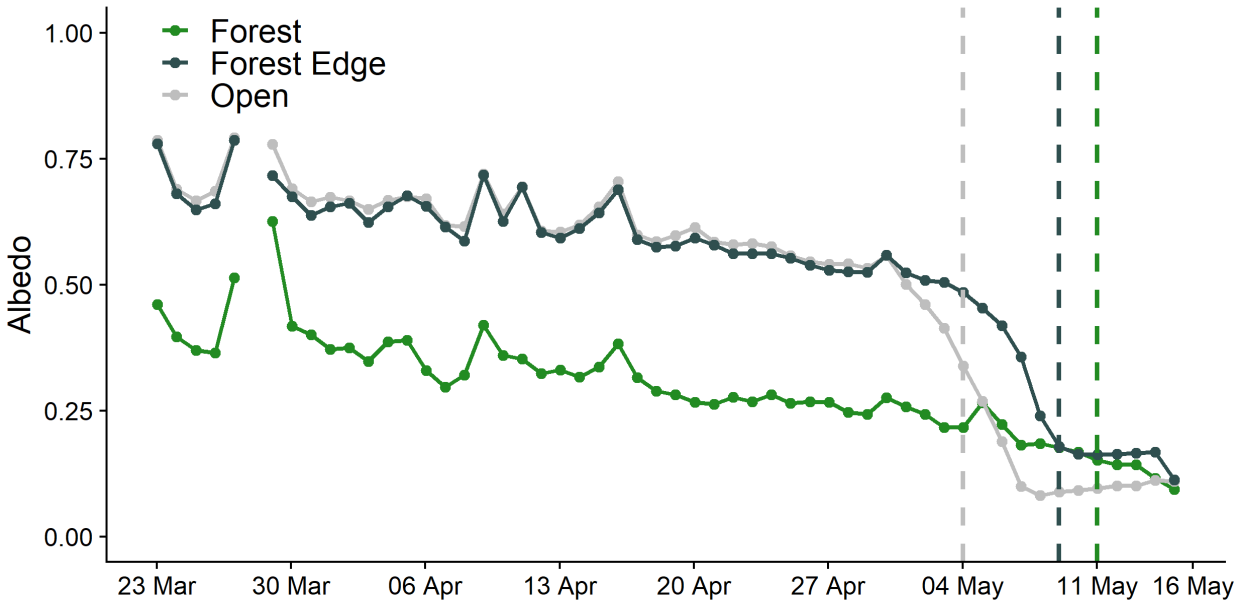

Figure 3. 5: Daily mean snow albedo, vertical dashed vertical lines indicate snow disappearance date per station.

3.3.3 Longwave radiation

The longwave radiation component of the snowpack energy budget was consistently larger in the Forest compared with Forest Edge and Open stations. The Forest station had greater incoming longwave radiation from the surrounding trees (Figure 3.7). For both the Open and Forest Edge stations, the atmosphere is the source of incoming longwave radiation and is only significant during cloudy periods. The Open and Forest Edge sites experienced relatively the same amount of incoming and outgoing longwave radiation (Figure 3.7, Figure 3.8). There was about an 18% difference in incoming longwave radiation greater at the Forest station than the Open station during the period of observation.

Net longwave radiation was negative at the Open and Forest Edge stations throughout the period of observation (Figure 3.6). Net longwave radiation was only slightly negative to slightly positive at the Forest station during the period of observation. During the period of observation, net longwave radiation differed by more than 44 Wm^{-2} between the Forest (-1.1 Wm^{-2}) and Open (-45 Wm^{-2}) stations.

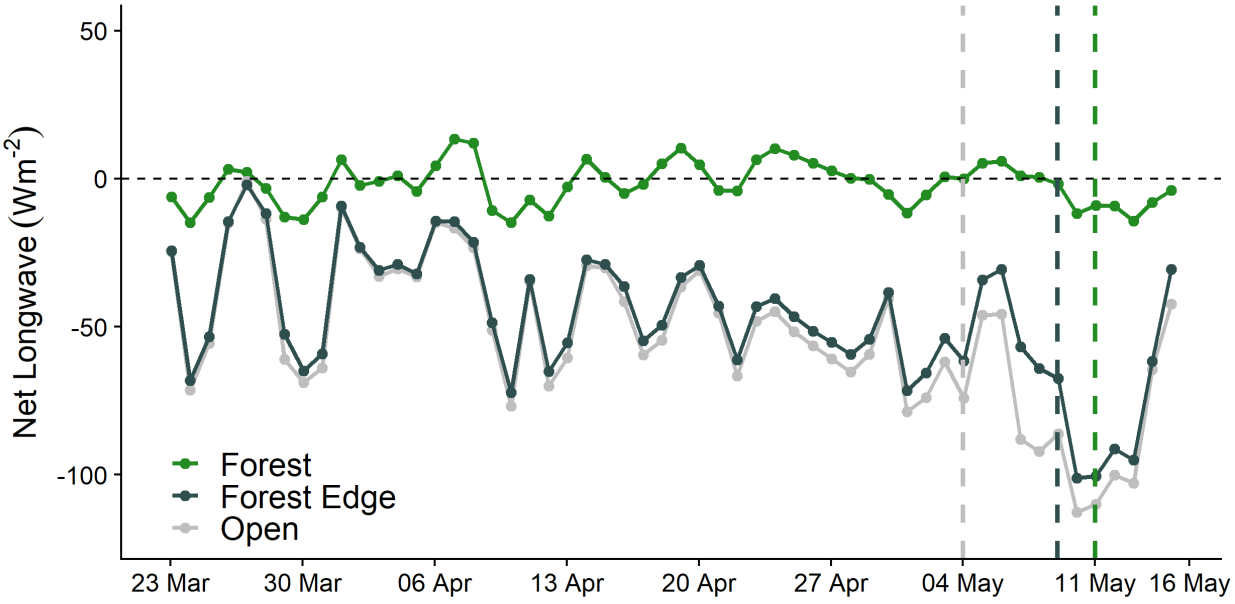

Figure 3. 6: Daily mean longwave radiation, vertical dashed lines indicate snow disappearance date.

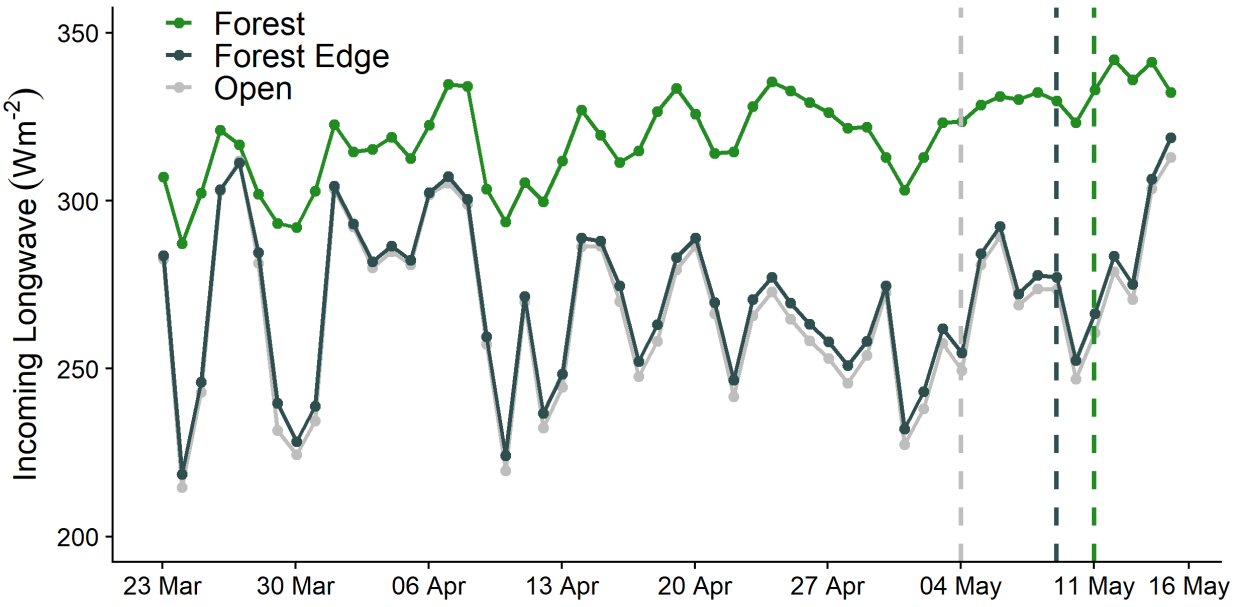

Figure 3. 7: Daily mean incoming longwave radiation, vertical dashed lines indicate snow disappearance date.

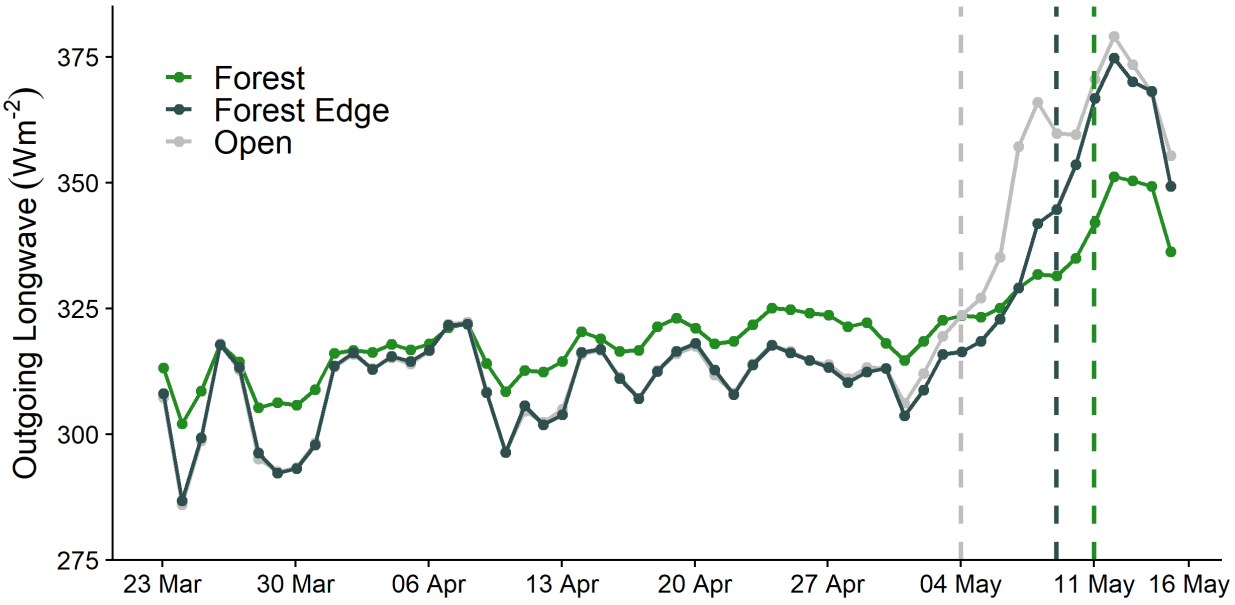

Figure 3. 8: Daily mean outgoing longwave radiation, vertical dashed lines indicate snow disappearance date.

3.3.4 Sensible Heat Fluxes

Figure 3.9 shows that sensible heat flux was consistently positive in direction and the second largest contributing component for snowmelt at all three stations during the period of observation. This was due to a temperature gradient from the warmer overlying air to the colder snow surface (Appendix A, Appendix B). At the Forest station wind speeds were reduced and lead to reduced sensible heat fluxes; roughly half of what was measured at the other two stations. At the Open and Forest Edge stations sensible heat fluxes were greater due to higher wind speeds. After SDD, these stations experienced a shift to negative sensible heat fluxes.

Our results of the observed sensible heat fluxes across the three stations can be explained by measurements of air temperature and snow surface temperature that created temperature gradients of different magnitude. Air temperature was measured at two different heights at each station. The Forest and Open stations both had mean air temperatures of 3.0 ˚C (lower height) and 3.2 ˚C (higher height) through the period of observation. The Forest Edge station had a mean air temperature of 3.4 ˚C (lower height) and 3.5 ˚C (higher height) through the period of observation. The three stations all shared a similar mean elevation of 1941 m which removed differences in elevation as a factor for different air temperatures.

At the Open and Forest Edge stations there were observed large diurnal shifts and greater variability in snow surface temperature (T_s) (Appendix C). The Open station had a mean T_s of -3.2 ˚C and the Forest Edge station had a mean T_s of -2.4 ˚C. The Forest station mean T_s was warmer -1.1˚C. These differences can be explained by forest density, the Forest station is affected by the surrounding trees, vegetation, and above canopy that can heat the sub-canopy greater.

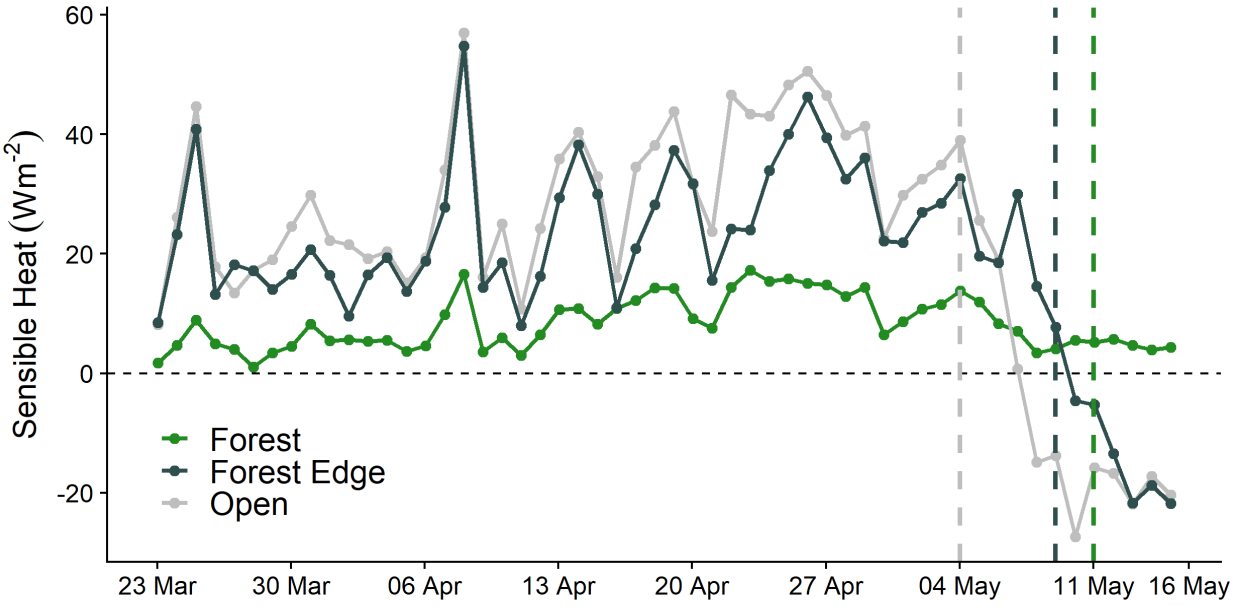

Figure 3. 9: Daily sensible heat flux, vertical dashed lines indicate snow disappearance date.

3.3.5 Latent Heat Fluxes

Figure 3.10 shows that latent heat fluxes were negative in direction and were large a large contributing component for cooling the snowpack at all three stations during the period of observation. Relative humidity at the same two heights as air temperature was measured from at all three stations. Measured relative humidity was similar at all three sites (Appendix C). Saturated air was greater closer to the snow surface and decreased vertically at all three stations across the study period. The air near the snowpack surface was more saturated with water vapor and decreased in saturation vertically above the surface. The vapor pressure gradient from the snowpack surface upwards created a vertical transfer of energy and cooling of the snowpack. During the period of observation daily magnitudes of latent heat fluxes at the Open and Forest Edge stations were roughly triple those measured at the Forest station through the period of observation.

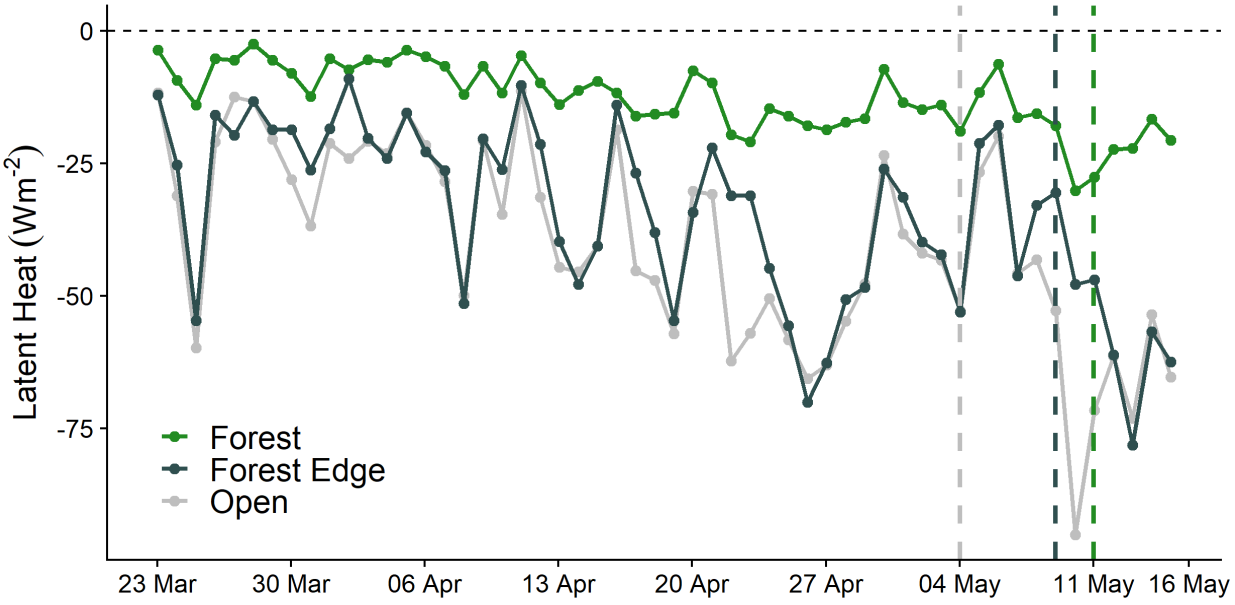

Figure 3. 10: Mean daily latent heat fluxes, vertical dashed lines indicate snow disappearance date.

3.3.6 Turbulent Fluxes Combined

Figure 3.11 shows the total net turbulent energy exchange at all three stations through the period of observation. The turbulent fluxes combined (sensible and latent) largely cancelled in magnitude at all three stations. Latent heat flux was always negative in direction and sensible heat flux was almost always positive. Due to a slightly greater latent heat flux at all three stations, net turbulent energy was slightly negative and contributed to cooling of the snowpack. As the surrounding snowpack around the Open and Forest Edge stations began melting out towards the end of April net turbulent energy flux became more negative.

Our results showed the observed differences both turbulent fluxes across the three stations can be explained by measurements of wind speed (Figure 3.12). At the Forest station, wind speed rarely exceeded 1 m s^{-1} and average wind speed was 0.5 m s^{-1}. Downwind of the Forest station; the Open and Forest Edge stations received greater average wind speeds. The Open station had an average wind speed of 1.4 m s^{-1} and the Forest Edge station had an average wind speed of 1.2 m s^{-1}. These stations experienced similar wind conditions because they both lack barriers that dampen turbulence from forest

stands or forest edge effects (the Forest Edge station is an upwind edge). Therefore, wind travels directly to both sites uninterrupted.

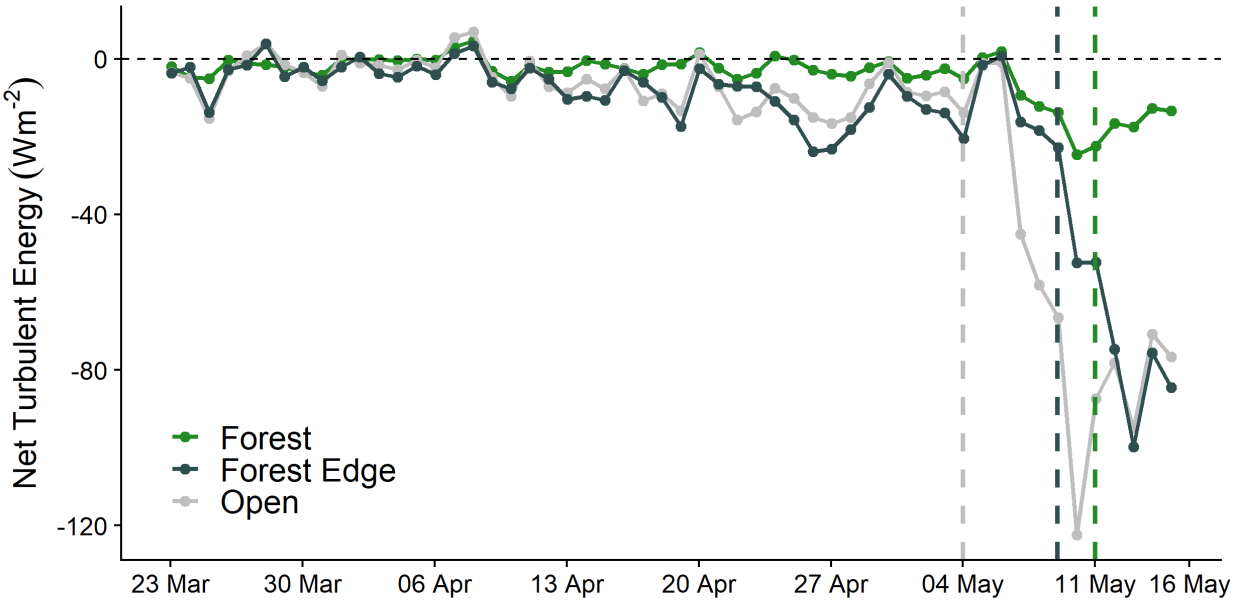

Figure 3. 11: Mean daily net turbulent fluxes, vertical dashed lines indicate snow disappearance date.

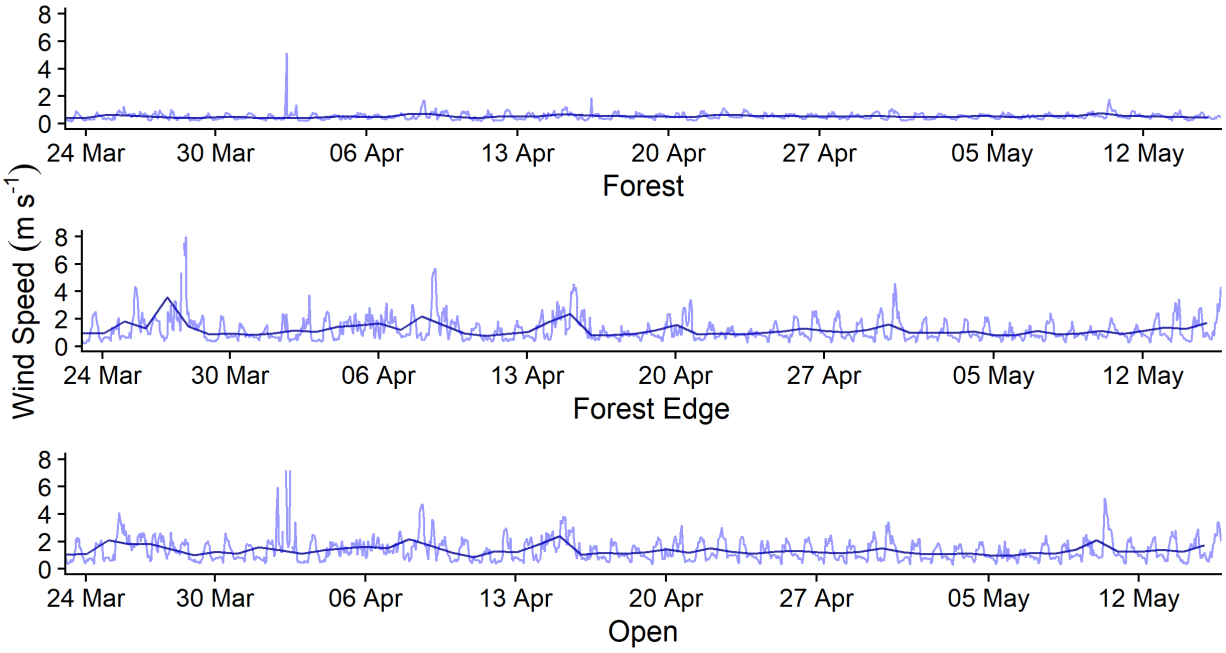

Figure 3. 12: Daily wind speed, solid blue line is daily mean value and light blue line is daily range of values.

3.3.7 Ground Heat Fluxes

Ground heat fluxes were positive and similar for all three sites during period of observation. Soil composition varied across the forest density gradient which created minor differences in the total ground heat flux. Liquid water at the base of the snowpack was observed in the immediate vicinity of the Open station during the snowmelt period. Figure 3.13 illustrates ground heat fluxes at all three stations. The contributions were all <1 Wm^{-2}. As the snowpack melted and underlying surface became exposed ground heat flux decreased at the Open and Forest Edge site, I removed these measurements from Figure 3.13.

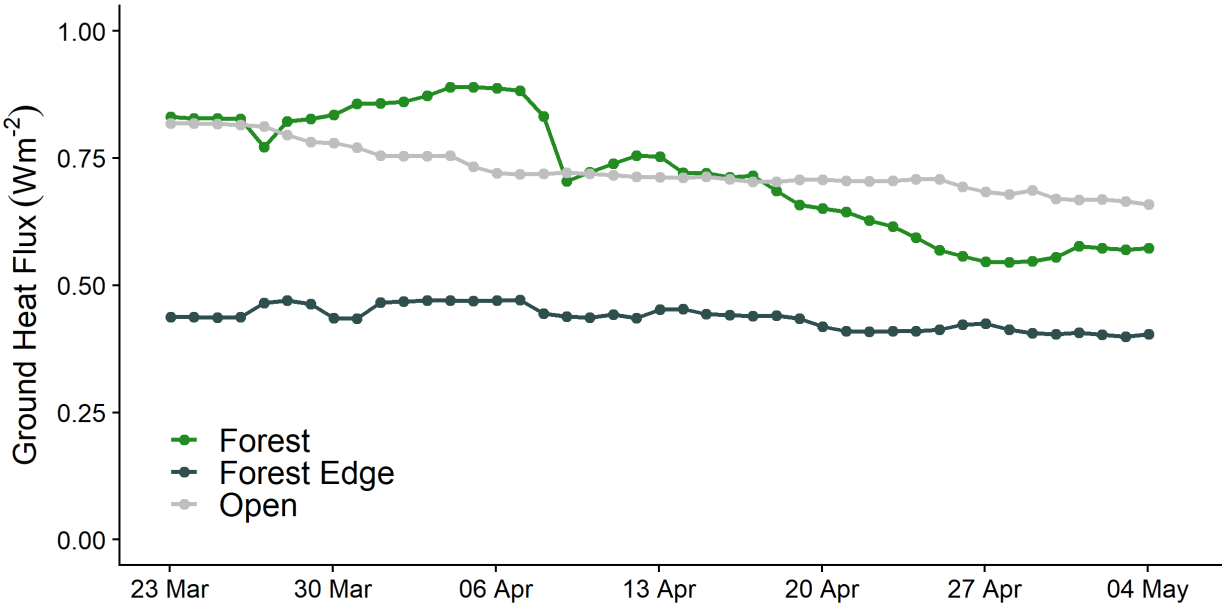

Figure 3. 13: Daily mean ground heat flux. Dates are removed past 3 May 2019 due to snow disappearance at the stations beginning.

3.3.8 Total Energy Budget

Figure 3.14, 3.15, and 3.16 shows the total energy at all three stations, total energy increased during the period of observation thereby causing snowmelt. The Open station had 6% greater total daily energy than the Forest Edge station and 15% greater total daily energy than the Forest station. The greater total daily energy melted the Open station five days before the Forest Edge station and a week at the Forest station. Both the Forest Edge and Forest station required slightly more sum of total energy to melt the snowpack than the Open station required. Net shortwave radiation was the dominant energy budget component at all three stations but played a much greater role at the Open and Forest Edge stations.

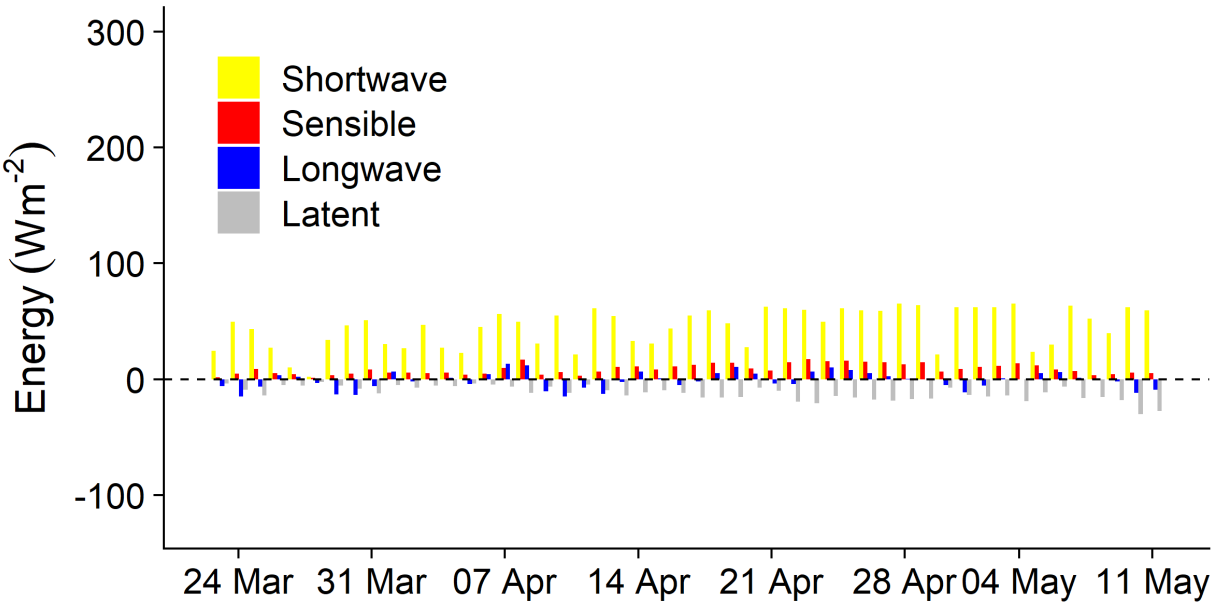

Figure 3. 14: S1 (Forest) daily mean energy budget components (bars), measurements end on snow disappearance date.

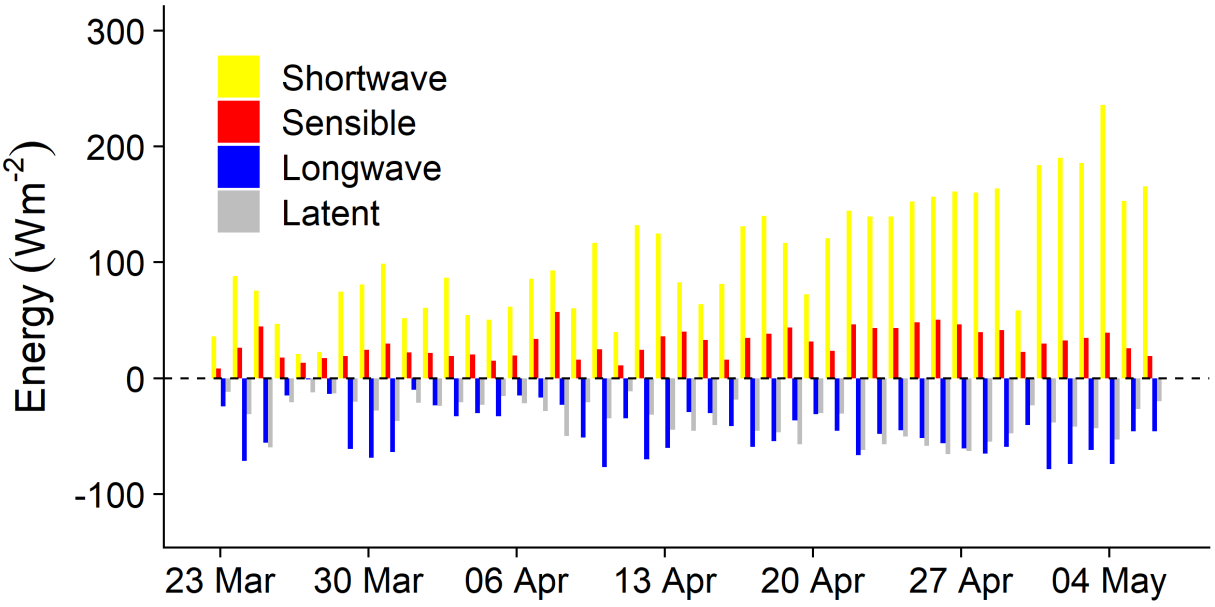

Figure 3. 15: S3 (Open) daily mean energy budget components (bars), measurements end on snow disappearance date.

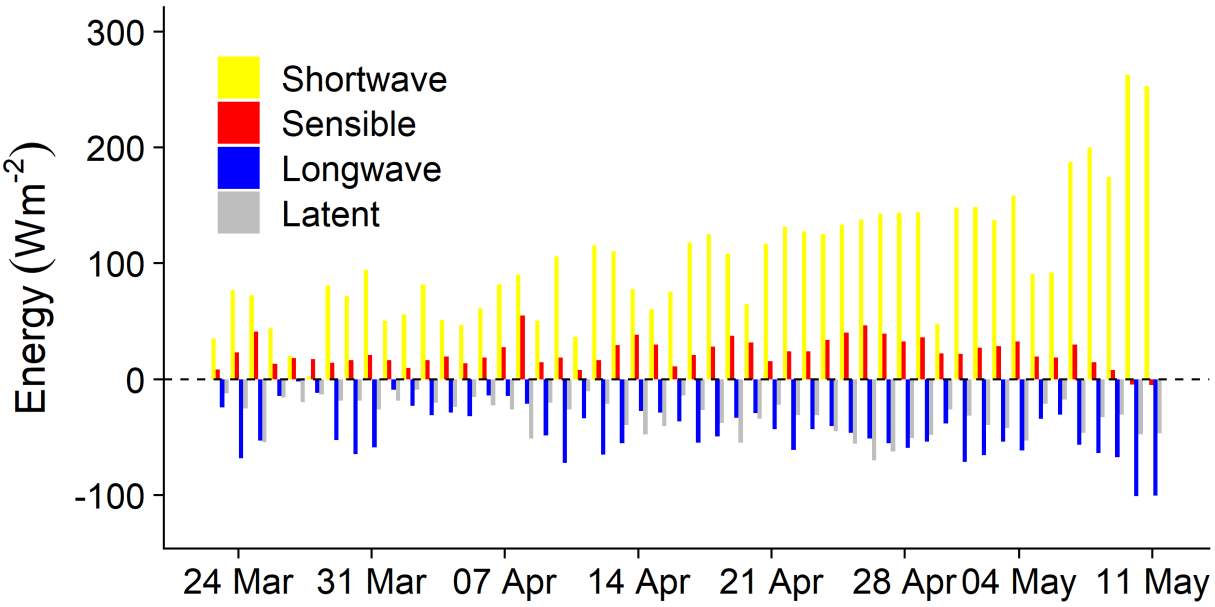

Figure 3. 16: S4 (Forest Edge) daily mean energy budget components (bars), measurements end on snow disappearance date.

3.3.9 Net Shortwave Radiation and the Relation to Broadband Snow Albedo

Net shortwave radiation was the dominant snowpack energy budget component at each of the three stations. To understand the effect of broadband albedo on net shortwave radiation budget at S1, S3, and S4 a relationship was formed between daily values of net shortwave radiation and snow albedo. Figure 3.17 shows that under a forest canopy where incoming solar radiation is low (Table 3.5), the net shortwave radiation is not affected by snow albedo. At S1, there is weak but significant relationship between net shortwave radiation and broadband albedo (Table 3.4). As incoming shortwave radiation increases at S4 and S3 (Table 3.5), broadband albedo plays a greater role in determining net shortwave radiation. As albedo decreases over the period of observation, net shortwave radiation increases at S4 and S3, and there is a statistically significant relationship between the two variables (Table 3.4).

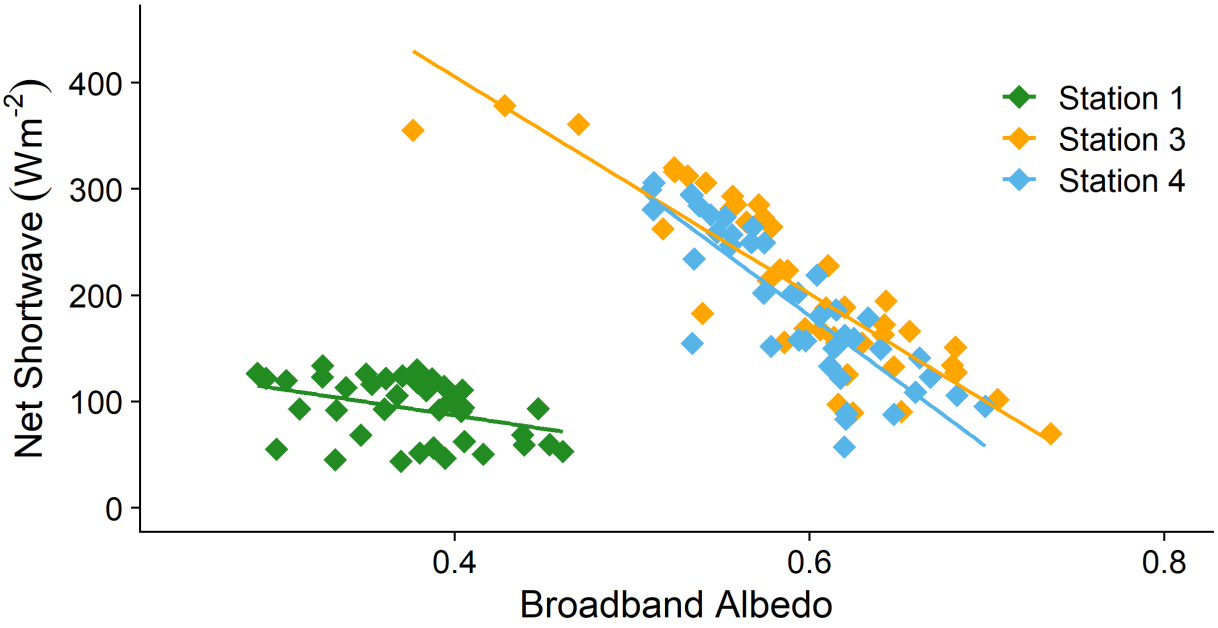

Figure 3. 17: Daily values of net radiometer measured broadband snow albedo and net shortwave radiation during the end of the accumulation and entire ablation period.

Table 3. 4: Reported statistical values of broadband snow albedo and net shortwave radiation.

Location	**R^2**	**P-value**
S1 (Forest)	0.19	P = 0.001606
S4 (Forest Edge)	0.65	P < 0.00001
S3 (Open)	0.79	P < 0.00001

Table 3. 5: Accumulation (acc.) and ablation (abl.) period daily average broadband albedo and incoming shortwave radiation with LiDAR forest metrics at each station. Standard deviations are reported in parentheses.

Location	**Albedo (acc.)**	**Albedo (abl.)**	**SW_{in} ($W\ m^{-2}$) (acc.)**	**SW_{in} ($W\ m^{-2}$) (abl.)**	**Canopy Cover (%)**	**Tree Height (m)**
S1 (Forest)	0.45 (±0.06)	0.37 (±0.03)	262 (±151)	306 (±128)	69 (±12)	18 (±2)
S4 (Forest Edge)	0.71 (±0.07)	0.61 (±0.05)	622 (±250)	745 (±239)	60 (±19)	5 (±1)
S3 (Open)	0.71 (±0.04)	0.62 (±0.05)	658 (±236)	768 (±233)	None	None

3.4 Error Assessment

Each instrument on the stations has a nominal accuracy and precision (Table 3.2). Here, I describe any additional uncertainties associated with the measurements.

3.4.1 CNR4 net radiometers

The Kipp & Zonen CNR4 is a 4-way net radiometer composed of a pair of pyranometers and pyrgeometers (upward and downward). The pyranometer has an expected daily accuracy of ± 10% the daily reported values and < 5% uncertainty in daily totals. The pyrgeometer has a < 10% uncertainty in daily totals. On both the pyranometer and pyrgeometer the upward facing detector field of view (FOV) measures 180˚, the lower facing detector FOV measures 150˚ to prevent illumination at low zenith angles.

A significant source of error in the net radiation measurements is due to precipitation. During and after snowfall events, the upward pointing instruments were blocked by snow. I monitored precipitation events

in order to clear off the upward-pointing pyranometers and pyrgeometers. I noted these events and omitted data that may have been affected. Vegetation within the FOV of the instruments can also influence both pyranometer and pyrgeometer measurements. Shading and sun-speckle can influence incoming solar radiation. Reflections from vegetation can also affect measured radiation at the downward-pointing pyranometer. Longwave radiation from vegetation will also affect measurements at the upward and downward-pointing pyrgeometers.

3.4.2 Energy Budget Calculation

In order to calculate the sensible and latent heat flux at each station atmospheric stability had to be accounted for and I used the bulk Richardson number with a bulk aerodynamic approach. A minimum wind speed threshold was created (<0.29 m s^{-1}) that assumed neutral stability. Positive values of Ri_B indicated a stable atmosphere and negative Ri_B indicated an unstable atmosphere. Values for Ri_B had to be constrained to times that it was within reasonable bounds. The use of bulk aerodynamic theory assumes log-linear profiles and scaling lengths for temperature and humidity are equal to the roughness length which can introduce bias to calculated and modeled turbulent fluxes (Moore, 1983). In addition, turbulent heat fluxes over patchy snow are variable due to advective heat transport (Essery et al., 2006) and noticed towards the end of the ablation period patchy snow around the Open and Forest Edge stations.

3.5 Discussion

3.5.1 Snowpack Energy Budget Component Variability

Snowpack energy budget results show that net shortwave radiation contributed the largest sum of energy for snowmelt through the period of observation similar to Marks and Dozier (1992). Spatial variability of snowpack energy budget components is due to forest density, denser forest reduces the magnitude of all energy budget components and shifts the date of snow disappearance. Our study took place across a uniform elevation gradient and did not evaluate variability due to elevation that was discovered in warm maritime forests in the Pacific Northwest (Dickerson-Lange et al., 2017). However, our study site represents a low elevation and warm maritime forest. Previous studies (Roth & Nolin, 2017) have shown

that elevation is important for snowpack energy budgets in forests and creates differences in snowmelt. Future work at the Sagehen Field Site should measure the snowpack energy budget with elevation gradients incorporated.

3.5.2 Shortwave Radiation

Net shortwave radiation is controlled primarily by snow albedo at both the Open and Forest edge stations and by canopy shading and snow albedo at the Forest station. Net shortwave radiation contributed the most energy to the snowpack at the Open, Forest Edge, and Forest stations but at the Forest station there is half the amount of net shortwave radiation received because of canopy shading. Roth and Nolin (2017) showed the large difference in net shortwave radiation when comparing open to forested areas which align with our results. Snow albedo was lowest (22%) in the forest through the period of observation, but canopy shading effectively reduces net shortwave radiation in the forest and factors into the importance of snow albedo. Future work requires this relationship to be tested during both the entire accumulation period and ablation period, and by incorporating forest metrics, for example canopy gap and canopy leaf area. The use of net radiometers is invaluable to sub-canopy net shortwave radiation and albedo measurements.

3.5.3 Longwave Radiation

Across the forest density gradient net longwave radiation had no significant effect on snowmelt. Previous studies have found that in forests net longwave radiation is a key snowpack energy budget component and is greater in denser forest or warm forested regions, similar to our study in the California Sierra (Essery et al., 2008; John W. Pomeroy et al., 2009; Roth & Nolin, 2017) Net longwave radiation was relatively minimal at our Forest station and always negative at the exposed Open and Forest Edge stations. This may be due to forest structure and the timing of our measurements which missed the accumulation season when storms and the atmosphere can increase longwave radiation inputs. Studies have shown greater energy inputs from net longwave radiation during the peak accumulation period (e.g. Marks & Dozier.,

1992). Future work is needed to assess the role of longwave radiation with different forest structures and in different snow climates.

3.5.4 Turbulent Fluxes

Forest density drives the magnitude of sensible and latent heat fluxes across the forest density, turbulence is greater in the open and less in the forest. Open areas of forest are more exposed and receive greater daily solar insolation, diurnal temperature shifts, and turbulence (e.g. wind) consistent with Boon (2009). Our results showed that the turbulent fluxes mirrored each other in direction and primarily canceled each other across the forest density gradient through the period of observation. This result is similar to Marks and Dozier., (1992) that found the turbulent fluxes cancelled out and had opposite direction in a higher elevation and more exposed watershed in the Central California Sierra Nevada. Sensible and latent heat fluxes were always greater at the Open and Forest Edge stations than the Forest station due to increased wind speed.

3.5.5 Snowmelt

Forest density created differences in the sum and magnitude of energy budget components that influenced snow disappearance dates. The Open and Forest edge stations had about a third more snow-water equivalent than the Forest site. However, the Open station melted a week earlier than the Forest station. The greater total daily energy received at the Open station which was largely net shortwave radiation melted the snowpack faster. There was less total daily energy in magnitude for all snowpack energy budget components at the Forest station, but net shortwave radiation was the primary component of energy for snowmelt at the Forest station. The snowpack melted seven days earlier at the Open station compared to the Forest station and melted five days earlier then at the Forest Edge station. These results show the importance of net shortwave radiation and snowmelt across the forest density gradient and our similar to findings of forest metrics explaining difference in snow ablation rates in mixed conifer forests (Musselman et al., 2012). Field observations noted the meadow surrounding the open station rapidly

melted. While snowmelt at and around the Forest station was slower, especially in areas with denser canopy coverage there were observations of ablation remnants that remained.

3.5.6 Conclusion

Our results demonstrate the importance of understanding how forest density can affect the magnitudes of the individual energy budget components. These results show that canopy shading and snow albedo are important for the net shortwave radiation budget in the forest. However, in large open areas of the forest snow albedo is the major control on the net shortwave radiation budget. Therefore, correctly representing snow albedo in open parts of the forest is critical for snowmelt models across watersheds with large open areas and forest gaps. This study highlights the importance of accurately measuring the radiation components of the snowpack energy budget across in forested because radiation contributes the most energy to snowmelt. These results illustrate the need to further study snowpack energy budget components in different types of forests and snow climates. Future work will calculate the entire snowpack energy budget for a complete snow season and test relationships between snowpack energy budget components and forest density metrics.

4 Synthesis of the Research

4.1 Key findings

Our key findings highlight the spatial and temporal differences of snow albedo and net shortwave radiation across a forest density gradient in the California Sierra Nevada. First, I find that differences in snow albedo are primarily driven by forest litter concentration, which changes across the forest density gradient and changes over time-since-last snowfall. Additionally, there is a strong relationship established between forest density metrics and snow albedo, snow albedo is effectively reduced near or under the forest canopy. Second, I find that in the forest, net shortwave radiation depends on the amount of solar radiation reaching the snow surface, rather than snow albedo. This contrasts with what was seen in the open areas where net shortwave radiation is strongly dependent on snow albedo. Lastly, I find that in the forest, net shortwave radiation is a reduced component of the total snow energy budget when compared to

open forest. As forest density decreases, albedo and net shortwave radiation are more important for snowpack energy budget. This implies that, for estimating energy budget in snowy forests, inaccuracies in snow albedo are less consequential in sub-canopy snow albedo relative to open areas.

4.2 Effects of Forest Litter and Light Absorbing Particles

Forest litter and light absorbing particles (e.g. black carbon) are highest in the forest and tend to concentrate in the surface layer of the snowpack. Snow albedo is always lowest in the forest, even after a new snow event. This is because forest litter accumulates on the snowpack either during or immediately after snowfall. Forest litter and light absorbing particles increase in concentration as snow ages and is particularly pronounced as the snow ablation period progresses.

Results finding black carbon in the surface and sub-surface snow samples was surprising, and this analysis was not able to identify a source for these light absorbing particles. Black carbon was consistently highest in snow samples collected in the forest, declining towards the open sites. This suggests that the forest may act as a filter for particulates carried by wind, causing them to be deposited through dry deposition in the forest gaps or indirectly through mass unloading of canopy snow. Questions around black carbon deposition in forests remain a topic for future research.

4.3 Effects of Forest on Net Solar Radiation

Canopy shading reduces solar insolation in the forest and therefore affects net solar radiation and energy budget. Our measurements show that incoming solar radiation is four times greater at the open site compared with the forested site during the ablation period. As a result, net shortwave radiation is two times greater in the open area than in the forest during the ablation period. I also find that there is no statistically significant relationship between broadband albedo and net shortwave radiation in the forest. This implies that snow albedo in dense forests is not a significant determinant of net shortwave radiation. Furthermore, it suggests that estimates of snow albedo in forested areas do not need to be highly accurate in order to adequately represent net shortwave radiation in the snow energy budget in forests. The open site had a significant relationship between broadband snow albedo and net shortwave radiation indicating

the importance of accurate albedo estimates. This suggests that the need for albedo accuracy increases with decreasing canopy cover while at the same time, forest litter decreases with decreasing canopy cover. Even during times of high insolation, the net shortwave radiation accounted for 50% less towards the total energy budget in the forest. Accounting for snow albedo in the areas and large forest gaps is critical to accurately estimate snow energy budget and snowmelt processes.

4.4 Bigger Picture

Our measurements, results, and key findings build on the exemplary work of several previous studies. Wiscombe and Warren (1980), Warren and Wiscombe (1980) provided the physical basis for snow albedo in solar spectrum. They showed that presence of dust and soot reduce snow albedo in the visible wavelengths and increasing grain size reduces snow albedo in the near-infrared wavelengths. Our results show that snow deposited in forests is not pure and becomes increasingly darkened by forest litter (as well as black carbon) as the snow ages and especially during snow ablation.

In a boreal forest study, Melloh et al. (2001) measured forest litter deposited on snow and they also modeled its effect on snow albedo. They found that it is more important to consider the role of forest litter and snow albedo during the ablation season as litter accumulates on the snow surface and has the greatest effect to reduce snow albedo. Their boreal forest results are similar to those presented here.

Boon, 2009 and Winkler & Boon, 2010 point to the importance of forest structure and forest litter on snow albedo and the snowpack energy budget. Our results align well with their findings that snow albedo needs to be accurately accounted for in areas of a forest where net shortwave radiation is the greatest. I show that the forest edge, and likely large forest gaps, receive substantial incoming shortwave radiation while concurrently having deposition of forest litter on the snow. This suggests that the net shortwave radiation in forest-adjacent areas is perhaps most sensitive to the effects of changing snow albedo due to forest litter.

Gleason et al. (2013) and Gleason & Nolin (2017) evaluated snow albedo across a forest and a burned forest and the overall importance of fires and snow albedo across the western US (Gleason et al. 2019). Gleason et al. (2013) demonstrated that charred woody debris deposited onto a snowpack following wildfire significantly affects snow albedo and that decreased canopy cover increases net solar radiation at the surface. Our results show that unburned forest litter is effective at reducing snow albedo and concentrations reduce from the forest to open areas of a forest. However, unlike Gleason et al. (2013) our results find that the reduction of snow albedo has little impact on net solar radiation because the forest remains intact. Gleason (2019) highlighted the importance of measuring snow albedo across different forest regions and snow climates. Our results show that spatial differences in snow albedo exist across a temperate mixed-coniferous forest and suggest that snow albedo variability may be affected by regional differences in forest structure and snow climate.

Previous energy budget studies in forests (e.g. Boon, 2009; T. Link & Marks, 1999; Marks et al., 1992; Roth & Nolin, 2017) found net radiation to be the dominant snowpack energy budget component. At open sites, net shortwave radiation as the primary component of positive energy into the snowpack for melt and snow albedo is a critical snow parameter needed (Marks et al., 1992).Our results were similar for the open site but not so for the dense forest site. Clearly measuring net shortwave radiation and snow albedo in the open parts of a forest are important to correctly model snowmelt timing. However longwave radiation increasingly dominates the energy budget with increasing forest density (Roth & Nolin, 2017). In the dense forest, it is more important to correctly determine the net longwave component than the net shortwave component of the energy budget.

4.5 Recommendations for future research

This study illustrates a future need for field-based snow albedo research in different types of forests, looking at relationships with forest structure, species composition, and snow climate. Transects of in-situ hyperspectral snow albedo measurements were a valuable addition to station-based broadband albedo measurements. Future snow field campaigns should incorporate both hyperspectral and broadband albedo

measurements across forest density gradients and over time; snow grain size and snow sample analysis offered critical insights into causes of snow albedo differences. Ground-based observations of snow albedo and snow characteristics (including forest litter) are critical for developing accuracy requirements for airborne snow campaigns and a future snow-monitoring satellite mission.

Our results will help inform how snow albedo is represented in land surface models. Clearly, forest litter affects snow albedo and therefore should be considered in modeled albedo decay parameterizations. Further research to fully account for the effects of forest litter on snow albedo and how forest density affects both litter concentrations and net shortwave radiation. In locations where incoming solar radiation is high, a static albedo value or a single albedo decay function will likely result in inaccurate snow ablation rates. This suggests the need for look up tables or libraries of albedo decay functions based on forest structure. Empirical equations can be created that relate forest structure to changes in snow albedo based on multiple forest metric variables, time, and snowfall events. However, in dense forests, and where incoming solar radiation is relatively low, a simple albedo representation is likely to be sufficient. Thus, measurements of forest structure over a range of forest types and snow climates are needed to understand the variability in, and relative importance of snow albedo.

5 References

Anderson, E. A. (1968). Development and testing of snow pack energy balance equations. *Water Resources Research*, *4*(1), 19–37. https://doi.org/10.1029/WR004i001p00019

Anderson, Eric A. (1976). *A point energy and mass balance model of a snow cover* (Vol. 19). US Department of Commerce, National Oceanic and Atmospheric Administration~….

Bair, E. H., Rittger, K., Skiles, S. M. K., & Dozier, J. (2019). An Examination of Snow Albedo Estimates From MODIS and Their Impact on Snow Water Equivalent Reconstruction. *Water Resources Research*, *55*(9). https://doi.org/10.1029/2019WR024810

Barnett, T. P., Adam, J. C., & Lettenmaier, D. P. (2005). Potential impacts of a warming climate on water availability in snow-dominated regions. In *Nature*. https://doi.org/10.1038/nature04141

Baumgardner, D., Kok, G., & Raga, G. (2004). Warming of the Arctic lower stratosphere by light absorbing particles. *Geophysical Research Letters*, *31*(6), n/a-n/a. https://doi.org/10.1029/2003gl018883

Betts, A. K., & Ball, J. H. (1997). Albedo over the boreal forest. *Journal of Geophysical Research: Atmospheres*, *102*(D24), 28901–28909. https://doi.org/10.1029/96JD03876

Boon, S. (2009). Snow ablation energy balance in a dead forest stand. *Hydrologic Processes*, *2274*(November 2008), 2267–2274. https://doi.org/10.1002/hyp

Brown, R. D., & Robinson, D. A. (2011). Northern Hemisphere spring snow cover variability and change over 1922-2010 including an assessment of uncertainty. *Cryosphere*, *5*(1), 219–229. https://doi.org/10.5194/tc-5-219-2011

Brutsaert, W. (1982). Evaporation into the atmosphere: Theory. *History, and Applications. D. Reidel*.

Cline, D. W. (1997). Snow surface energy exchanges and snowmelt at a continental, midlatitude Alpine site. *Water Resources Research*, *33*(4), 689–701. https://doi.org/10.1029/97WR00026

Daniel, W. (1990). Applied nonparametric statistics. 2^ sup a^ ed. *PlusKent. Boston, MA, EEUU*.

DeWalle, D. R., & Rango, A. (2008). *Principles of snow hydrology*. Cambridge University Press.

Dickerson-Lange, S. E., Gersonde, R. F., Hubbart, J. A., Link, T. E., Nolin, A. W., Perry, G. H., Roth, T. R., Wayand, N. E., & Lundquist, J. D. (2017). Snow disappearance timing is dominated by forest effects on snow accumulation in warm winter climates of the Pacific Northwest, United States. *Hydrological Processes*. https://doi.org/10.1002/hyp.11144

Dozier, J. (1984). *Snow Reflectance from LAN DSAT-4 Thematic Mapper*. *3*, 323–328.

Dozier, J. (1989). *Spectral Signature of Alpine Snow Cover from the Landsat Thematic Mapper* (Vol. 28).

Dozier, J., Green, R. O., Nolin, A. W., & Painter, T. H. (2009). Interpretation of snow properties from imaging spectrometry. *Remote Sensing of Environment*, *113*(SUPPL. 1), S25–S37. https://doi.org/10.1016/j.rse.2007.07.029

Essery, R. (2013). Large-scale simulations of snow albedo masking by forests. *Geophysical Research Letters*, *40*(20), 5521–5525. https://doi.org/10.1002/grl.51008

Essery, R., Granger, R., & Pomeroy, J. (2006). Boundary-layer growth and advection of heat over snow and soil patches: modelling and parameterization. *Hydrological Processes: An International Journal*, *20*(4), 953–967.

Essery, R., Pomeroy, J., Ellis, C., & Link, T. (2008). Modelling longwave radiation to snow beneath forest canopies using hemispherical photography or linear regression. *Hydrological Processes*, *22*(15), 2788–2800. https://doi.org/10.1002/hyp.6930

Evolution, S. (2014). *SR-3500 Series Spectroradiometer / SM-3500 Series Spectrometer Operator ' s Manual*.

Flanner, M. G., Zender, C. S., Randerson, J. T., & Rasch, P. J. (2007a). Present-day climate forcing and response from black carbon in snow. *Journal of Geophysical Research Atmospheres*, *112*(11), 1–17. https://doi.org/10.1029/2006JD008003

Flanner, M. G., Zender, C. S., Randerson, J. T., & Rasch, P. J. (2007b). Present-day climate forcing and response from black carbon in snow. *Journal of Geophysical Research Atmospheres*. https://doi.org/10.1029/2006JD008003

Gelfan, A. N., Pomeroy, J. W., & Kuchment, L. S. (2004). Modeling forest cover influences on snow accumulation, sublimation, and melt. *Journal of Hydrometeorology*, *5*(5), 785–803. https://doi.org/10.1175/1525-7541(2004)005<0785:MFCIOS>2.0.CO;2

Gleason, K. E., McConnell, J. R., Arienzo, M. M., Chellman, N., & Calvin, W. M. (2019a). Four-fold increase in solar forcing on snow in western U.S. burned forests since 1999. *Nature Communications*, *10*(1). https://doi.org/10.1038/s41467-019-09935-y

Gleason, K. E., McConnell, J. R., Arienzo, M. M., Chellman, N., & Calvin, W. M. (2019b). Four-fold increase in solar forcing on snow in western U.S. burned forests since 1999. *Nature*

Communications, *10*(1), 1–8. https://doi.org/10.1038/s41467-019-09935-y

Gleason, K. E., & Nolin, A. W. (2016). *Charred forests accelerate snow albedo decay : parameterizing the post- fi re radiative forcing on snow for three years following fi re*. *3870*(June), 3855–3870. https://doi.org/10.1002/hyp.10897

Gleason, K. E., Nolin, A. W., & Roth, T. R. (2013). Charred forests increase snowmelt: Effects of burned woody debris and incoming solar radiation on snow ablation. *Geophysical Research Letters*. https://doi.org/10.1002/grl.50896

Hadley, O. L., & Kirchstetter, T. W. (2012). Black-carbon reduction of snow albedo. *Nature Climate Change*, *2*(6), 437–440. https://doi.org/10.1038/nclimate1433

Hansen, J., & Nazarenko, L. (2004). Soot climate forcing via snow and ice albedos. *Proceedings of the National Academy of Sciences of the United States of America*, *101*(2), 423–428. https://doi.org/10.1073/pnas.2237157100

Hardy, J. P., Davis, R. E., Jordan, R., Ni, W., & Woodcock, C. E. (1998). Snow ablation modelling in a mature aspen stand of the boreal forest. *Hydrological Processes*, *12*(10–11), 1763–1778. https://doi.org/10.1002/(SICI)1099-1085(199808/09)12:10/11<1763::AID-HYP693>3.0.CO;2-T

Hardy, J. P., Melloh, R., Koenig, G., Marks, D., Winstral, A., Pomeroy, J. W., & Link, T. (2004). Solar radiation transmission through conifer canopies. *Agricultural and Forest Meteorology*. https://doi.org/10.1016/j.agrformet.2004.06.012

Hardy, J. P., Melloh, R., Robinson, P., & Jordan, R. (2000). *Incorporating effects of forest litter in a snow process model*. *3237*(May), 3227–3237.

Harpold, A. A., Biederman, J. A., Condon, K., Merino, M., Korgaonkar, Y., Nan, T., Sloat, L. L., Ross, M., & Brooks, P. D. (2014). Changes in snow accumulation and ablation following the Las Conchas Forest Fire, New Mexico, USA. *Ecohydrology*, *7*(2), 440–452. https://doi.org/10.1002/eco.1363

Henderson-Sellers, A., & Wilson, M. F. (1983). • Scat. *Review of Geophysics and Space Physics*, *21*(8), 1743–1778.

Hiemstra, C. A., Liston, G. E., & Reiners, W. A. (2002). Snow Redistribution by Wind and Interactions with Vegetation at Upper Treeline in the Medicine Bow Mountains, Wyoming, U.S.A. *Arctic, Antarctic, and Alpine Research*, *34*(3), 262–273. https://doi.org/10.1080/15230430.2002.12003493

Hiemstra, C. A., Liston, G. E., & Reiners, W. A. (2006). Observing, modelling, and validating snow

redistribution by wind in a Wyoming upper treeline landscape. *Ecological Modelling*, *197*(1–2), 35–51. https://doi.org/10.1016/j.ecolmodel.2006.03.005

Jennings, K., & Jones, J. A. (2015). Precipitation-snowmelt timing and snowmelt augmentation of large peak flow events, western Cascades, Oregon. *Water Resources Research*, *51*(9), 7649–7661. https://doi.org/10.1002/2014WR016877

Jost, G., Weiler, M., Gluns, D. R., & Alila, Y. (2007). The influence of forest and topography on snow accumulation and melt at the watershed-scale. *Journal of Hydrology*, *347*(1–2), 101–115. https://doi.org/10.1016/j.jhydrol.2007.09.006

Klok, E. J., Greuell, W., & Oerlemans, J. (2004). Temporal and spatial variation of the surface albedo of Morteratschgletscher, Switzerland, as derived from 12 Landsat images. *Journal of Glaciology*, *49*(167), 491–502. https://doi.org/10.3189/172756503781830395

Kustas, W. P., Rango, A., & Uijlenhoet, R. (1994). A simple energy budget algorithm for the snowmelt runoff model. *Water Resources Research*, *30*(5), 1515–1527.

Lek, P. C. H., & Ramaswamy, V. (1983). *Albedo of soot-contaminated snow*. *88*(3), 837–843.

Lemke, P., Alley, R. B., Allison, I., Carrasco, J., Flato, G., Fujii, Y., Kaser, G., Mote, P., Thomas, R. H., & Zhang, T. (2007). Observations: Changes in Snow, Ice and Frozen Ground BT - Climate Change 2007: The Physical Science Basis. Contribution of Working Group I to the Fourth Assessment Report of the Intergovernmental Panel on Climate Change . *Climate Change 2007: The Physical Science Basis. Contribution of Working Group I to the Fourth Assessment Report of the Intergovernmental Panel on Climate Change , February 2015*, 1–48. papers2://publication/uuid/0D287704-646B-4B00-84D1-862C7838CA54

Link, T. E., & Marks, D. (1999). Point simulation of seasonal snow cover dynamics beneath boreal forest canopies. *Journal of Geophysical Research Atmospheres*, *104*(D22), 27841–27857. https://doi.org/10.1029/1998JD200121

Link, T., & Marks, D. (1999). Distributed simulation of snowcover mass- and energy-balance in the boreal forest. *Hydrological Processes*, *13*(14–15), 2439–2452. https://doi.org/10.1002/(SICI)1099-1085(199910)13:14/15<2439::AID-HYP866>3.0.CO;2-1

Male, D. H., & Granger, R. J. (1981). Snow surface energy exchange. *Water Resources Research*, *17*(3), 609–627. https://doi.org/10.1029/WR017i003p00609

Marks, D., & Dozier, J. (1992). *Climate and Energy Exchange at the Snow Surface in the Alpine Region*

of the Sierra Nevada 2 . Snow Cover Energy Balance Rv , o [anirr. *28*(11), 3043–3054.

Marks, D., Dozier, J., & Davis, R. E. (1992). *Climate and Energy Exchange at the Snow Surface in the Alpine Region of the Sierra Nevada 2 . Snow Cover Energy Balance Rv , o [anirr*. *28*(11), 3043–3054.

Marks, D., & Winstral, A. (2001). Comparison of snow deposition, the snow cover energy balance, and snowmelt at two sites in a semiarid mountain basin. *Journal of Hydrometeorology*, *2*(3), 213–227. https://doi.org/10.1175/1525-7541(2001)002<0213:COSDTS>2.0.CO;2

MARSH, P., & POMEROY, J. W. (1996). Meltwater Fluxes At an Arctic Forest-Tundra Site. *Hydrological Processes*, *10*(10), 1383–1400. https://doi.org/10.1002/(sici)1099-1085(199610)10:10<1383::aid-hyp468>3.3.co;2-n

Mazurkiewicz, A. B., Callery, D. G., & McDonnell, J. J. (2008). Assessing the controls of the snow energy balance and water available for runoff in a rain-on-snow environment. *Journal of Hydrology*, *354*(1–4), 1–14. https://doi.org/10.1016/j.jhydrol.2007.12.027

Melloh, R. A., Hardy, J. P., Davis, R. E., & Robinson, P. B. (2001). Spectral albedo/reflectance of littered forest snow during the melt season. *Hydrological Processes*. https://doi.org/10.1002/hyp.1043

Moore, R. D. (1983). A comparison of the snowmelt energy budgets in two alpine basins. *Archives for Meteorology, Geophysics, and Bioclimatology, Series B*, *33*(1–2), 1–10.

Musselman, K. N., Molotch, N. P., & Brooks, P. D. (2008). Effects of vegetation on snow accumulation and ablation in a mid-latitude sub-alpine forest. *Hydrological Processes*, *22*(15), 2767–2776. https://doi.org/10.1002/hyp.7050

Musselman, K. N., Molotch, N. P., Margulis, S. A., Kirchner, P. B., & Bales, R. C. (2012). Influence of canopy structure and direct beam solar irradiance on snowmelt rates in a mixed conifer forest. *Agricultural and Forest Meteorology*, *161*, 46–56. https://doi.org/10.1016/j.agrformet.2012.03.011

Nolin, A. W., & Dozier, J. (1993). *Estimating Snow Grain Size Using AVIRIS Data* (Vol. 44).

Nolin, A. W., & Dozier, J. (2000). A hyperspectral method for remotely sensing the grain size of snow. *Remote Sensing of Environment*. https://doi.org/10.1016/S0034-4257(00)00111-5

O'Neill, A. D. J., & Gray, D. M. (1973). *Spatial and temporal variations of the albedo of a prairie snowpack, The Role of Snow and Ice in Hydrology: Proceedings of the Banff Symposium*. Unesco/WMO/IAHS, Geneva-Budapest-Paris.

Painter, T. H., Dozier, J., Roberts, D. A., Davis, R. E., & Green, R. O. (2003). *Retrieval of subpixel snow-covered area and grain size from imaging spectrometer data*. *85*, 64–77. https://doi.org/10.1016/S0034-4257(02)00187-6

Painter, T. H., Rittger, K., McKenzie, C., Slaughter, P., Davis, R. E., & Dozier, J. (2009). Retrieval of subpixel snow covered area, grain size, and albedo from MODIS. *Remote Sensing of Environment*. https://doi.org/10.1016/j.rse.2009.01.001

Pomeroy, J. W., Parviainen, J., Hedstrom, N., & Gray, D. M. (1998). Coupled modelling of forest snow interception and sublimation. *Hydrological Processes*, *12*(15), 2317–2337. https://doi.org/10.1002/(SICI)1099-1085(199812)12:15<2317::AID-HYP799>3.0.CO;2-X

Pomeroy, John W., Marks, D., Link, T., Ellis, C., Hardy, J., Rowlands, A., & Granger, R. (2009). The impact of coniferous forest temperature on incoming longwave radiation to melting snow. *Hydrological Processes*, *23*(17), 2513–2525. https://doi.org/10.1002/hyp.7325

Rinehart, A. J., Vivoni, E. R., & Brooks, P. D. (2008). Effects of vegetation, albedo, and solar radiation sheltering on the distribution of snow in the Valles Caldera, New Mexico. *Ecohydrology*, *1*(3), 253–270. https://doi.org/10.1002/eco.26

Roth, T. R., & Nolin, A. W. (2017). Forest impacts on snow accumulation and ablation across an elevation gradient in a temperate montane environment. *Hydrology and Earth System Sciences*, *21*(11). https://doi.org/10.5194/hess-21-5427-2017

Serreze, M. C., Clark, M. P., Armstrong, R. L., McGinnis, D. A., & Pulwarty, R. S. (1999). Characteristics of the western United States snowpack from snowpack telemetry (SNOTEL) data. *Water Resources Research*, *35*(7), 2145–2160. https://doi.org/10.1029/1999WR900090

Skiles, S. M., Painter, T. H., Deems, J. S., Bryant, A. C., & Landry, C. C. (2012). *Dust radiative forcing in snow of the Upper Colorado River Basin : 2 . Interannual variability in radiative forcing and snowmelt rates*. *48*, 1–11. https://doi.org/10.1029/2012WR011986

Stephens, M., Turner, N., & Sandberg, J. (2003). Particle identification by laser-induced incandescence in a solid-state laser cavity. *Applied Optics*, *42*(19), 3726. https://doi.org/10.1364/ao.42.003726

Stroeve, J., Nolin, A., & Steffen, K. (1997). Comparison of AVHRR-derived and in situ surface albedo over the Greenland ice sheet. *Remote Sensing of Environment*, *62*(3), 262–276. https://doi.org/10.1016/S0034-4257(97)00107-7

Sturm, M., Durand, M., Robinson, D., & Serreze, M. (2017). Got snow? *The Need to Monitor Earth's*

Snow Resources.

Varhola, A., Coops, N. C., Weiler, M., & Moore, R. D. (2010). Forest canopy effects on snow accumulation and ablation: An integrative review of empirical results. *Journal of Hydrology*, *392*(3–4), 219–233. https://doi.org/10.1016/j.jhydrol.2010.08.009

Warren_Wiscombe_1980_P2.pdf. (n.d.).

Warren, S. G. (1982). Optical properties of snow. *Reviews of Geophysics*, *20*(1), 67–89. https://doi.org/10.1029/RG020i001p00067

Winkler, R., Boon, S., Zimonick, B., & Baleshta, K. (2010a). Assessing the effects of post-pine beetle forest litter on snow albedo. *Hydrological Processes*. https://doi.org/10.1002/hyp.7648

Winkler, R., Boon, S., Zimonick, B., & Baleshta, K. (2010b). Assessing the effects of post-pine beetle forest litter on snow albedo. *Hydrological Processes*, *24*(6), 803–812. https://doi.org/10.1002/hyp.7648

Winkler, R. D., Spittlehouse, D. L., & Golding, D. L. (2005). Measured differences in snow accumulation and melt among clearcut, juvenile, and mature forests in southern British Columbia. *Hydrological Processes*, *19*(1), 51–62. https://doi.org/10.1002/hyp.5757

Wiscombe, W. J., & Warren, S. G. (1980). A Model for the Spectral Albedo of Snow. I: Pure Snow. *Journal of the Atmospheric Sciences*, *37*(12), 2712–2733. https://doi.org/10.1175/1520-0469(1980)037<2712:AMFTSA>2.0.CO;2

6 Appendices

Appendix A: Daily air temperature, solid black line is daily mean value and light grey line is daily range of values.

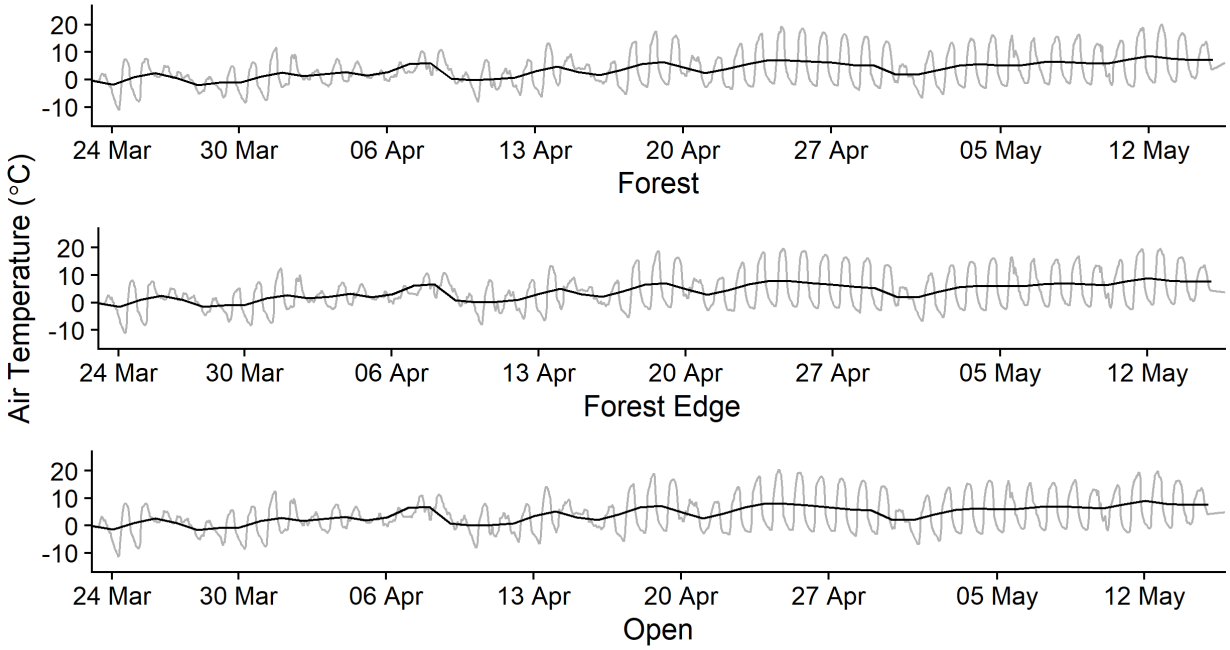

Appendix B: Daily snow surface temperature, solid black line is daily mean value and dark grey line is daily range of values.

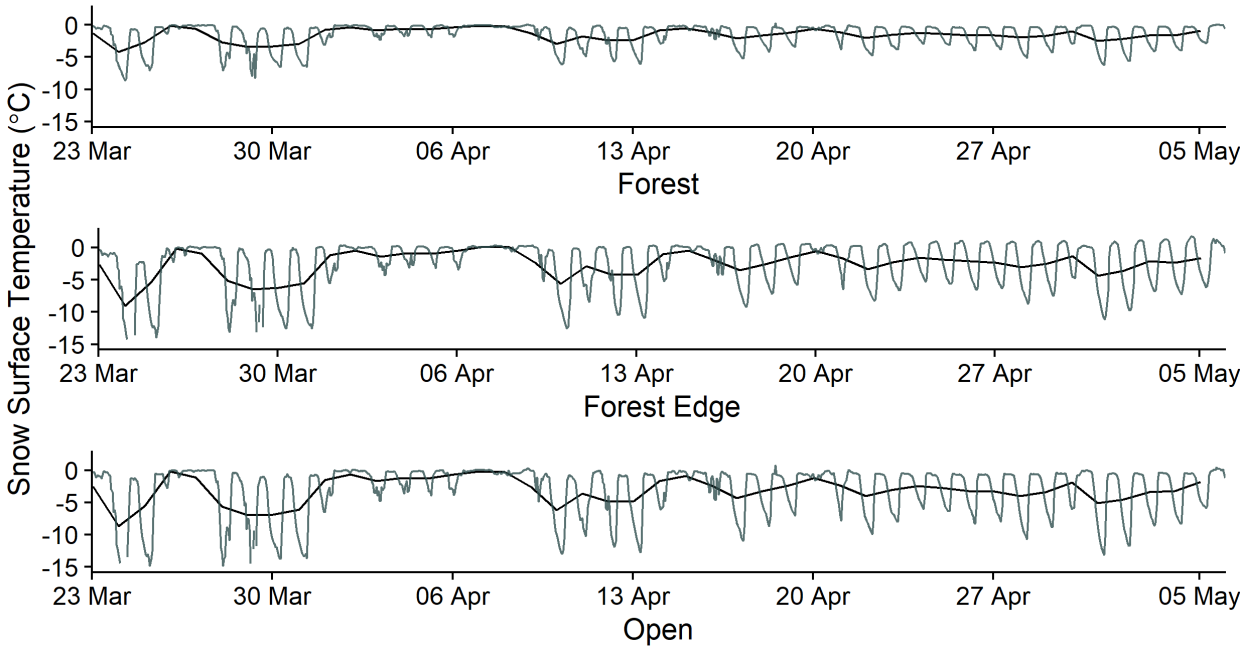

Appendix C: Daily relative humidity values, solid blue line is daily mean value and light grey line is daily range of values.